Finite-Quark-Mass Effects on the Higgs Production Cross Section in the Gluon-Gluon Fusion Channel

Dissertation

zur Erlangung des Doktorgrades an der Fakultät für Mathematik, Informatik und Naturwissenschaften

Fachbereich Physik der Rheinisch-Westfälischen Technischen Hochschule

vorgelegt von

Tom Claus Rudolf Schellenberger

Aachen
1. Juli 2025

Finite-Quark-Mass Effects on the Higgs Production Cross Section in the Gluon-Gluon Fusion Channel

GUTACHTER DER DISSERTATION:

Prof. Dr. Michał Czakon
Prof. Dr. Robert Harlander

ZUSAMMENSETZUNG DER PRÜFUNGSKOMMISSION:

Prof. Dr. Michał Czakon
Prof. Dr. Robert Harlander
TBA
TBA

VORSITZENDER DER PRÜFUNGSKOMMISSION:

TBA

DATUM DER DISPUTATION:

TBA

DEKAN DER FAKULTÄT MIN:

Prof. Dr. Carsten Honerkamp

ABSTRACT

This is my Abstract

ZUSAMMENFASSUNG

Dies ist meine Zusammenfassung

ACKNOWLEDGMENTS

Here is where I thank god.

PUBLICATIONS

During my PhD studies, I co-authored the following publications:

[1] Michał Czakon, Felix Eschment, and Tom Schellenberger. "Revisiting the double-soft asymptotics of one-loop amplitudes in massless QCD." In: *JHEP* 04 (2023), p. 065. DOI: 10.1007/JHEP04(2023)065. arXiv: 2211.06465 [hep-ph]

[2] Michał Czakon, Felix Eschment, and Tom Schellenberger. "Subleading effects in soft-gluon emission at one-loop in massless QCD." In: *JHEP* 12 (2023), p. 126. DOI: 10.1007/JHEP12(2023)126. arXiv: 2307.02286 [hep-ph]

[3] Michał Czakon et al. "Top-Bottom Interference Contribution to Fully Inclusive Higgs Production." In: *Phys. Rev. Lett.* 132.21 (2024), p. 211902. DOI: 10.1103/PhysRevLett.132.211902. arXiv: 2312.09896 [hep-ph]

[4] Michał Czakon et al. "Quark mass effects in Higgs production." In: *JHEP* 10 (2024), p. 210. DOI: 10.1007/JHEP10(2024)210. arXiv: 2407.12413 [hep-ph]

Among these, only the last two are directly relevant to this dissertation.

CONTENTS

ACRONYMS

SM	Standard model
VEV	Vacuum expectation value
SSB	Spontaneous symmetry breaking
PDF	Parton distribution function
QCD	Quantum chromodynamics
QED	Quantum electrodynamics
RGE	Renormalization group equation
LO	Leading order
DR	Dimensional regularization
UV	Ultraviolet
IR	Infrared
LO	Leading order
NLO	Next-to-leading order
NNLO	Next-to-next-to-leading order
OS	On-shell renormalization
RG	Renormalization group
RGE	Renormalization group equation
LHC	Large hadron collider
FS	Flavor scheme
MC	Monte-Carlo
LME	Large mass expansion
HEL	High-energy limit
HTL	Heavy-top limit
rHTL	Rescaled heavy-top limit
SCET	Soft-collinear effective theory
IBP	Integration-by-parts

NOTATION, CONSTANTS AND CONVENTIONS

- In this thesis, I will be using the *Einstein summation convention*, by which any index—be it a Lorentz, color or flavor index—which appears twice is implicitly summed over.

- I will be using natural units

$$\hbar = c = 1. \tag{0.1}$$

- The electron charge is

$$-e, \quad e > 0. \tag{0.2}$$

- The metric is

$$g_{\mu\nu} = \begin{pmatrix} 1 & & & \\ & -1 & & \\ & & -1 & \\ & & & -1 \end{pmatrix}. \tag{0.3}$$

- The normalization of the Levi-Civita anti-symmetric tensor $\epsilon_{\mu\nu\rho\sigma}$ is

$$\epsilon_{0123} = +1 \tag{0.4}$$

- The Pauli matrices are defined as

$$\sigma^1 \equiv \begin{pmatrix} 0 & 1 \\ 1 & 0 \end{pmatrix}, \quad \sigma^2 = \begin{pmatrix} 0 & -i \\ i & 0 \end{pmatrix}, \quad \sigma^3 = \begin{pmatrix} 1 & 0 \\ 0 & -1 \end{pmatrix}, \quad \tau^i \equiv \sigma^i. \tag{0.5}$$

- Unless specifically specified otherwhise we will use the following values for appearing physical constants

    - $G_F = 1.16637 \times 10^{-5} \text{ GeV}^{-2}$

    - $m_H = 125.00 \text{ GeV}$

    - $m_t = 173.06 \text{ GeV}$

    - $\overline{m}_t(\overline{m}_t) = 162.7 \text{ GeV}$

    - $m_b = 4.78 \text{ GeV}$

    - $\overline{m}_b(\overline{m}_b) = 4.18 \text{ GeV}$

    - $\overline{m}_c(\overline{m}_c) = 1.27 \text{ GeV}$

    - $m_Z = 91.1876 \text{ GeV}$

- We use the `NNPDF31_nnlo_as_0118` and `NNPDF31_nnlo_as_0118_nf_4`PDF set in the 5FS and 4FS respectively.

- α_s is extracted from the PDF set at the Z^0 mass.

1 | INTRODUCTION

General introductions

2 | THE STANDARD MODEL OF PARTICLE PHYSICS

2.1 ELECTROWEAK SYMMETRY BREAKING

The standard model (SM) of particle physics is a theory describing all known matter and their fundamental interactions except for gravity. It unifies the electromagnetic, weak, and strong forces under a single theoretical framework. The matter content of the SM is classified into two primary groups: *fermions* and *bosons*. The fermions have spin 1/2, they are further subcategorized into *quarks* and *leptons*. Quarks participate in strong interactions, while leptons interact only via the electromagnetic and weak forces. In contrast, bosons have integer spin. There exists a single particle with spin 0, the *Higgs* boson, and four vector bosons, namely the gluon, the photon, and the W and Z boson. The vector bosons act as force carrier for the strong, the electromagnetic and the weak force respectively. Fermions are organized into three generations, with each generation containing two types of quarks (up-type and down-type) and two leptons (a charged lepton and its corresponding neutrino). These generations are shown in Fig. 2.1, along with their masses, charges, and spins.

The interactions between SM particles are described by a non-abelian gauge theory of the $\mathrm{SU}(3)_C \times \mathrm{SU}(2)_L \times \mathrm{U}(1)_Y$ group. Here $\mathrm{SU}(3)_C$ governs the strong interactions. It applies to all *colored* particles, i.e. quarks and gluons. The quarks transform under the fundamental representation of the $\mathrm{SU}(3)_C$ group. $\mathrm{SU}(2)_L \times \mathrm{U}(1)_Y$ governs electroweak interactions. The $\mathrm{SU}(2)_L$ transformation acts non-trivially only on *left-handed* fermions which form doublets

$$L_{iL} \equiv \begin{pmatrix} \nu_{iL} \\ l_{iL} \end{pmatrix}, \quad Q_{iL} \equiv \begin{pmatrix} u_{iL} \\ d_{iL} \end{pmatrix},$$

$$\nu_i = (\nu_e, \nu_\mu, \nu_\tau), \quad l_i = (e, \mu, \tau), \quad u_i = (u, c, t), \quad d_i = (d, s, b). \tag{2.1}$$

The phase transformation $\mathrm{U}(1)_Y$ acts on all particles except neutrinos according to their quantum number, the *hypercharge Y*. The symmetry is spontaneously broken to $\mathrm{SU}(3)_C \times \mathrm{U}(1)_Q$, where the $\mathrm{U}(1)_Q$ group corresponds to gauge transformation of the electromagnetic interaction, hence the subscript Q for the *electric charge*. To ensure that the particles have the correct charges, the hypercharge must satisfy the *Gell-Mann–Nishijima relation*:

$$\frac{Y}{2} = Q - I^3. \tag{2.2}$$

With the particle charges displayed in Fig. 2.1 we then get

	L_{iL}	Q_{iL}	ν_{iR}	l_{iR}	u_{iR}	d_{iR}
$\frac{Y}{2}$	$-\frac{1}{2}$	$\frac{1}{6}$	0	-1	$\frac{2}{3}$	$-\frac{1}{3}$

Figure 2.1: Elementary particles of the SM. The was image generated with the help of Ref. [5].

The transformation properties of the gauge bosons is dictated by the covariance of the covariant derivative

$$D_\mu \equiv \partial_\mu - ig A_\mu^a T_R^a - ig_2 W_\mu^a I^a + ig_Y \frac{Y}{2} B_\mu$$

$$T_R^a = \begin{cases} T^a & \text{for quarks,} \\ 0 & \text{for leptons,} \end{cases} \qquad I^a = \begin{cases} \frac{\tau}{2} & \text{for left-handed fermions,} \\ 0 & \text{for right-handed fermions,} \end{cases} \tag{2.3}$$

where T^a and τ^a are the *Gell-Mann* and *Pauli* matrices.

Before spontaneous symmetry breaking, the Lagrangian which governs the evolution of all matter fields must be invariant under the $\mathrm{SU(3)}_C \times \mathrm{SU(2)}_L \times \mathrm{U(1)}_Y$ gauge group. Up to a $\mathbb{CP}$ violating term[1] the SM Lagrangian is the most general mass-dimension four Lagrangian for the described particle content

$$\mathcal{L}_{\mathrm{SM}} = \mathcal{L}_G + \mathcal{L}_F + \mathcal{L}_Y + \mathcal{L}_H. \tag{2.4}$$

---

1 The absence of the $\mathbb{CP}$ violating term $\theta \frac{g^2}{64\pi^2} \epsilon^{\mu\nu\alpha\beta} F_{\mu\nu}^a F_{\alpha\beta}^a$ is an unsolved problem of particle physics, known as the strong CP problem.

The gauge-field Lagrangian $\mathcal{L}_G$ describes the free propagation and in the case of the non-abelian groups $SU(3)_C$ and $SU(2)_L$ also the self-interaction of the gauge bosons. It is given by

$$
\begin{aligned}
\mathcal{L}_G &= -\frac{1}{4}G^a_{\mu\nu}G^{a\,\mu\nu} - \frac{1}{4}W^a_{\mu\nu}W^{a\,\mu\nu} - \frac{1}{4}B_{\mu\nu}B^{\mu\nu}, \\
G^a_{\mu\nu} &\equiv \partial_\mu A^a_\nu - \partial_\nu A^a_\mu + g f^{abc}A^b_\mu A^c_\nu, \\
W^a_{\mu\nu} &\equiv \partial_\mu W^a_\nu - \partial_\nu W^a_\mu + g_2\epsilon^{abc}W^b_\mu W^c_\nu, \\
B_{\mu\nu} &\equiv \partial_\mu B_\nu - \partial_\nu B_\mu.
\end{aligned}
\tag{2.5}
$$

The propagation of the fermions and their interaction with the gauge bosons is described by

$$
\mathcal{L}_F = \bar{L}_{iL}i\slashed{D}L_{iL} + \bar{\nu}_{iR}i\slashed{D}\nu_{iR} + \bar{l}_{iR}i\slashed{D}l_{iR} + \bar{Q}_{iL}i\slashed{D}Q_{iL} + \bar{u}_{iR}i\slashed{D}u_{iR} + \bar{d}_{iR}i\slashed{D}d_{iR}.
\tag{2.6}
$$

The Higgs field is a doublet of the $SU(2)_L$ group. We want the field to have a non-vanishing vacuum expectation value (VEV) to dynamically generate the fermion and boson masses. Of course, the vacuum cannot carry an electric charge, which means that the Higgs field must be electrically neutral along the direction of *spontaneous symmetry breaking* (SSB). We choose this to be the second component of the doublet. With the Gell-Mann–Nishijima relation we can then deduce that hypercharge of the doublet must be $Y = +1$. The Higgs doublet field thus takes the form

$$
\Phi = \begin{pmatrix} \phi^+ \\ \phi^0 \end{pmatrix},
\tag{2.7}
$$

where the superscript indicates the electic charge.

In order to generate a non-vanishing VEV, the Higgs field must be in a potential with a global minimum away from zero. Hence, the only gauge invariant mass-dimension four Lagrangian we can construct is

$$
\begin{aligned}
\mathcal{L}_H &= (D_\mu\Phi)^\dagger (D^\mu\Phi) - V(\Phi) \\
V(\Phi) &= \lambda(\Phi^\dagger\Phi)^2 - \mu^2\Phi^\dagger\Phi, \quad \mu^2, \lambda > 0.
\end{aligned}
\tag{2.8}
$$

The minimum of the Higgs potential V is at

$$
\Phi^\dagger_0\Phi_0 = \frac{\mu^2}{2\lambda} \equiv \frac{v^2}{2} \neq 0.
\tag{2.9}
$$

After (SSB) we can expand the Higgs field around its minimum

$$
\Phi = \begin{pmatrix} \phi^+ \\ \frac{1}{\sqrt{2}}(v + H + i\xi). \end{pmatrix}
\tag{2.10}
$$

The real scalar field H is the famous Higgs boson, whereas the fields $\phi^\pm$ and ξ are unphysical since they can always be eliminated through a gauge transformation (*would-be Goldstone bosons*). After inserting the expansion in the Higgs Lagrangian, the mass of the Higgs can be read off from its square term

$$
m_H = \sqrt{2}\mu.
\tag{2.11}
$$

SSB enables the generation of vector boson masses without breaking the gauge symmetry explicitly. If we insert the expanded Higgs field in the Higgs Lagrangian, we get quadratic terms of the gauge boson fields

$$
\begin{aligned}
\mathcal{L}_H &\supsetneq \frac{v^2}{2}\left\{ g_2^2 \begin{pmatrix} 0 & 1 \end{pmatrix} I^a I^b \begin{pmatrix} 0 \\ 1 \end{pmatrix} W_\mu^a W^{b\,\mu} - g_2 g_Y \begin{pmatrix} 0 & 1 \end{pmatrix} I^a \begin{pmatrix} 0 \\ 1 \end{pmatrix} W_\mu^a B^\mu + \frac{g_Y^2}{4} B_\mu B^\mu \right\} \\
&= \frac{v^2}{2}\left\{ \frac{g_2^2}{4}\left[(W^1)^2 + (W^2)^2 \right] + \frac{1}{4} \begin{pmatrix} B^\mu & W^{3\,\mu} \end{pmatrix} \begin{pmatrix} g_Y^2 & g_Y g_2 \\ g_Y g_2 & g_2^2 \end{pmatrix} \begin{pmatrix} B_\mu \\ W_\mu^3 \end{pmatrix} \right\}.
\end{aligned}
\tag{2.12}
$$

By diagonalizing the mass matrix we obtain the physical states

$$
\begin{pmatrix} A_\mu^\gamma \\ Z_\mu \end{pmatrix} = \begin{pmatrix} \cos\theta_W & -\sin\theta_W \\ \sin\theta_W & \cos\theta_W \end{pmatrix} \begin{pmatrix} B_\mu \\ W_\mu^3 \end{pmatrix}, \quad \cos\theta_W = \frac{g_2}{\sqrt{g_Y^2 + g_2^2}}, \sin\theta_W = \frac{g_Y}{\sqrt{g_Y^2 + g_2^2}}. \tag{2.13}
$$

In this new basis, we have one massless boson A_μ^γ, which we identify as the photon and a charge neutral boson of mass

$$
m_Z = \frac{v}{2}\sqrt{g_Y^2 + g_2^2}. \tag{2.14}
$$

The vector bosons W^1 and W^2 are not eigenstates of the charge operator. We therefore define the new states

$$
W_\mu^\pm = \frac{1}{\sqrt{2}}\left(W_\mu^1 \mp i W_\mu^2 \right), \qquad Q W_\mu^\pm = \pm W_\mu^\pm, \tag{2.15}
$$

which are eigenstates of Q and have mass

$$
m_W = \frac{v}{2} g_2. \tag{2.16}
$$

Last but not least, we discuss the Yukawa sector of the SM Lagrangian. Before SSB, fermions cannot generate masses because a mass term would mix the left- and right-handed components of the fields, thereby breaking the chiral gauge symmetry. Here, once again, the Higgs field comes to the rescue: by coupling the fermions with the Higgs field through a Yukawa interaction[2]

$$
\mathcal{L}_Y = -\left(y_{ij}^\nu \bar{L}_{iL} \Phi^c \nu_{jR} + y_{ij}^l \bar{L}_{iL} \Phi l_{jR} + y_{ij}^d \bar{Q}_{iL} \Phi d_{jR} + y_{ij}^u \bar{Q}_{iL} \Phi^c u_{jR} \right) + \text{h.c.}, \tag{2.17}
$$

where Φ^c is the charge-conjugated field to Φ, we do not explicitly break the symmetry. However, after SSB this Lagrangian will generate exactly the required mixing between left- and right-handed fields to generate the fermion masses. The Yukawa-interaction matrices $y_{ij}^{\nu,l,d,u}$ can be shifted from the Yukawa sector to the fermion sector through a field redefinition. Indeed, if we apply the *singular value decomposition* of the Yukawa matrix

$$
y = U_L^\dagger y_{\text{diag}} U_R, \quad \text{with} \quad (y_{\text{diag}})_{ij} = \sqrt{2} Y_i \delta_{ij} \quad \text{and} \quad U_{L,R} \in \mathrm{U}(3), \tag{2.18}
$$

and redefine our fermion fields to be

$$
f_{iR} \longrightarrow U_{Rij} f_{jR}, \qquad f_{iL} \longrightarrow U_{Lij} f_{jL}, \qquad f = \nu, l, u, d \tag{2.19}
$$

the Yukawa Lagrangian becomes

$$
\mathcal{L}_Y = -\sum_i \left(m_{\nu_i} \bar{\nu}_i \nu_i + m_{l_i} \bar{l}_i l_i + m_{u_i} \bar{u}_i u_i + m_{d_i} \bar{d}_i d_i \right)\left(1 + \frac{H}{v} \right). \tag{2.20}
$$

---

2 In the original formulation of the SM, there are no neutrino Yukawa interactions, since they were believed to be massless. Neutrino oscillation experiments have shown however, that neutrinos do in fact have finite masses.

Here we identified the Yukawa coupling as $Y_i = m_i/v$ in order to generate the required mass terms. Consequently, we observe that the Yukawa coupling of the Higgs to the fermions is proportional to the mass of that fermion. The field redefinition is a change from a flavor eigenbasis, which is diagonal in the couplings to the gauge bosons, to a mass eigenbasis. In the mass eigenbasis the part of fermion Lagrangian which contains the interaction to the electroweak gauge bosons after SSB is

$$
\begin{aligned}
\mathcal{L}_F \supsetneq &\sum_f (-Q_f)e\bar{f}_i \slashed{A}^\gamma f_i + \sum_f \frac{e}{\sin\theta_W \cos\theta_W} \bar{f}_i(I_f^3 \gamma^\mu P_L - \sin^2\theta_W Q_f \gamma^\mu) f_i Z_\mu \\
&+ \frac{e}{\sqrt{2}\sin\theta_W} \left(\bar{u}_i \gamma^\mu P_L (V_{\text{CKM}})_{ij} d_j W_\mu^+ + \bar{d}_i \gamma^\mu P_L (V_{\text{CKM}}^\dagger)_{ij} u_j W_\mu^- \right) \\
&+ \frac{e}{\sqrt{2}\sin\theta_W} \left(\bar{\nu}_i \gamma^\mu P_L (V_{\text{PMNS}}^\dagger)_{ij} l_j W_\mu^+ + \bar{l}_i \gamma^\mu P_L (V_{\text{PMNS}})_{ij} v_j W_\mu^- \right).
\end{aligned}
\tag{2.21}
$$

Here we identified the electromagnetic coupling constant

$$
e = \frac{g_2 g_Y}{\sqrt{g_2^2 + g_Y^2}},
\tag{2.22}
$$

as the factor in front of the photon interaction term. The operators $P_{L,R}$ are just the projectors onto the left- and right-handed components

$$
P_{L,R} = \frac{1 \mp \gamma^5}{2}.
\tag{2.23}
$$

The *CKM* and *PMNS matrices*[3] are the results of the field redefinitions

$$
V_{\text{CKM}} \equiv U_L^{u\dagger} U_L^d, \qquad V_{\text{PMNS}} \equiv U_L^{l\,\dagger} U_L^\nu.
\tag{2.24}
$$

Typically, one prefers to work in the mass eigenbasis of the quarks, while the neutrinos are kept in the flavor eigenbasis, in which case one encounters flavor changes (*neutrino oscillations*) through propagation. This is why the PMNS matrix is defined in terms of the complex conjugate of the CKM matrix equivalent in the lepton sector.

2.2 CROSS SECTIONS

Cross sections offer the possibility to directly test the SM and many of the great successes of the SM are its *cross section* predictions. The cross section is simply defined as the probability to create some final state from some initial state per unit of time per target particle normalized by the incoming particle flux. This definition allows for straightforward measurement through counting experiments. For instance, experiments like `CMS` and `ATLAS` collide particles and count how often a particular final state is produced within a given time interval.

From a theoretical perspective, cross sections can be calculated using

$$
d\hat{\sigma}_{ij \to n} = \frac{1}{F} d\Phi_n |M_{ij \to n}|^2,
\tag{2.25}
$$

where F denotes the *flux factor*[4]

$$
F \equiv 4 p_1 \cdot p_2,
\tag{2.26}
$$

---

3 Named after Cabibbo, Kobayashi and Maskawa, and Pontecorvo, Maki, Nakagawa and Sakata.
4 In the following we assume that the initial state particles are massless.

$\mathrm{d}\Phi_n$ is the *Lorentz invariant phase space measure*

$$\mathrm{d}\Phi_n = \left[\prod_{i=1}^{n} \frac{\mathrm{d}^4 q_i}{(2\pi)^4} (2\pi)\delta(q_i^2 - m_i^2)\Theta(q_i^0) \right] (2\pi)^4 \delta^{(4)}\left(p_1 + p_2 - \sum_{i=1}^{n} q_i \right), \qquad (2.27)$$

and M_{fi} is the *scattering amplitude* describing the short distance interactions.

The computation of cross sections involves three basic steps:

1. Calculation of the hard scattering amplitude,

2. Phase-space integration,

3. And the convolution with *parton distribution functions* (PDFs).

We will discuss each step in detail below.

2.2.1 The Hard Scattering Amplitude

The Hard Scattering Amplitude describes the transition probability from a specific initial state to a particular finial state. Since the scattering is **hard**, it implies that the energy transfer between particles during scattering is large compared to the QCD scale. Thus, we operate within the perturbative regime of QCD and can perform an expansion in terms of the coupling constant

$$M_{ij\to n} = \alpha_s^{n_{\mathrm{Born}}} \left(M_{ij\to n}^{(0)} + \frac{\alpha_s}{\pi} M_{ij\to n}^{(1)} + \left(\frac{\alpha_s}{\pi} \right)^2 M_{ij\to n}^{(2)} + \mathcal{O}\big(\alpha_s^3\big) \right). \qquad (2.28)$$

Here, n_{Born} denotes the power of the coupling constant at *leading order* (LO). The coefficients in this series can be computed graphically using *Feynman rules*. These are the set of all allowed propagators and vertices together with the corresponding mathematical prescription. The Feynman rules for the complete SM are listed in Appendix A. To calculate the coefficient $M_{ij\to n}^{(l)}$ for a specific process, one has to draw all possible connected and amputated Feynman diagrams with the initial state (i,j) and final state n, that contain $2(n_{\mathrm{Born}} + l)$ vertices[5]. Then one uses the Feynman rules to get the mathematical translation, keeping in mind that momentum must be conserved at every vertex and also taking into account possible symmetry factors.

Starting from $M_{ij\to n}^{(1)}$, but for some processes, called *loop induced processes*, even from $M_{ij\to n}^{(0)}$, we will encounter loops in the diagrams. Inside a loop, the momentum of the edges cannot be uniquely determined through momentum conservation. Consequently, we must leave momentum unspecified and integrate over all possible values. Typically, it is the computation of these *loop integrals* that makes the calculation of hard scattering amplitudes so challenging. A plethora of powerful techniques has been developed over the years to tackle this daunting task. Still, the computation of loop integrals remains a highly active field of research and two-loop amplitudes with 5 or more scales are only just becoming available. A detailed description of modern techniques is beyond the scope of this thesis. For a comprehensive overview see Ref. [6].

Loop integrals are notorious for exhibiting divergences. To tame these, we introduce *regulators*, i.e. we introduce a parameter, such that the integral becomes function of that parameter with a singularity at the physical value. The most commonly used regularization scheme is

---

5 Quartic vertices are counted twice.

dimensional regularization (DR), here we make the loop-integral a function of the dimension by replacing

$$\int \frac{\mathrm{d}^4 k}{(2\pi)^4} \left(\cdots\right) \longrightarrow \bar{\mu}^{2\epsilon} \int \frac{\mathrm{d}^d k}{(2\pi)^d} \left(\cdots\right), \quad d \equiv 4 - 2\epsilon \in \mathbb{C}, \quad \gamma_E = 0.5772\ldots. \tag{2.29}$$

The dimensionally regularized integral satisfies the usual integral properties like linearity, translation invariance and rescaling. The mass scale,

$$\bar{\mu}^2 = \frac{\mu^2}{4\pi} e^{\gamma_E} \tag{2.30}$$

was introduced to retain the mass dimension of the measure to 4, while absorbing some common factors of loop integrals. The physical limit then corresponds to $\epsilon \to 0$. A divergent integral in four dimensions will hence have ϵ-poles in DR. The poles are categorized as *ultraviolet* poles if their origin are large loop momenta, i.e. the four dimensional integral diverges for $k \to \infty$. Further we categorize poles as *infrared* poles if the singularity arises from loop momenta which are either soft $(k \to 0)$ or *collinear* $(k \cdot p_i \to 0)$ to one of the external massless legs. UV and IR singularities are mutually exclusive since they originate from different regions of the phase space. This means that the poles do not multiply together, and we may only get a single UV pole per loop integration. The soft and collinear singularities are **not** exclusive, meaning that IR singularities can develop one double pole per loop integration.

The IR singularities cancel for inclusive observables as we shall discuss in detail in section 2.2.3. UV poles on the other hand, are removed through a method called *renormalization*. Renormalization hinges on the idea, that the fields, constants and masses we observe in nature are not necessarily the same as the one in our Lagrangian. Instead, they are related through a *renormalization constant*

$$\begin{aligned}
W_\mu^{B,a} &= \left(Z_3^W\right)^{1/2} W_\mu^{R,a} \\
B_\mu^B &= \left(Z_3^Z\right)^{1/2} B_\mu^R \\
A_\mu^{B,a} &= \left(Z_3^A\right)^{1/2} A_\mu^{R,a} \\
\Phi^B &= \left(Z^\Phi\right)^{1/2} \Phi^R \\
Q_{iL}^B &= \left(Z_{2i}^L\right)^{1/2} Q_{iL}^R \\
u_{iR}^{B,a} &= \left(Z_{2i}^{u,R}\right)^{1/2} u_{iR}^{B,a} \\
d_{iR}^{B,a} &= \left(Z_{2i}^{d,R}\right)^{1/2} d_{iR}^{B,a} \\
g^B &= Z_g g^R \\
g_Y^B &= Z_Y g_Y^R \\
g_2^B &= Z_2 g_2^R \\
\left(\mu^2\right)^B &= Z_\mu \left(\mu^2\right)^R \\
\lambda^B &= Z_\lambda \lambda^R \\
y_{ij}^{d,B} &= Z_{y,ij}^d y_{ij}^{d,R} \\
y_{ij}^{u,B} &= Z_{y,ij}^u y_{ij}^{u,R}
\end{aligned} \tag{2.31}$$

In these equations B refers to *bare* quantities appearing within our Lagrangian while R signifies renormalized quantities that are finite by definition. In the SM, it can be shown [7, 8] that we can choose renormalization constants, such that *Green's functions*, i.e. vacuum expectation values of time ordered products of local renormalized fields, are free of UV divergences. Scattering amplitudes, generally do not depend on the unphysical fields, which is why the fields can be kept unrenormalized in this case. Since at LO Green's functions do not require renormalization, all renormalization constants are equal to the identity at this order.

The definition of the renormalization constants is not unique. Indeed, the renormalization constants were designed to absorb singularities, but the finite part is a priori unconstrained. We call a prescription which uniquely determines the renormalization constants a *renormalization scheme*. The most widely used renormalization scheme is the $\overline{\text{MS}}$ scheme. Here, beyond the leading 1 and a universal factor of $\bar{\mu}^{\epsilon\rho_i}$, the renormalization constants **only** consist of poles, i.e. the renormalization constants have the structure

$$Z_i(\alpha) = \bar{\mu}^{\epsilon\rho_i}\left(1 + \frac{z_1}{\epsilon}\frac{\alpha}{4\pi} + \left(\frac{z_{22}}{\epsilon^2} + \frac{z_{21}}{\epsilon}\right)\left(\frac{\alpha}{4\pi}\right)^2 + \dots\right). \tag{2.32}$$

ρ_i is the mass dimension of the operator in units of ϵ, so that the factor $\bar{\mu}^{\epsilon\rho_i}$ corrects for the mismatch in mass dimensions between the four-dimensional renormalized and the d-dimensional bare quantities. For example: the coupling constant g^B has mass dimension ϵ, hence the renormalized coupling g^R has mass dimension zero and $\rho_i = 1$.

$\overline{\text{MS}}$-renormalized masses are generally different from the pole mass. The *on-shell renormalization* (OS) scheme, is an alternative to the $\overline{\text{MS}}$ scheme specifically designed, such that the renormalized mass matches the pole mass. It is therefore the suitable choice for external particles that are asymptotically free. Bare quantities are independent of the chosen renormalization scheme. The invariance under the change of the renormalization scheme defines a group, the *renormalization group* (RG). In the $\overline{\text{MS}}$ scheme, the change from one scale $\bar{\mu}$ to another defines a continuous subgroup of the RG. This means we can formulate the invariance in terms of a differential equation

$$0 = \frac{\mathrm{d}}{\mathrm{d}\log\mu}a^B = a^R\frac{\mathrm{d}Z_a^{\overline{\text{MS}}}}{\mathrm{d}\log\mu} + Z_a^{\overline{\text{MS}}}\frac{\mathrm{d}a^R}{\mathrm{d}\log\mu}, \tag{2.33}$$

where a could be a mass or a coupling. Eq. (2.33) is called the *renormalization group equation* (RGE) and it can be leveraged to determine the scale dependence, also called the *running*, of the observable.

The final step in calculating the hard scattering amplitude involves the application of the *Lehmann-Symanzik-Zimmermann* (LSZ) reduction formula. It relates the scattering amplitudes to Green's functions, and it is the reason why we only considered amputated Feynman diagrams. In practice, one just has to multiply each external field with the square root of the corresponding LSZ constant. These constants are defined as the proportionality factor between the propagator of the interacting and the free theory[6]. As such, they are numerically identical to the OS field renormalization constants.

---

6 The interacting field theory might have an additional continuous spectrum.

2.2.2 The Parton Distribution Functions

In hadron collisions, the initial state is not made up of elementary particles, but are bound states thereof. This means that during an inelastic scattering event, the partons which take part in the short-range interaction only carry a fraction of the original hadron momentum

$$p_1 = x_1 P_1, \qquad p_2 = x_2 P_2. \tag{2.34}$$

Here p_1 and p_2 denote the momenta of the partons and P_1 and P_2 are the momenta of the hadrons. Since the momentum of the parton can not be larger than that of the hadron, $x_{1,2}$ is restricted to be less than one. Furthermore, since the energy of the parton must be positive the momentum fraction must also be positive. Otherwise, the momentum fraction is a priori unconstrained, we therefore integrate over all allowed values of x_1 and x_2

$$\begin{aligned}
\mathrm{d}\sigma_{H_1 H_2 \to n}(S) &= \int_0^1 \mathrm{d}x_1 \mathrm{d}x_2 \, f_{H_1,i}(x_1) f_{H_2,j}(x_2) \mathrm{d}\hat{\sigma}_{ij \to n}(x_1 P_1, x_2 P_2, \mu_R) \\
&= \int_0^1 \frac{\mathrm{d}\tau}{\tau} \mathcal{L}_{ij}(\tau) \mathrm{d}\hat{\sigma}_{ij \to n}(\tau S, \mu_R)
\end{aligned} \tag{2.35}$$

where $S = 2P_1 \cdot P_2$ is hadronic center of mass energy. $f_{H_k,i}(x_k)$ are the (unrenormalized) *parton distribution functions* (PDFs). They describe the probability of finding a parton i with momentum fraction x_k inside the hadron H_k. Lorentz invariance of the partonic cross section allowed us to conclude that it can only depend on the partonic center of mass energy $\hat{s}$

$$\mathrm{d}\hat{\sigma}_{ij \to n}(x_1 P_1, x_2 P_2, \mu_R) = \mathrm{d}\hat{\sigma}_{ij \to n}(x_1 x_2 S, \mu_R). \tag{2.36}$$

We then defined the *partonic luminosity*

$$\mathcal{L}_{ij}(\tau) \equiv (\tilde{f}_{H_1,i} \otimes \tilde{f}_{H_2,j})(\tau) \equiv \int_0^1 \mathrm{d}x_1 \mathrm{d}x_2 \, \tilde{f}_{H_1,i}(x_1) \tilde{f}_{H_2,j}(x_2) \delta(\tau - x_1 x_2), \tag{2.37}$$

where $\tilde{f}_{H,i}(x) \equiv x f_{H,i}(x)$, to arrive at the second line of Eq. (2.35).

At this stage the partonic cross section can still exhibit singularities whenever a finial state parton becomes collinear to one of the initial state partons. At LO for example, the divergence due to initial-state collinear emissions reads

$$\mathrm{d}\hat{\sigma}_{ab \to cX}(s, \mu_R)\Big|_{\mathrm{div.}} = -\frac{\alpha_s}{2\pi} \frac{1}{\epsilon} \int_0^1 \mathrm{d}z \, \left(P_{db}^{(0)}(z) \mathrm{d}\hat{\sigma}_{ad \to X}(zs, \mu_R) + P_{da}^{(0)}(z) \hat{\sigma}_{db \to X}(zs, \mu_R) \right), \tag{2.38}$$

where $P_{ij}^{(0)}$ are the LO *Altarelli-Parisi splitting kernels*[7]:

$$\begin{aligned}
P_{qq}^{(0)}(x) &= C_F \left[\frac{1 + x^2}{(1-x)_+} + \frac{3}{2} \delta(1-x) \right], \\
P_{qg}^{(0)}(x) &= T_F \left[x^2 + (1-x)^2 \right], \\
P_{gq}^{(0)}(x) &= C_F \left[\frac{1 + (1-x)^2}{x} \right], \\
P_{gg}^{(0)}(x) &= 2 C_A \left[\frac{x}{(1-x)_+} + \frac{1-x}{x} + x(1-x) \right] + \delta(1-x) \frac{\beta_0}{2}.
\end{aligned} \tag{2.39}$$

---

[7] The definition of β_0 can be found in Eq. (4.49)

We absorb these collinear singularities into the PDFs through a process called *collinear renormalization*, by defining the renormalized PDFs $f_{H,i}(x, \mu_F)$ via

$$f_{H,i}(x) \equiv (Z_{ij}(\cdot, \mu_F) \otimes f_{H,j}(\cdot, \mu_F))(x). \tag{2.40}$$

Beyond the pole term, the renormalization constants are generally scheme dependent. From Eq. (2.38) we see that the $\overline{\text{MS}}$ renormalization constant at NLO are given by

$$Z_{ij}(z, \mu_R, \mu_F) = \delta(1-z)\delta_{ij} + \frac{\alpha_s}{2\pi}\frac{1}{\epsilon}P_{ij}^{(0)}(z) + \mathcal{O}(\alpha_s^2). \tag{2.41}$$

Now the sum

$$\mathrm{d}\sigma_{H_1 H_2 \to cX} + \mathrm{d}\sigma_{H_1 H_2 \to X} \tag{2.42}$$

is guaranteed to be free initial-state collinear divergences.

Since the initial state collinear divergences are of a completely different origin than the UV divergences, we introduce a new scale μ_F, called the factorization scale. This scale separates the long-distance (non-perturbative) physics, contained in the PDFs, from the short-distance (perturbative) physics, contained in the partonic cross sections.

Figure 2.2: The various PDFs multiplied by x as a function of x. The plot was created using the LHAPDF6 [9] interface to the NNPDF31_nnlo_as_0118 [10] PDF set at a scale of $\mu_F = m_H/2$.

Figure 2.3: Displayed is the partonic luminosity for combinations of various partons. The luminosities are defined as $\mathcal{L}_{qg} = 2\times\sum_i(\mathcal{L}_{q_i g}+\mathcal{L}_{\bar{q}_i g})$, $\mathcal{L}_{q\bar{q}} = 2\times\sum_i \mathcal{L}_{q_i \bar{q}_i}$, $\mathcal{L}_{qq'} = \sum_{i,j}(\mathcal{L}_{q_i q_j}+\mathcal{L}_{q_i \bar{q}_j}+\mathcal{L}_{\bar{q}_i \bar{q}_j})-\mathcal{L}_{q\bar{q}}$. The setup is the same as in Fig. 2.2.

The factorization theorem (2.35) is central in the SM as it tells us that the PDFs are universal quantities, i.e. they are not specific to any one process. It is a postulate of the parton model, in which hadrons are thought of as collection of the free elementary particles. In QCD however, the

theorem requires proof [11]! The PDF for all light partons are displayed in Fig. 2.2. In Fig. 2.3 we show the partonic luminosity for exemplary parton combinations. PDFs describe long range interactions, a regime in which QCD is non-perturbative. As such, PDFs are non-perturbative objects which have to be measured in experiments or be calculated non-pertubatively, e.g. on the lattice.

The factorization scale in unphysical in the sense that it is not a parameter in our theory, nor can it be measured in an experiment. As usual we can apply the RGE to determine the running of the renormalized PDFs

$$0 = \frac{\mathrm{d}}{\mathrm{d}\ln\mu_F} f_{H,i}(x) = \frac{\mathrm{d}}{\mathrm{d}\ln\mu_F}(Z_{ij} \otimes f_{H,j}(\cdot,\mu_F))(x). \tag{2.43}$$

This can be rewritten to

$$\begin{aligned} \frac{\mathrm{d}f_{H,i}(x,\mu_F)}{\mathrm{d}\ln\mu_F} &= 2\alpha_s \left(Z_{ij}^{-1} \otimes \frac{\mathrm{d}Z_{jk}^{(1)}}{\mathrm{d}\alpha_s} \otimes f_{H,k}(\cdot,\mu_F) \right)(x,\mu_F) \\ &= \frac{\alpha_s}{\pi} \left(P_{ij}^{(0)} \otimes f_{H,j}(\cdot,\mu_F) \right)(x) + \mathcal{O}(\alpha_s^2), \end{aligned} \tag{2.44}$$

where $Z_{ij}^{(1)}$ is the residue of the renormalization constant. So even though the PDFs are non-perturbative, their dependence on the factorization scale is. Eq. (2.44) is the famous *Dokshitzter-Gribow-Lipatow-Altarelli-Parisi-evolution equation* (DGLAP equations) [12, 13, 14].

In the derivation above, we have treated the partons inside the hadrons as massless, which leads to real collinear singularities. In reality, all quarks have finite masses, so the phase-space integration only yields logarithmic mass enhancements of the form $\ln(\hat{s}/m_q^2)$ instead of actual singularities. The DGLAP equations then automatically resum these logarithms. For most applications at the LHC, the typical hard scattering scale is orders of magnitudes larger than all quark masses except for the top quark mass. It is therefore beneficial to treat them as massless partons, as the appearance of the large logarithms would otherwise completely destroy the perturbative convergence. However, treating quarks as massless also implies that we neglect their mass-dependent effects in the hard-scattering matrix elements. If the scattering process is sensitive to the quark masses—for example, in processes involving Higgs couplings to quarks—these mass effects might be lost.

The number of quark flavors treated as active (massless) partons defines our *flavor scheme* (FS). For instance, if we treat the lightest four flavors (up, down, strange, charm) as massless, while considering the bottom and top quarks as massive, we are working in the 4FS. Analogously, if the bottom quark is also considered massless, we are working in the 5FS, and so on.

2.2.3 The Phase-Space Integration

Even after renormalization and collinear renormalization can the amplitude exhibit divergences. The scatting amplitude in and of itself is not a physical observable; therefore, it is not required to be finite. Physical observables are cross sections, which are obtained by performing phase-space integrations over the squared amplitudes. However, even after integrating over the phase space, the cross section is not guaranteed to be finite. The reason is that the Born process is indistinguishable from processes with additional infrared radiation. Indeed, no

matter how precise a detector is, below a certain resolution, it becomes impossible to detect a very soft photon or to distinguish two highly collinear jets. Hence, computing a cross section with a fixed final state does not make physical sense. Instead, one must consider sufficiently inclusive observables—so called *IR-safe observables*. For these, Kinoshita, Lee and Nauenberg proved that in unitary theories all IR singularities cancel [15, 16]. This is known as the Kinoshita-Lee-Nauenberg (KLN) theorem.

An example of an observable which is trivially IR safe is the fully inclusive cross section

$$\hat{\sigma}_{ij \to n+X} = \sum_{k=1}^{\infty} \hat{\sigma}_{ij \to n+k}, \quad \text{for} \quad \hat{\sigma}_{ij \to n}^{(0)} \quad \text{finite}, \tag{2.45}$$

where $n + k$ indicates that in addition to the final state n we now have k massless partons of whatever flavor. In perturbation theory, the infinite sum is truncated at a given order and at each order

$$\hat{\sigma}_{ij \to n+X}^{(l)} = \sum_{k=0}^{l} \hat{\sigma}_{ij \to n+k}^{(l-k)}, \tag{2.46}$$

summed together with the contribution from collinear renormalization will be finite. For example at NLO, the finite inclusive cross section reads

$$\hat{\sigma}_{ij \to n+X}^{(1)} = \hat{\sigma}_{ij \to n}^{R} + \hat{\sigma}_{ij \to n}^{V} + \hat{\sigma}_{ij \to n}^{C}, \tag{2.47}$$

where

$$\hat{\sigma}_{ij \to n}^{R} = \frac{1}{F} \int \mathrm{d}\Phi_{n+1} \sum_{c} |M_{ij \to n+c}^{(0)}|^2 \tag{2.48}$$

is the real correction,

$$\hat{\sigma}_{ij \to n}^{V} = \frac{1}{F} \int \mathrm{d}\Phi_{n} \, 2\mathrm{Re} \left(\left(M_{ij \to n}^{(0)} \right)^* M_{ij \to n}^{(1)} \right) \tag{2.49}$$

is the virtual correction, and

$$\hat{\sigma}_{ij \to n}^{C} = \frac{1}{F} \int \mathrm{d}\Phi_{n} \frac{\alpha_s}{2\pi} \frac{1}{\epsilon} \left(\frac{\mu_R^2}{\mu_F^2} \right)^{\epsilon} \sum_{c} \int_0^1 \mathrm{d}z \left[P_{ci}^{(0)}(z)|M_{cj \to n}^{(0)}|^2 + P_{cj}^{(0)}(z)|M_{ic \to n}^{(0)}|^2 \right] \tag{2.50}$$

are the corrections from collinear renormalization. Figure 2.4 provides a pictorial representation of the required partonic cross sections for Higgs boson production in the gluon fusion channel at various perturbative orders.

Although the sum of the contributions to the cross section is guaranteed to be finite due to the KLN theorem, the presence of IR singularities in individual terms poses significant challenges for practical calculations. These singularities prevent a straightforward evaluation of the phase-space integrals. To overcome this, we once again have to introduce regulators (such as dimensional regularization) to make the integrals well-defined. Over the years, numerous techniques have been developed to compute phase-space integrals efficiently. These techniques can generally be categorized into two main types: *Analytic methods*, and *numerical methods*.

As the name suggests, in the former class, the phase-space integrals are solved analytically. One noteworthy member of this class is the *reverse-unitarity method* [17], which was first applied to Higgs production in the gluon fusion channel. The method uses unitarity, to rewrite the phase-space integrals in terms of loop integrals over cut-propagators. One can then apply the remarkable techniques developed for Feynman integrals to these phase-space integrals and

Figure 2.4: Pictorial representation of the needed partonic cross sections at various perturbative orders of the fully inclusive hadronic cross section. The graphic shows the example of Higgs production in the gluon fusion channel.

solve them analytically. The mayor downside of this approach is that it is highly process and observable dependent, meaning that for every process and every observable we have to start over from scratch. Furthermore, by the very nature of the method, you are always restricted to inclusive jet observables. Nevertheless, it has been successfully applied to, among others, Higgs-rapidity and Higgs-p_T distributions [18].

Among the numerical methods, there are two mayor approaches: *slicing* and *subtraction methods*. The former rely on a variable that isolates the IR-sensitive region of the phase space. Consider once again the example of Higgs production. Here, the IR-sensitive region of the phase space corresponds to configurations where the transverse momentum of the Higgs boson, p_T, approaches zero. The phase-space integral can then be decomposed into

$$\int_0^{p_T} \mathrm{d}k_T \, \mathrm{d}\hat{\sigma}_{ij \to H+c} = \int_0^{p_T^{\text{cut}}} \mathrm{d}k_T \, \mathrm{d}\hat{\sigma}_{ij \to H+c} + \int_{p_T^{\text{cut}}}^{p_T} \mathrm{d}k_T \, \mathrm{d}\hat{\sigma}_{ij \to H+c}. \tag{2.51}$$

The first integral on the right-hand side is now finite and can be computed numerically, e.g. using *Monte-Carlo* (MC) techniques. If we choose p_T^{Cut} small enough, then we can approximate the integrand in the second integral, by its IR limit and solve the integral analytically. The pole of the integral should then cancel against the poles in the virtual integration and the counter term from collinear renormalization. The mayor advantage of this method is its simplicity. One big downside is its dependence on the unphysical cutoff scale. Ideally it is chosen very small, such that the approximation introduces little to no error. But if chosen too small, the

integrations will have huge logarithmic enhancements which can easily spoil the numerical precision. Another disadvantage is that not all processes or observables have easily identifiable slicing variables, or the analytic integration is very challenging. For example, p_T slicing only works for color singlet production, indeed if we have a jet in the final state, we can encounter collinear divergences also at finite transverse momenta of the jet. For processes involving jets, a possible slicing variable is the N-jettiness

$$\mathcal{T}_N \equiv \sum_k \min_i \left\{ \frac{2p_i \cdot q_k}{Q_i} \right\}, \tag{2.52}$$

with N, the number of jets, q_k, the momenta of the unresolved partons, p_i, the momenta of the resolved jets, and Q_i a normalization factor which can for example be set to the jet energy. However, the analytic integration becomes highly non-trivial and is a matter of active research. Currently, the N-jettiness beam functions are known at N^{3}LO [19], the 0-jettiness soft function is known at N^{3}LO [20, 21] and NNLO 1-jettiness soft functions and jet functions are also known [22, 23, 24, 25].

Subtraction methods on the other hand, work by subtracting the infrared limits at the integrand level. In the *Frixione-Kunszt-Signer subtraction scheme* (FKS subtraction scheme) one first isolates the IR divergence by partitioning the phase space into *sectors* using *selector functions*. These functions isolate specific infrared limits by approaching unity when a particular limit is approached (e.g., when an unresolved parton becomes soft or collinear) and vanish in other limits. For a single unresolved parton, a possible selector function is

$$\mathcal{S}_{n+1,k} \equiv \frac{1}{d_{n+1,k}} \left(\sum_k \frac{1}{d_{n+1,k}} \right)^{-1}, \quad \text{where} \quad d_{n+1,k} \equiv \left(\frac{E_{n+1}}{\sqrt{\hat{s}}} \right)^\alpha (1 - \cos\theta_{n+1,k})^\beta. \tag{2.53}$$

The first index $n+1$ is the index of the unresolved parton, while the second index is the index of the reference parton. E_{n+1} denotes the energy of the unresolved parton, this factor is therefore to identify soft singularities. Consequently, the power α can be set to zero if the unresolved parton is a quark. Other than that, the powers must be strictly positive $\alpha, \beta > 0$. If $n+1$ now becomes collinear to one of the partons, say parton i, then the selector function $\mathcal{S}_{n+1,i}$ will approach one. And since the selector functions are strictly positive and form a decomposition of unity

$$\sum_k \mathcal{S}_{n+1,k} = 1, \tag{2.54}$$

all other selector functions will go to zero simultaneously.

The real emission cross section can then be written as a sum over sectors:

$$\hat{\sigma}_{ij \to n+u} = \frac{1}{F} \sum_k \int d\Phi_{n+1} |M^{(0)}_{ij \to n+u}|^2 \mathcal{S}_{n+1,k}. \tag{2.55}$$

Now say we found a way to factorize the phase space, such that the infrared limits of a specific sector, are isolated (see for example Ref. [26]). Then in each sector, we will have two unit integrations over ξ and η which parameterize the soft and collinear limit respectively, i.e. if $\xi \to 0$, then the momentum of the unresolved parton goes to zero and if $\eta \to 0$, the unresolved parton will become collinear to the reference momentum of that sector. The amplitude has the singular scaling $|M^{(0)}_{ij \to n+u}|^2 \sim \xi^{-2}\eta^{-1}$, leading to an integral of the form

$$\int_0^1 \frac{d\eta}{\eta^{1+\epsilon}} \frac{d\xi}{\xi^{1+2\epsilon}} f(\eta, \xi, \cdots), \tag{2.56}$$

where f is a function regular in the limits $\eta, \xi \to 0$. If we now apply the distributional identity

$$\frac{1}{x^{1-\epsilon}} = \frac{1}{\epsilon}\delta(x) + \sum_{k=0} \frac{\epsilon^k}{k!} \left(\frac{\ln^k x}{x} \right)_+ , \qquad (2.57)$$

we can explicitly carry out all integrations.

The *sector improved residue subtraction scheme* [27] extends the FKS subtraction scheme to NNLO. As of today, it is the only subtraction scheme capable of computing any QCD phase-space integral. Beyond NNLO, developing efficient and general subtraction schemes remains an open challenge in perturbative QCD.

3 | THE HIGGS AS A WINDOW TO NEW PHYSICS

3.1 STABILITY OF THE HIGGS POTENTIAL

3.2 THE HIERARCHY PROBLEM

4 | HADRONIC HIGGS PRODUCTION

4.1 MOTIVATION (BETTER TITLE NEEDED!)

Here I list various application for the Higgs production cross section and explain why precise predictions are so central. Maybe just put this in the chapter description?

4.2 THE LEADING-ORDER CROSS SECTION

Having established, that the gluon-fusion Higgs production cross section is central for many phenomenological applications, we now want to perform the actual LO calculation, which was first demonstrated by Georgi et al. in 1978 [28]. The calculation not only serves as an instructive example on cross section calculation, and thereby allows us to put our experience from section 2.2 to good use, but it already introduces many important concepts we can transfer to the NNLO computation.

At LO, there are only two possible Feynman diagrams we can draw. They are depicted in Fig. 4.1. As we can see. Gluon-fusion is a loop induced process with two scales: the mass of
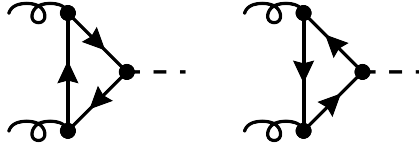
Figure 4.1: LO Feynman diagrams for Higgs production in the gluon-fusion channel.

the quark running in the loop m_q, and the Higgs mass m_H which must simultaneously be the partonic center of mass energy. The initial state gluons carry on the on-shell momenta p_1 and p_2. Let us then define

$$i\mathcal{M} = i\mathcal{M}^{\mu\nu,ab}\varepsilon_\mu^a(p_1)\varepsilon_\nu^b(p_2). \tag{4.1}$$

With the Feynman rules presented in appendix A we find

$$i\mathcal{M}^{\mu\nu,ab} = -\int \frac{\mathrm{d}^4k}{(2\pi)^4}$$

$$\times \mathrm{Tr}\left[\frac{-im_q}{v}\delta_{ij}\frac{i(\slashed{k}+\slashed{p}_1+\slashed{p}_2+m_q)}{(k+p_1+p_2)^2-m_q^2}(ig\gamma^\nu T_{ik}^a)\frac{i(\slashed{k}+\slashed{p}_1+m_q)}{(k+p_1)^2-m_q^2}(ig\gamma^\mu T_{kj}^b)\frac{i(\slashed{k}+m_q)}{k^2-m_q^2}\right] \tag{4.2}$$

$$+ \{p_1 \longleftrightarrow p_2, \mu \longleftrightarrow \nu, a \longleftrightarrow b\},$$

where the extra minus sign in front stems from the fermion trace.

Even without performing the explicit calculation can we already anticipate the general structure of the amplitude. Color wise, the amplitude must be proportional to δ^{ab}, because it is the

only available rank-two tensor. Since it is symmetric, the Lorentz structure must also be symmetric in order to satisfy *Bose symmetry*. The only building blocks we have available are $g^{\mu\nu}$, $(p_1^\mu p_2^\nu + p_2^\mu p_1^\nu)$, $p_1^\mu p_1^\nu$, and $p_2^\mu p_2^\nu$, but since all transverse parts drop out of the physical amplitude, the relevant tensors are only $g^{\mu\nu}$ and $p_2^\mu p_1^\nu$. Lastly, we know that the amplitude must satisfy the *Ward identity*, which allows us to restrict the tensor even further, such that we end up with

$$i\mathcal{M}^{\mu\nu,ab} = i\frac{\alpha_s}{\pi}\frac{1}{v}\delta^{ab}\left(p_2^\mu p_1^\nu - (p_1\cdot p_2)g^{\mu\nu}\right)\mathcal{C}(m_H, m_q). \tag{4.3}$$

Notice that we have only made use of very general properties of the amplitude. This is why the decomposition in Eq. (4.3) will hold at every order of α_s. The function $\mathcal{C}(m_H, m_q)$ is called the *Higgs-gluon form factor*. It has mass dimension 0, i.e. its functional dependence on m_q and m_H must be through a mass ratio

$$\mathcal{C}(m_H, m_q) = \mathcal{C}(z), \quad \text{with} \quad z \equiv \frac{m_H^2}{4m_q^2}. \tag{4.4}$$

The factor of $1/4$ was introduced, so that the *normal threshold* is located at $z = 1$. Mathematically, this means that $z = 1$ is a solution of the *Landau equations*. Physically, we can interpret the singularity as the point where we have enough energy to produce the quark pair on-shell. We can now project onto the form factor with

$$\mathcal{C}(z) = \frac{\pi v}{i\alpha_s}\frac{1}{N_c^2 - 1}\delta^{ab}\frac{1}{(p_1\cdot p_2)^2(d-2)}\left(p_{2\,\mu}p_{1\,\nu} - (p_1\cdot p_2)g_{\mu\nu}\right)i\mathcal{M}^{\mu\nu,ab}. \tag{4.5}$$

Let us define the pertubative expansion of the Higgs-gluon form factor as

$$\mathcal{C} = \mathcal{C}^{(0)} + \frac{\alpha_s}{\pi}\mathcal{C}^{(1)} + \left(\frac{\alpha_s}{\pi}\right)\mathcal{C}^{(2)} + \cdots \tag{4.6}$$

If we now insert the LO expression of Eq. (4.2) and perform some basic manipulations we find for the leading coefficient

$$\mathcal{C}^{(0)}(z) = T_F\frac{1}{2-2\epsilon}\frac{1}{z}\int\frac{\mathrm{d}^d k}{i\pi^{d/2}}\frac{1}{[k^2 - m_q^2 + i0^+][(k+p_1+p_2)^2 - m_q^2 + i0^+]}$$
$$\times\left(2\epsilon + \frac{m_H^2}{[(k+p_1)^2 - m_q^2 + i0^+]}\left(\frac{1}{z} + \epsilon - 1\right)\right), \tag{4.7}$$

which, after inserting integrals and expanding in ϵ, finally reduces to

$$\mathcal{C}^{(0)}(z) = T_F\frac{1}{z}\left\{1 - \left(1 - \frac{1}{z}\right)\left[\frac{1}{2}\ln\left(\frac{\sqrt{1-1/z} - 1}{\sqrt{1-1/z} + 1}\right)\right]^2\right\}. \tag{4.8}$$

We see that the Higgs-gluon form factor is roughly proportional to the square of the mass of the quark running in the loop. One power of m_q is hereby picked up from the Yukawa coupling. The other factor m_q is a consequence of the scalar coupling to Higgs. Indeed, without the quark mass, the trace in Eq. (4.2) would contain an odd number of gamma matrices and vanish consequently. Physically, we can interpret this as a helicity flip of the internal quark at the Higgs interaction vertex. And since massless QCD conserves helicity, the other helicity flip is provided by the mass. Similarly, since the two incoming gluons are vector bosons which should form a spinless final state, we would expect them to always carry opposite spins. This intuition is indeed confirmed by the tensor structure of the amplitude (4.3), as it always vanishes once contracted with two polarization vectors of the same helicity[1].
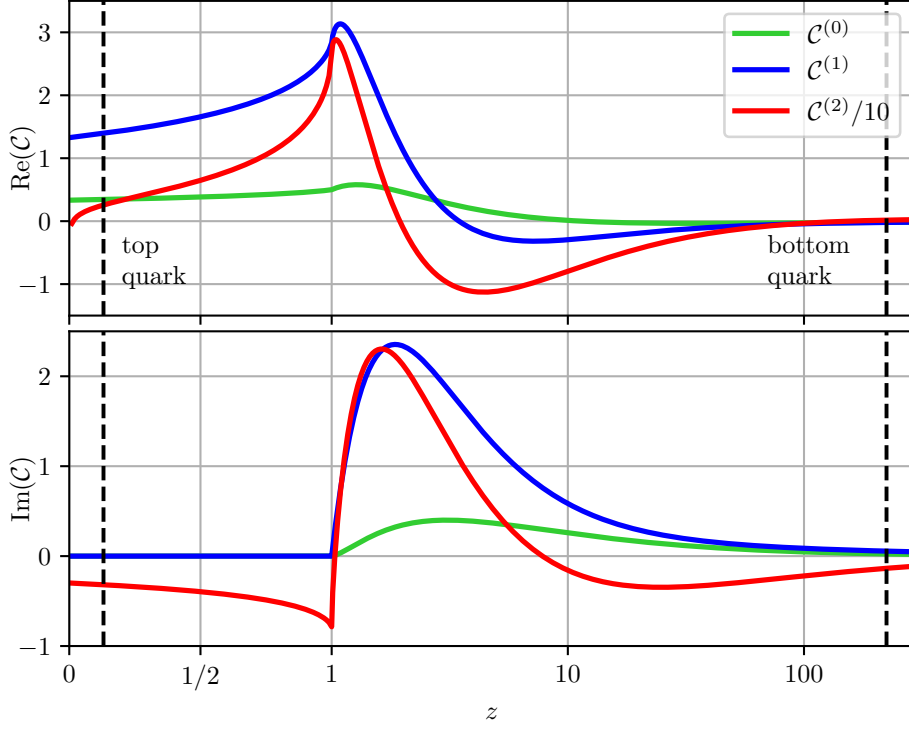
Figure 4.2: Real and imaginary part of the finite part of the Higgs-gluon form factor at various perturbative. NNLO is divided by ten for better visibility. NNLO results also depend on the number of light quark flavors, which has been set to 5 (5FS). Top-quark is renormalized in the OS scheme. Infrared divergences are subtracted in the $\overline{\text{MS}}$ scheme with the help of the **Z** operator (see e.g. Ref. [29]). Vertical lines indicate the z values for the top- (on-shell) and bottom-quark ($\overline{\text{MS}}$) masses. The plot was created using the results of Ref. [30].

The LO Higgs-gluon form factor is plotted in Fig. 4.2. As expected, we pick up an imaginary part starting from the normal threshold at $z = 1$. If we expand the form factor around large quark masses, i.e. we perform a *large mass expansion* (LME), we find that it approaches a constant

$$\mathcal{C}^{(0)}(z) = T_F \left(\frac{2}{3} + \frac{7}{45}z + \frac{4}{63}z^2 + \mathcal{O}(z^3) \right). \tag{4.9}$$

We will discuss the infinite mass limit in more detail in section 4.3. On the other side of the spectrum we can see that if the mass of the Higgs is far greater than the mass the internal quark, the form factor is approximately

$$\mathcal{C}^{(0)}(z) = \frac{T_F}{4z} \left[4 - \log^2(-4z) + \frac{1}{z} \left(\log(-4z) + \log^2(-4z) \right) + \mathcal{O}(1/z^2) \right]. \tag{4.10}$$

This expansion is known as *high-energy limit* HEL. The appearing double logarithms $\log^2(m_q^2/m_H^2)$ originate from a soft quark exchange. In fact, the quark mass acts as an infrared regulator of the integral in Eq. 4.7, so the appearance of these logarithms is not entirely unexpected. Numerically, these logarithms can be very large. The bottom quark, for example will yield a double logarithm of about 46. I.e., although suppressed by a factor of m_q^2/m_H^2, the contributions from lighter quark flavors are logarithmically enhanced and hence highly significant for precision predictions.

---

1 This can be seen easily by boosting to the center of mass frame and using $\epsilon^\mu(-\mathbf{p}, \lambda) \propto \epsilon^\mu(\mathbf{p}, -\lambda)$.

If we now apply Eq. (2.25) and perform the phase space integration, which for a single particle is trivial because of the momentum conserving delta function, we get for the partonic cross section

$$\hat{\sigma}_{gg \to H}(\tau S) = \frac{\pi}{64v^2} m_H^2 \left(\frac{\alpha_s}{\pi}\right)^2 |\mathcal{C}(z)|^2 \delta(\tau S - m_H^2) \frac{1}{1 - \epsilon}. \tag{4.11}$$

The initial state was averaged over spin and color. In conventional dimensional regularization, the gluons have $d - 2 = 2(1 - \epsilon)$ spin degrees. Finally, after the convolution with the partonic luminosity we arrive at the LO cross section

$$\sigma_{pp \to HX}^{\text{LO}}(S) = \frac{\pi}{64v^2} \left(\frac{\alpha_s}{\pi}\right)^2 \mathcal{L}_{gg}\left(\frac{m_H^2}{S}\right) |\mathcal{C}^{(0)}(z)|^2. \tag{4.12}$$

From Fig. 4.2 we can see that the top quark exerts the largest impact on the Higgs-gluon form factor and hence the LO hadron cross section. We can read off the partonic luminosity from Fig. 2.3 and find that the cross section for the top quark induces Higgs production reads[2]

$$\sigma_{pp \to HX}^{\text{LO}}(t) = 16.30 \text{ pb} \tag{4.13}$$

at a hadronic center of mass energy of 13 TeV. Although expected to have a less significant impact, we can also include the effects of finite bottom quark masses by coherently summing together the corresponding form factors. We find

$$\sigma_{pp \to HX}^{\text{LO}}(t + b) = 15.23 \text{ pb}, \tag{4.14}$$

i.e. the bottom quark lowers the cross section by around 6.5% at LO.

Without the inclusion of electro-weak corrections, we can always decompose the gluon fusion cross section in terms of the Yukawa couplings Y_i:

$$\sigma_{pp \to HX} = \sum_{i \leq j} Y_i Y_j \sigma_{ij}. \tag{4.15}$$

We call

$$\sigma_{i \times j} = Y_i Y_j \sigma_{ij}, \tag{4.16}$$

the *i-j-interference contribution* and

$$\sigma_i = Y_i^2 \sigma_{ii} \tag{4.17}$$

the *pure-i contribution* to the cross section. Both contributions are depicted at LO in Fig. 4.3. Clearly, the dominant contribution for the lighter quark flavors comes from the interference with the top-quark. The pure-bottom contribution is already below a percent and the pure-charm quark mass effects are completely negligible. The inclusion of the charm quark lowers the total cross section by around 1%.

4.3 THE HEAVY-TOP LIMIT

The computation of the Higgs production cross section in full QCD is quite challenging. As we saw above, even at leading order we encounter loop integrals with two mass scales. It is therefore maybe not surprising that the first NLO corrections to this process were actually computed in an approximation framework [31]. In the approximation, we assume that the

---

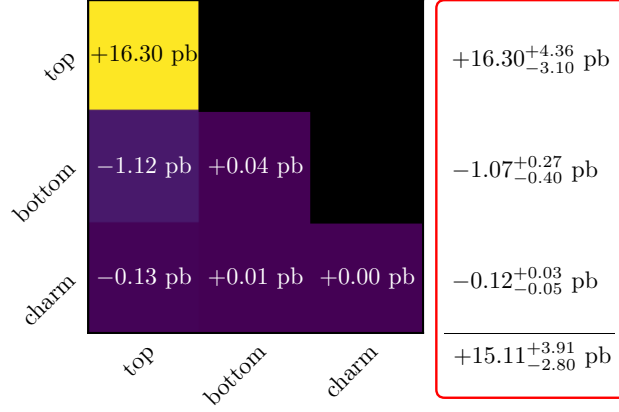2 Values of masses and coupling constants are provided in the conventions.

Figure 4.3: σ_i (diagonals) and $\sigma_{i \times j}$ (off-diagonals) at LO for the three heaviest quark flavors. The red box indicates the sum of each row, and hence the combined effects of each additional flavor. The computational setup is described in the conventions. We use the on-shell mass value for the top quark and $\overline{\mathrm{MS}}$ masses for the bottom- and charm-quark. Scale uncertainties are computed with 7-point-variation.

quark, which is coupling to the Higgs is infinitely heavy. That means we are only interested in the leading term of the LME.

The finite distance interaction of the gluon and the Higgs will therefore shrink down to a point like vertex, which we can describe with the effective Lagrangian

$$\mathcal{L}_{\mathrm{HTL}}^{(0)} = \mathcal{L}_{\mathrm{QCD}}^{(n_f - 1)} - C_1 \frac{H}{v} \frac{1}{4} G_{\mu\nu}^a G^{a\,\mu\nu}. \tag{4.18}$$

We see that the coupling constant now has mass dimension -1, so the theory will not be UV renormalizable. That means that we cannot absorb all UV divergences into multiplicative renormalization constants as we did for the SM (see Eq. (2.31)), but we will generate more and more independent terms in our Lagrangian to cancel all appearing divergences. On the other hand, as long as we restrict ourselves to QCD corrections, and hence only single operator insertions, we can treat the color singlet Higgs as a constant, and renormalize only the gauge invariant operator

$$\mathcal{O}_1 \equiv -1/4 G_{\mu\nu}^a G^{a\,\mu\nu}. \tag{4.19}$$

To indicate the pertubative order we gave the Lagrangian in Eq. (4.18) a superscript. The superscript $n_f - 1$ of the QCD Lagrangian specifies the number of active flavors. It was reduced by one, since the heaviest quark flavor was integrated out. The constant C_1 is called a *Wilson coefficient*, and it needs to be matched to the full theory in the infinite quark mass limit. At LO for example, we find that the Higgs-gluon form factor in the effective theory simply reads

$$C_1 = -\frac{\alpha_s}{\pi} \mathcal{C}^{(0)} + \mathcal{O}\big(\alpha_s^2\big). \tag{4.20}$$

If we compare this to the leading term of our LME (4.9), we find

$$C_1 = -\frac{\alpha_s}{\pi} \frac{2}{3} T_F + \mathcal{O}\big(\alpha_s^2\big). \tag{4.21}$$

The main benefit of the approximation lies in the reduced complexity. By integrating out the top quark, we have reduced a loop-induced process to a tree-level process. Moreover, the top-quark mass is eliminated as a scale, hence the appearing Feynman integrals will generally be much simpler to solve.

4.3.1   Renormalization of Gauge Invariant Operators

Beyond LO gauge invariant operator like $\mathcal{O}_1$ can mix under renormalization with other gauge invariant operators but notably also with operators which are not gauge invariant. In general, we distinguish two types of operators: *Type-II operators*, which give zero when sandwiched between physical states, and *type-I operators*, which can give non-zero matrix elements. The type-II operators can be further subcategorized into operators vanishing by the equation of motion (*type-II$_a$ operators*), and all other operators (*type-II$_b$ operators*). For a polynomial operator with ghost number zero satisfying

$$s\mathcal{O} = 0, \tag{4.22}$$

where s is the *linearized Slavnov operator*, one can proof [32, 33, 34] that

$$\mathcal{O} = sF + \text{gauge invariant operators}. \tag{4.23}$$

Operators of the form sF are also called *Bechi-Rouet-Stora-Tyutin-* (BRST-) *exact operators*, and they vanish between physical states. For $\mathcal{O}_1$ the above conditions are met, allowing us to conclude that the $\mathcal{O}_{II}$ operators are BRST-exact. This can be leveraged to find the complete operator basis:

$$
\begin{aligned}
\mathcal{O}_I &\begin{cases} \mathcal{O}_1 = -\frac{1}{4} G^a_{\mu\nu} G^{a\,\mu\nu}, \\ \mathcal{O}_2 = \sum_{i=1}^{n_l} m_i \bar{q}_i q_i, \end{cases} \\
\mathcal{O}_{II_a} &\begin{cases} \mathcal{O}_3 = \sum_{i=1}^{n_l} \bar{q}_i \left(\frac{i}{2} \overleftrightarrow{\slashed{D}} - m \right) q_i, \end{cases} \\
\mathcal{O}_{II_b} &\begin{cases} \mathcal{O}_4 = A^{a\,\mu} D^\nu G^a_{\nu\mu} + g \sum_{i=1}^{n_l} \bar{q}_i \slashed{A} q_i - \partial^\mu \bar{c}^a \partial_\mu c^a, \\ \mathcal{O}_5 = D_\mu \partial^\mu \bar{c}^a c^a. \end{cases}
\end{aligned}
\tag{4.24}
$$

The operator basis is constructed only of light fields, and the light fields are defined in a decoupled theory.

Since operators of type II cannot generate non-vanishing S-matrix elements through renormalization the renormalization matrix must have the general structure

$$
\begin{pmatrix} \mathcal{O}_I^R \\ \mathcal{O}_{II}^R \end{pmatrix} = \begin{pmatrix} z^{I,I} & z^{I,II} \\ 0 & z^{II,II} \end{pmatrix} \begin{pmatrix} \mathcal{O}_I^B \\ \mathcal{O}_{II}^B \end{pmatrix}. \tag{4.25}
$$

The final form of our effective Lagrangian therefore reads

$$\mathcal{L}_{\mathrm{HTL}} = \mathcal{L}_{\mathrm{QCD}}^{(5)} + \frac{H}{v} \sum_{i=1}^{5} C_i^B \mathcal{O}_i^B. \tag{4.26}$$

As usual, we replace the bare quantities by their renormalized counter parts

$$C_i^B \mathcal{O}_i^B = C_i^B Z_{ij}^{-1} \mathcal{O}_j^R, \tag{4.27}$$

and we identify

$$C^R = (Z^{-1})^T C^B. \tag{4.28}$$

Using the RGE we find that the *anomalous dimension* matrix of the Wilson coefficients is determined through

$$\frac{\mathrm{d}C^R}{\mathrm{d}\ln\mu} = \left(Z\frac{\mathrm{d}(Z^{-1})}{\mathrm{d}\ln\mu}\right)^T C^R = -\left(\frac{\mathrm{d}Z}{\mathrm{d}\ln\mu}Z^{-1}\right)^T C^R \equiv \gamma^T C^R. \tag{4.29}$$

With the structure of the renormalization matrix (4.25), we arrive at an important conclusion: The Wilson coefficients of type-II operators cannot mix into the Wilson coefficients of type-I operators through the running in the scale. Since the type-II operators render no contribution to the scattering matrix element, we can focus our attention on the gauge invariant operators and their Wilson coefficients.

We now want to determine the I, I part of the renormalization matrix, i.e. $z^{I,I}$ to determine the running of the Wilson coefficients. Let us start by defining the generating functional

$$Z[J] \equiv z[J]/z[0], \quad z[J] \equiv \int \prod_i \mathcal{D}\Phi_j \, e^{i(S+J\cdot\Phi)}, \quad S = S[A,c,\bar{c},q,\bar{q}] \equiv \int \mathrm{d}^d x \, \mathcal{L},$$
$$J = \left(J^\mu, \bar{J}, J, \bar{\eta}, \eta\right), \quad \Phi = \left(\frac{1}{g}A_\mu, c, \bar{c}, q, \bar{q}\right), \tag{4.30}$$

with the Lagrangian

$$\mathcal{L} \equiv -\frac{1}{4g^2}F^a_{\mu\nu}F^{a\,\mu\nu} - \frac{1}{2\xi g^2}\left(\partial\cdot A\right)^2 + \partial^\mu\bar{c}^a D_\mu c^a + \bar{q}\left(\frac{i}{2}\overleftrightarrow{\slashed{D}} - m_q\right)q. \tag{4.31}$$

The Lagrangian is the QCD Lagrangian with only one active quark flavor and rescaled gauge fields

$$A^a_\mu \longrightarrow \frac{1}{g}A^a_\mu. \tag{4.32}$$

The operators in Eq. (4.24) can now be generated by applying the differential operators[3]

$$D_1 = -\frac{1}{2}g\frac{\partial}{\partial g} + \xi\frac{\partial}{\partial\xi} - \frac{1}{2}J_\mu\cdot\frac{\delta}{\delta J_\mu},$$
$$D_2 = -m_q\frac{\partial}{\partial m_q}, \tag{4.33}$$

on the generating functional

$$z_{\mathcal{O}_k}[J] \equiv \int \prod_j \mathcal{D}\Phi_j \, \hat{\mathcal{O}}_k(0)e^{i(S+J\cdot\Phi)} = -iD_k z[J]. \tag{4.34}$$

Here $\hat{\mathcal{O}}_k(0)$ is the Fourier transform of the operator $\mathcal{O}(x)$ at zero momentum. The normalization of the generating functional then properly subtracts the vacuum expectation value of the operators

$$-iD_k Z[J] = \frac{1}{z[0]}\int \prod_j \mathcal{D}\Phi_j \left(\hat{\mathcal{O}}_k(0) - \langle\Omega|\mathcal{O}_k(0)|\Omega\rangle\right)e^{i(S+J\cdot\Phi)} \equiv Z_{\mathcal{O}_k}. \tag{4.35}$$

In the $\overline{\mathrm{MS}}$ scheme, the R-operation commutes with the differential operators in Eq. (4.33), i.e. the renormalized operators can be generated from the renormalized generating functional

$$Z_{\mathcal{O}_k^R} = -iD_k Z^R[J], \tag{4.36}$$

---

3 We only provide the operators for the type-I operators, since they are the only ones necessary for computing physical amplitudes.

where the renormalized generating functional is defined as

$$Z^R[J] = z^R[J]/z^R[0],$$

$$z^R[J] = \int \prod_i \mathcal{D}\Phi_j \, e^{i(S^R + J \cdot \Phi)},$$

(4.37)

$$S^R \equiv S[Z_3'^{1/2} A^R, Z_3'^{-1/2} c^R, \tilde{Z}_3^{-1/2} \bar{c}^R, Z_2^{1/2} q^R, Z_2^{1/2} \bar{q}^R, Z_g g, Z_m m_q, Z_g^{-2} Z_3' \xi^R].$$

Using the chain rule we find that

$$-iD_k z^R[J] = \int \prod_j \mathcal{D}\Phi_j \left[\hat{O}_k(0) + \sum_i (D_k \ln Z_i) \frac{\partial S^R}{\partial \ln Z_i} \right] e^{iS^R + J \cdot \Phi}, \quad Z_i \in \{Z_3', \tilde{Z}_3, Z_2, Z_g, Z_m\}.$$

(4.38)

And with

$$Z_g \frac{\partial S^R}{\partial Z_g} = -2\hat{\mathcal{O}}_1(0), \quad \text{and} \quad Z_m \frac{\partial S^R}{\partial Z_m} = -\hat{\mathcal{O}}_2(0),$$

(4.39)

we find that the renormalization constants are given by

$$z_{11}^{I,I} = 1 - 2D_1 \ln Z_g = 1 + g \frac{\partial \ln Z_g}{\partial g}, \quad z_{12}^{I,I} = -D_1 \ln Z_m = \frac{g}{2} \frac{\partial \ln Z_m}{\partial g}$$

$$z_{21}^{I,I} = 0, \qquad\qquad\qquad\qquad z_{22}^{I,I} = 1.$$

(4.40)

Here we made use of the fact, that the $\overline{\text{MS}}$-renormalization constants are independent of the quark mass and the gauge parameter. We can rewrite the appearing derivatives in terms of the β-function and the mass-anomalous dimension. Indeed,

$$\frac{4\pi}{\alpha_s} \bar{\beta} \equiv \frac{d \ln \alpha_s}{d \ln \mu} = -\frac{d \ln Z_{\alpha_s}}{d \ln \mu} = -\left(\frac{\partial \ln Z_{\alpha_s}}{\partial \ln \alpha_s} \frac{d \ln \alpha_s}{d \ln \mu} + \frac{\partial \ln Z_{\alpha_s}}{\partial \ln \mu} \right) = -\left(\frac{4\pi}{\alpha_s} \bar{\beta} \frac{\partial \ln Z_{\alpha_s}}{\partial \ln \alpha_s} + 2\epsilon \right)$$

$$\Rightarrow \frac{\partial \ln Z_{\alpha_s}}{\partial \ln \alpha_s} = g \frac{\partial \ln Z_g}{\partial g} = -1 - 2\epsilon \frac{\alpha_s}{4\pi \bar{\beta}} = -1 + \frac{1}{1 - \frac{\beta}{2\epsilon} \frac{4\pi}{\alpha_s}},$$

(4.41)

where in the last step we used the relation between the d- and four-dimensional β-functions

$$\bar{\beta} = \beta - 2\epsilon \frac{\alpha_s}{4\pi}.$$

(4.42)

Similarly, we find

$$\gamma_m \equiv -\frac{d \ln m_q}{d \ln \mu} = \frac{d \ln Z_m}{d \ln \mu} = \frac{\partial \ln Z_m}{\partial \ln \alpha_s} \frac{\partial \ln \alpha_s}{\partial \ln \mu} = \frac{\partial \ln Z_m}{\partial \ln \alpha_s} \frac{4\pi}{\alpha_s} \bar{\beta}$$

$$\Rightarrow \frac{\partial \ln Z_m}{\partial \ln \alpha_s} = g \frac{\partial \ln Z_m}{\partial g} = \frac{\alpha_s}{4\pi} \frac{1}{\bar{\beta}} \gamma_m = -\frac{\gamma_m}{2\epsilon} \frac{1}{1 - \frac{\beta}{2\epsilon} \frac{4\pi}{\alpha_s}}$$

(4.43)

Finally, we want to use the above results to calculate the anomalous dimension matrix in Eq. (4.29). The entries of the renormalization constant only depend on scale through the coupling constant, i.e.

$$\gamma^{I,I} = -\frac{dz^{I,I}}{d \ln \mu} (z^{I,I})^{-1} \bigg|_{\epsilon=0} = -\frac{\partial z^{I,I}}{\partial \alpha_s} (z^{I,I})^{-1} 4\pi \bar{\beta} \bigg|_{\epsilon=0} = \frac{\partial z^{I,I\,(1)}}{\partial \alpha_s} 2\alpha_s.$$

(4.44)

Where we used that $z^{I,I}$ consists only of poles in the $\overline{\text{MS}}$ scheme, and once again applied the relation between the β-functions in Eq. (4.42). $z^{I,I\,(1)}$ denotes the residue of the renormalization matrix

$$z^{I,I} = \mathbb{1} + \sum_{i=1} z^{I,I\,(i)} \epsilon^{-i}.$$

(4.45)

We then find for the anomalous dimension matrix

$$\gamma^{I,I} = \begin{pmatrix} 4\pi\alpha_s \frac{d}{d\alpha_s}\left(\frac{\beta}{\alpha_s}\right) & -\alpha_s \frac{d\gamma_m}{d\alpha_s} \\ 0 & 0 \end{pmatrix}. \tag{4.46}$$

The structure of this matrix reveals, that the C_1 Wilson coefficient, which is relevant coefficient for the HTL, is completely independent of the other Wilson coefficients. The RGE for the Wilson coefficient (4.29) can now be written as

$$\frac{\partial C_1}{\partial \alpha_s}4\pi\beta + \frac{\partial C_1}{\partial \ln \mu} = 4\pi\alpha_s \frac{d}{d\alpha_s}\left(\frac{\beta}{\alpha_s}\right)C_1. \tag{4.47}$$

The β-function has the general expansion

$$\beta = \left(\frac{\alpha_s}{4\pi}\right)^2 \sum_{i=0} \beta_i \left(\frac{\alpha_s}{4\pi}\right)^i. \tag{4.48}$$

For example at one-, and two-loop, it can be shown [35, 36, 37, 38, 39, 40]

$$\begin{aligned} \beta_0 &= \frac{11}{3}C_A - \frac{4}{3}T_F n_f, \\ \beta_1 &= \frac{34}{3}C_A^2 - \frac{20}{3}C_A T_F n_f - 4C_F T_F n_f. \end{aligned} \tag{4.49}$$

We can solve the partial differential equation in Eq. (4.47) perturbatively by proposing the Ansatz

$$\begin{aligned} C_1 &= \frac{\alpha_s}{4\pi}C_1^{(0,0)} + \left(\frac{\alpha_s}{4\pi}\right)^2\left(C_1^{(1,0)} + C_1^{(1,1)}\ln\frac{\mu}{\mu_0}\right) \\ &\quad + \left(\frac{\alpha_s}{4\pi}\right)^3\left(C_1^{(2,0)} + C_1^{(2,1)}\ln\frac{\mu}{\mu_0} + C_1^{(2,2)}\ln^2\frac{\mu}{\mu_0}\right) + \cdots. \end{aligned} \tag{4.50}$$

The constants coefficients $C_1^{(i,0)}$ mark the initial conditions; they need to be matched to the full theory in the infinite mass limit. The coefficients of the logarithms on the other hand can be determined through a comparison of coefficients, they read

$$\begin{aligned} C_1^{(1,1)} &= 0, \\ C_1^{(2,1)} = C_1^{(0,0)}\beta_1 - C_1^{(1,0)}\beta_0, &\quad C_1^{(2,2)} = 0, \\ C_1^{(3,1)} = 2C_1^{(0,0)}\beta_2 - 2C_1^{(2,0)}\beta_0, \quad C_1^{(3,2)} = \beta_0^2 C_1^{(1,0)} - \beta_0\beta_1 C_1^{(0,0)}, &\quad C_1^{(3,3)} = 0. \end{aligned} \tag{4.51}$$

It is clear from the structure of the differential equation, that the all coefficients $C_1^{(i,i)}$ are in fact all zero except for $C_1^{(0,0)}$.

4.3.2 Matching of Wilson Coefficients

By expanding the Higgs-gluon form for large quark masses we were able to determine the LO Wilson coefficient. Of course, if we would need the full Higgs-gluon form factor to determine the Wilson coefficient, the HTL would be of little use, since it would not bring any simplifications. Fortunately, the large quark mass limit can already be used at the integrand level using the large mass expansion.

Alternatively, one may find the matching coefficients by means of *low-energy theorems* [41, 42, 43]:

$$-iG^B_{\mathcal{O}_1,\dots,\mathcal{O}_n,\bar{q}_iq_i}(p_1,\dots,p_{n-1},0)\Big|_{\text{connected}} = \frac{\partial}{\partial m^B_i}G^B_{\mathcal{O}_1,\dots,\mathcal{O}_n}(p_1,\dots,p_{n-1})\Big|_{\text{connected}}. \quad (4.52)$$

Here, $\mathcal{O}_1,\dots,\mathcal{O}_n$ are local operators and $G_{\mathcal{O}_1,\dots}\big|_{\text{connected}}$ denotes the momentum space representation of the corresponding connected Green's functions

$$\int\left(\prod_{i=1}^n \mathrm{d}^dx_i\, e^{ip_i\cdot x_i}\right)\langle\Omega|T\left[\mathcal{O}^B_1(x_1)\dots\mathcal{O}^B_n(x_n)\right]|\Omega\rangle\Big|_{\text{connected}}$$
$$\equiv (2\pi)^d\delta^{(d)}\left(\sum_{i=1}^n p_i\right)G^B_{\mathcal{O}_1,\dots,\mathcal{O}_n}(p_1,\dots,p_{n-1})\Big|_{\text{connected}}, \quad (4.53)$$

$|\Omega\rangle$ denotes the vacuum of the interacting theory and T is the *time ordering operator*. The theorem relates the mass derivative of a Green's function with a Green's function of the same operators but with the insertion of $\bar{q}_iq_i$ at zero momentum.

It follows upon application of the *Gell-Mann–Low formula*

$$\frac{\partial}{\partial m^B_i}\langle\Omega|T\left[\mathcal{O}^B_1(x_1)\dots\mathcal{O}^B_n(x_n)\right]|\Omega\rangle\Big|_{\text{connected}} =$$
$$\langle 0|T\left[\mathcal{O}^B_{1,I}(x_1)\dots\mathcal{O}^B_{n,I}(x_n)(-i)\int\mathrm{d}^dx\left(1+\frac{H^B_I(x)}{v}\right)\bar{q}^B_i(x)q^B_i(x)\exp\left(-i\int\mathrm{d}^dz\,\mathcal{H}^B_{\text{int},I}(z)\right)\right]|0\rangle \quad (4.54)$$

The subscript I indicates interaction picture fields, $|0\rangle$ is the vacuum state, now of the free theory, and $\mathcal{H}_{\text{int}}$ is the interaction part of the *Hamiltonian*. Without the inclusion of electroweak corrections, we can omit the field of the Higgs[4] in the intergral. This also implies, that all operators $\mathcal{O}_1,\dots,\mathcal{O}_n$, do not contain any electroweak fields. After switching to momentum space, we immediately arrive at Eq. (4.52).

Since the proof relied on relations on the level of the Lagrangian, the statement is only true for bare amplitudes and Green's functions beyond LO. It can be straightforwardly generalized to include an arbitrary number of massive particles, by simply summing over all massive particles. Lastly, we note that the differential operator does not act on masses in the operators themselves, should they contain any.

We can now apply the low-energy theorem on the gluon self energy. Let us consider first the *amputated* Green's function of two gluons with the insertion of the composite operator $\mathcal{O}_h = \bar{h}^Bh^B$. In momentum space, it reads

$$G^{B,ab\,\mu\nu}_{A,A,\mathcal{O}_h}(p,0)\Big|_{\text{amp.}} = \int\mathrm{d}^dx\,\mathrm{d}^dy\,e^{ip\cdot(x-y)}\langle\Omega|T\left[A^{B,a\mu}(x)A^{B,b\nu}(y)\mathcal{O}_h(0)\right]|\Omega\rangle\Big|_{\text{amp.}}$$
$$\equiv \delta^{ab}\left[-g^{\mu\nu}p^2 G^B_{A,A,\mathcal{O}_h}(p^2)\Big|_{\text{amp.}} + \text{terms proportional to } p^\mu p^\nu\right], \quad (4.55)$$

---

4 Not to be confused with the Higgs field.

where T denotes the time ordering operator and p is the momentum along the gluon line. As discussed in detail above, in the limit of infinite quark mass $m_h^B \to \infty$, the operator $\bar{h}h$ can be written in terms of a linear combination of the operators $\mathcal{O}_1, \ldots, \mathcal{O}_5$

$$
\begin{aligned}
&\left. G_{A,A,\mathcal{O}_h}^{B,ab\,\mu\nu}(p,0) \right|_{\text{amp.}} \simeq \\
&\quad -\int \mathrm{d}^d x\, \mathrm{d}^d y\, e^{ip\cdot(x-y)} \langle\Omega| T \left[A^{B,a\mu}(x) A^{B,b\nu}(y) \frac{\alpha_s}{\pi} \frac{1}{m_h^B} \sum_{i=1}^{5} C_i^B \mathcal{O}_i^B(0) \right] |\Omega\rangle \Big|_{\text{amp.}}.
\end{aligned}
\tag{4.56}
$$

The $\simeq$ indicates, that the relation holds only up to power corrections of order $1/m_h^{B\,2}$.

In the $\overline{\text{MS}}$ scheme, the *Appelquist-Carazzone decoupling theorem* [44] does not hold in its naïve sense, i.e. heavy degrees of freedom, do not decouple at low energy. The standard method to circumvent this issue, is by the introduction decoupling constants, which relate quantities at in the decoupled theory (denoted with a superscript (n_l)) with the full high energy theory:

$$
\begin{aligned}
g^{B,(n_l)} &= \zeta_g^B g^B, \quad m_i^{B,(n_l)} = \zeta_{m_i}^B m_i^B, \quad \xi^{B,(n_l)} - 1 = \zeta_3^B(\zeta^B - 1), \\
q_i^{B,(n_l)} &= \sqrt{\zeta_2^B} q_i^B, \quad A_\mu^{B,(n_l),a} = \sqrt{\zeta_3^B} A_\mu^{B,a}, \quad c^{B,(n_l),a} = \sqrt{\tilde{\zeta}_3^B} c^{B,a}.
\end{aligned}
\tag{4.57}
$$

The relations hold up to power corrections of $1/m_h^2$. The decoupling constants are functions of g^B, m_i^B and the scale μ, but the function arguments are left implicit. The amputated Green's functions then becomes[5]

$$
\begin{aligned}
&\left. G_{A,A,\mathcal{O}_h}^{B,ab\,\mu\nu}(p,0) \right|_{\text{amp.}} \simeq \\
&\quad -\zeta_3^B \int \mathrm{d}^d x\, \mathrm{d}^d y\, e^{ip\cdot(x-y)} \langle\Omega| T \left[A^{B,(n_l),a\mu}(x) A^{B,(n_l),b\nu}(y) \frac{\alpha_s}{\pi} \frac{1}{m_h^B} \sum_{i=1}^{5} C_i^B \mathcal{O}_i^B(0) \right] |\Omega\rangle \Big|_{\text{amp.}}
\end{aligned}
\tag{4.58}
$$

At LO in α_s, we will have only contributions from the operators $\mathcal{O}_1$ and $\mathcal{O}_4$, because all other operators would create disconnected contributions

$$
\begin{aligned}
&\left. G_{A,A,\mathcal{O}_h}^{B,ab\,\mu\nu}(p,0) \right|_{\text{amp.}} \simeq \\
&\quad -\frac{\alpha_s}{\pi} \frac{1}{m_h^B} \delta^{ab} \left(-g^{\mu\nu} p^2 \zeta_3^B \left(C_1^B + 2C_4^B \right) + \mathcal{O}(\alpha_s) \right) + \text{terms proportional to } p^\mu p^\nu.
\end{aligned}
\tag{4.59}
$$

We now set the mass of the light quarks in the QCD Lagrangian to zero; the light quark masses in the definition of the operators in Eq. (4.24) can still be non-vanishing. In the limit of vanishing gluon momentum $p \to 0$, the coefficient of the transverse part does not receive any α_s-corrections in DR, because all appearing Feynman integrals are necessarily scaleless. We have thus shown the all order result

$$
\left. G_{A,A,\mathcal{O}_h}^{B}(0,0) \right|_{\text{amp.}} \simeq -\frac{\alpha_s}{\pi} \frac{1}{m_h^B} \zeta_3^B \left(C_1^B + 2C_4^B \right).
\tag{4.60}
$$

By application of the LSZ reduction formula we can rewrite the amputated Green's functions in terms of connected ones. The operator $\mathcal{O}_h$ is hereby irrelevant as it is not considered to be

---

5 Keep in mind, that the amputated Green's function is an antilinear functional of the fields.

external, i.e. (4.52) holds for regular, connected and 1-particle-irreducible Green's functions. Application of Eq. (4.52) yields

$$\frac{\alpha_s}{\pi}\left(C_1^B + 2C_4^B\right) = \frac{\partial \ln \zeta_3^B}{\partial \ln m_h^B}. \tag{4.61}$$

We can repeat the same analysis for $G_{\bar{c},c,\mathcal{O}_h}(p,0)$ and $G_{\bar{c},c,g,\mathcal{O}_h}(p,p,0)$ and in the limit $p \to 0$ obtain

$$\begin{aligned}
\frac{\alpha_s}{\pi}\left(-C_4^B - C_5^B\right) &= \frac{\partial \ln \tilde{\zeta}_3^B}{\partial \ln m_h^B} \\
\frac{\alpha_s}{\pi}\left(-C_5^B\right) &= \frac{\partial}{\partial \ln m_h^B} \ln\left(\tilde{\zeta}_3^B \sqrt{\zeta_3^B}\zeta_g^B\right)
\end{aligned} \tag{4.62}$$

Eq. (4.61) and (4.62) form a linear system of equations which we can solve for the Wilson coefficients. The solution for the physical Wilson coefficient reads

$$\frac{\alpha_s}{\pi}C_1^B = -\frac{\partial \ln \zeta_g^{B\,2}}{\partial \ln m_h^B}. \tag{4.63}$$

In the $\overline{\text{MS}}$ scheme, the renormalization constant of the heavy quark mass is independent of the mass, i.e.

$$\frac{\partial}{\partial \ln m_h^B} = \frac{\partial}{\partial \ln m_h}. \tag{4.64}$$

With the renormalization matrix in Eq. (4.40) we can then find the renormalized version of Eq. (4.63)

$$\frac{\alpha_s}{\pi}C_1 = -\frac{\partial \ln \zeta_g^2}{\partial \ln m_h}. \tag{4.65}$$

The decoupling constants are known at two-, three-[45] and four-loop [46, 47] order. Notice that we only require the logarithmic dependence of the decoupling constants to obtain the Wilson coefficients. The logarithmic structure on the other hand may be reconstructed from lower order terms in combination with the β-function and the mass anomalous dimension [43]. The four-loop decoupling constant is therefore sufficient, to match the Wilson coefficient up to N^{4}LO. Here we only provide the Wilson coefficient up to N^{3}LO, as it is the highest order for which full cross section calculations are available at present

$$\begin{aligned}
C_1^{(0,0)} &= -\frac{4}{3} \\
C_1^{(1,0)} &= -\frac{44}{3} \\
C_1^{(2,0)} &= -\frac{5554}{27} + \frac{76}{3}\ln\left(\frac{m_h^2}{\mu^2}\right) + n_l\left[\frac{134}{9} + \frac{64}{9}\ln\left(\frac{m_h^2}{\mu^2}\right)\right] \\
C_1^{(3,0)} &= \frac{2892659}{486} - \frac{897943}{108}\zeta(3) + \frac{13864}{27}\ln\left(\frac{m_h^2}{\mu^2}\right) - \frac{836}{3}\ln^2\left(\frac{m_h^2}{\mu^2}\right) - \frac{64}{81}\ln^3\left(\frac{m_h^2}{\mu^2}\right) \\
&\quad + n_l\left[-\frac{40291}{243} + \frac{110779}{162}\zeta(3) + \frac{7040}{81}\ln\left(\frac{m_h^2}{\mu^2}\right) - \frac{184}{3}\ln^2\left(\frac{m_h^2}{\mu^2}\right)\right] \\
&\quad + n_l^2\left[\frac{13730}{729} + \frac{308}{81}\ln\left(\frac{m_h^2}{\mu^2}\right) + \frac{128}{27}\ln^2\left(\frac{m_h^2}{\mu^2}\right)\right].
\end{aligned} \tag{4.66}$$

Notice that the decoupling constant ζ_g is a function of $\alpha_s^{(n_l+1)}$, i.e. we must recursively apply the decoupling relations (4.57) to express everything in terms of decoupled quantities. The heavy mass m_h is the $\overline{\text{MS}}$ mass.

4.3.3 Higher-Order Corrections

With the effective theory matched, we are ready to discuss higher order corrections to the Higgs production cross section. In the HTL the cross section was computed up to N³LO in the literature [31, 48, 17, 49]. Here, we will briefly recapitulate the NLO calculation, as it nicely illustrates the methods introduces in section 2.2.

We start with the computation of the hard scattering amplitudes. At NLO we require the one-loop Higgs-gluon form factor, and the tree-level amplitudes for $q\bar{q} \to Hg$, $qg \to Hq$, and $gg \to Hg$.

The careful reader might wonder why we do not have to compute the $q\bar{q} \to H$ amplitude. The reason is, that these amplitudes will be zero to all orders. Indeed, the corresponding amplitude would be of the form

$$\mathcal{M}_{q\bar{q}\to H} = i\frac{\alpha_s}{\pi}\bar{v}(p_2)\left[\cdots\right]u(p_1)\delta_{c_1 c_2}\frac{1}{v}\mathcal{C}_{q\bar{q}H}, \tag{4.67}$$

where the dots indicate an a priori unknown number of γ-matrices. But since there is no external vector field, the γ-matrices must be fully contracted. The only available objects to contract a γ-matrix with, are either another γ-matrix, or the momenta p_1 or p_2. Contractions among the γ-matrices can always be reduced by applying the anti-commutation relations provided by the Clifford algebra of the γ-matrices. Afterwards, we are left only with contractions with p_1 or p_2. These on the other hand vanish in Eq. (4.67) because of the equation of motion.

The virtual contributions to the cross sections are obtained by evaluating the Feynman diagrams in Fig. 4.4. The result is the NLO correction to the Higgs-gluon form factor in the HTL and reads

$$\mathcal{C}(0) = \frac{1}{3}\left\{1 + \frac{\alpha_s}{\pi}\left(-\frac{m_H^2 + 0^+}{\mu^2}\right)^{-\epsilon}\left(-\frac{3}{2}\frac{1}{\epsilon^2} + \frac{11}{4} + \frac{\pi^2}{8}\right)\right\} \tag{4.68}$$

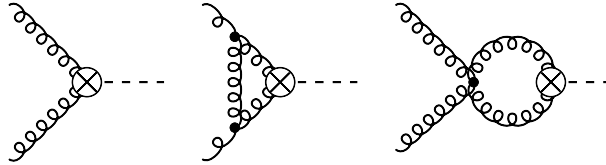Using Eq. (4.11) for the partonic $gg \to H$ cross section, we then find

Figure 4.4: One-loop corrections to the Higgs-gluon form factor. The first diagram contributes through the NLO Wilson coefficient.

$$\hat{\sigma}_{gg\to H} = \frac{\pi}{576v^2}\xi\left(\frac{\alpha_s}{\pi}\right)^2\delta(1-\xi)$$
$$\times\left[\left(1 + \epsilon + \mathcal{O}(\epsilon^2)\right) + \frac{\alpha_s}{\pi}\left(\frac{m_H^2}{\mu^2}\right)^{-\epsilon}\left(-\frac{3}{\epsilon^2} - \frac{3}{\epsilon} + \frac{5}{2} + \frac{7\pi^2}{4} + \mathcal{O}(\epsilon)\right) + \mathcal{O}(\alpha_s^2)\right] \tag{4.69}$$
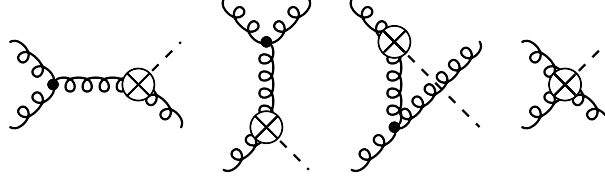
Figure 4.5: Feynman diagrams for the real radiation corrections in the gluon-gluon channel.

where we defined ξ as the of the Higgs mass over the partonic center of mass energy

$$\xi = \frac{m_H^2}{s} = \frac{m_H^2}{\tau S}. \tag{4.70}$$

As expected, the NLO partonic cross section is not finite on its own, because the IR divergences only cancel in inclusive observables. We must therefore also compute the real radiation corrections as well as the contributions from collinear renormalization. For the former, we evaluate the diagrams in Fig. 4.5 and obtain the averaged squared amplitude

$$\overline{|\mathcal{M}_{gg \to Hg}|^2} = \frac{1}{N_A^2 4(1-\epsilon)^2} \frac{\alpha_s^3}{v^2} \left(\frac{32}{3\pi}\right) \left[(1-2\epsilon) \frac{m_H^8 + s^4 + t^4 + u^4}{stu} + \frac{\epsilon}{2} \frac{\left(m_H^4 + s^2 + t^2 + u^2\right)^2}{stu} \right], \tag{4.71}$$

where N_A is the dimension of the adjoint representation, i.e. $N_A = N^2 - 1$ for $SU(N)$ groups. The symbols s, t and u denote the usual *Mandelstam variables*. Since the Mandelstam variables are not completely independent, as they must satisfy

$$s + t + u = m_H^2, \tag{4.72}$$

the squared matrix element only depends on the final state momenta through t or u. The phase-space integral is $2*d$ dimensional. We can reduce one of the d dimensional integrals via the momentum conserving delta function. Using spherical coordinates and the remaining two delta functions which ensure on-shellness of the Higgs and the final state gluon, we can carry out the energy and momentum magnitude integral explicitly. This is particularly simple in the center of mass frame. We are hence left with an integral over the $\mathcal{S}_1^{d-2}$ sphere. If we now apply the recursion relation

$$\int_{\mathcal{S}_1^{d-2}} = \int \mathrm{d}\cos\theta \, \sin^{d-4}\theta \int_{\mathcal{S}_1^{d-3}}, \tag{4.73}$$

and use that the amplitude only depends on the azimuthal angle, i.e. the scattering angle of the Higgs (or gluon), we can carry out the integral over the $\mathcal{S}_1^{d-3}$ sphere explicitly. In the end the phase-space integral is a single one-dimensional integral

$$\text{P.S.} = \frac{1}{8\pi} \frac{1}{\Gamma(1-\epsilon)} \left(\frac{s}{\mu^2 e^{\gamma_E}}\right)^{-\epsilon} (1-\xi)^{1-2\epsilon} \Theta(1-\xi) \int_0^1 \mathrm{d}\omega \, \omega^{-\epsilon}(1-\omega)^{-\epsilon}, \tag{4.74}$$

where ω is related to the scattering angle of the Higgs via

$$\omega = \frac{1 + \cos\theta}{2}. \tag{4.75}$$

The amplitude in Eq. (4.71) is proportional to $1/tu$, i.e. it diverges if the final state gluon becomes collinear to one of the initial state gluons. Consequently, we expect the appearance of

poles once we perform the phase-space integration. Indeed, we find after a straightforward integration

$$\hat{\sigma}_{gg \to Hg} = \frac{1}{576\pi^2} \frac{\alpha_s}{v^2} (1 - \xi)^{-1-2\epsilon} \left(\frac{s}{\mu^2} \right)^{-\epsilon} \Theta(1 - \xi)$$

$$\times \left[-\frac{3}{\epsilon} \left(1 + \xi^4 + (1 - \xi)^4 \right) - \frac{11}{2} (1 - \xi)^4 - 6(1 - \xi + \xi^2)^2 + \epsilon \left(\frac{3\pi^2}{2} - 6 + (1 - \xi) \cdot (\cdots) \right) \right].$$

$$(4.76)$$

The cross section also has a soft singularity at $\xi \to 1$, which can be regulated by applying the distributional identity in Eq. (2.57). The $\mathcal{O}(\epsilon)$ terms proportional to $(1 - \xi)$ we only hinted at in Eq. (4.76) will hence not contribute as they are only integrated together with the delta function $\delta(1 - \xi)$. The final result then reads

$$\hat{\sigma}_{gg \to Hg} = \frac{1}{576\pi^2} \frac{\alpha_s^3}{v^2} \left(\frac{s}{\mu^2} \right)^{-\epsilon} \Theta(1 - \xi) \left\{ \left[\frac{3}{\epsilon^2} + \frac{3}{\epsilon} + 3 - \frac{3\pi^2}{4} \right] \delta(1 - \xi) \right.$$

$$- \frac{6\xi}{\epsilon} \left[\frac{\xi}{(1 - \xi)_+} + \frac{1 - \xi}{\xi} + \xi(1 - \xi) \right] (1 + \epsilon) - \frac{11}{2} (1 - \xi)^3 \qquad (4.77)$$

$$\left. + 6 \left(\frac{\log(1 - \xi)}{1 - \xi} \right)_+ \left[1 + \xi^4 + (1 - \xi)^4 \right] \right\}.$$

The poles proportional to the delta function $\delta(1 - \xi)$ exactly cancel between real (4.77) and virtual contributions (4.11). The remaining divergences should cancel after coupling and collinear renormalization. According to Eq. (2.38), the additional contribution from collinear renormalization is

$$\hat{\sigma}_{gg \to Hg}^C = 2 \times \frac{\alpha_s}{2\pi} \frac{1}{\epsilon} \int_0^1 dz \, P_{gg}^{(0)}(z) \hat{\sigma}_{gg \to H}(zs) = \frac{1}{576\pi^2} \frac{\alpha_s^3}{v^2} \frac{1}{\epsilon} \xi P_{gg}(\xi)(1 + \epsilon). \qquad (4.78)$$

With the definition of the splitting kernel in Eq. (2.39), we see that the remaining poles in the real radiation contribution are indeed canceled. The additional pole introduced by the collinear renormalization is finally canceled by the charge renormalization. Gathering the fruits of our labor, we determined that the inclusive partonic cross section at NLO reads

$$\hat{\sigma}_{gg \to HX} = \frac{\alpha_s^2}{576\pi v^2} \Theta(1 - \xi) \left\{ \delta(1 - \xi) \right.$$

$$+ \frac{\alpha_s}{\pi} \left[\delta(1 - \xi) \left(\pi^2 + \frac{11}{2} \right) - \frac{11}{2} (1 - \xi)^3 + 6 \left(1 + \xi^4 + (1 - \xi)^4 \right) \left(\frac{\log(1 - \xi)}{1 - \xi} \right)_+ \qquad (4.79) \right.$$

$$\left. \left. + \xi P_{gg}(\xi) \log \left(\frac{s}{\mu^2} \right) \right] \right\}$$

We can carry out the same analysis for the $q\bar{q}$ and qg channel. The Feynman diagrams are depicted in Fig. 4.6. The amplitude for $q\bar{q} \to Hg$ does not exhibit any collinear or soft divergences, rendering collinear renormalization unnecessary. The result for the cross section reads

$$\hat{\sigma}_{q\bar{q} \to Hg} = \frac{1}{486\pi^2} \frac{\alpha_s^3}{v^2} \Theta(1 - \xi)(1 - \xi)^3. \qquad (4.80)$$
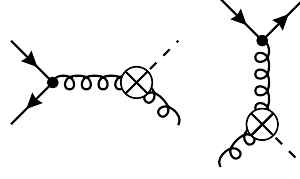
Figure 4.6: Feynman diagrams contributing to the $q\bar{q}$ (left) and qg (right) channel of the Higgs production cross section.

The qg-channel on the other hand has a collinear divergence when the final state quark becomes collinear to the initial state quark. After collinear renormalization we find for the cross section

$$\hat{\sigma}_{qg \to Hg} + \hat{\sigma}^C_{qg \to Hg} = \frac{\alpha_s^3}{576\pi^2 v^2} \Theta(1 - \xi)$$
$$\times \left\{ (1 - \xi) \frac{3\xi - 7}{3} + \frac{1}{2}\xi P_{gq}(\xi) \left[1 + \log\left(\frac{s}{\mu^2}\right) + 2\log(1 - \xi) \right] \right\}.$$
$$(4.81)$$
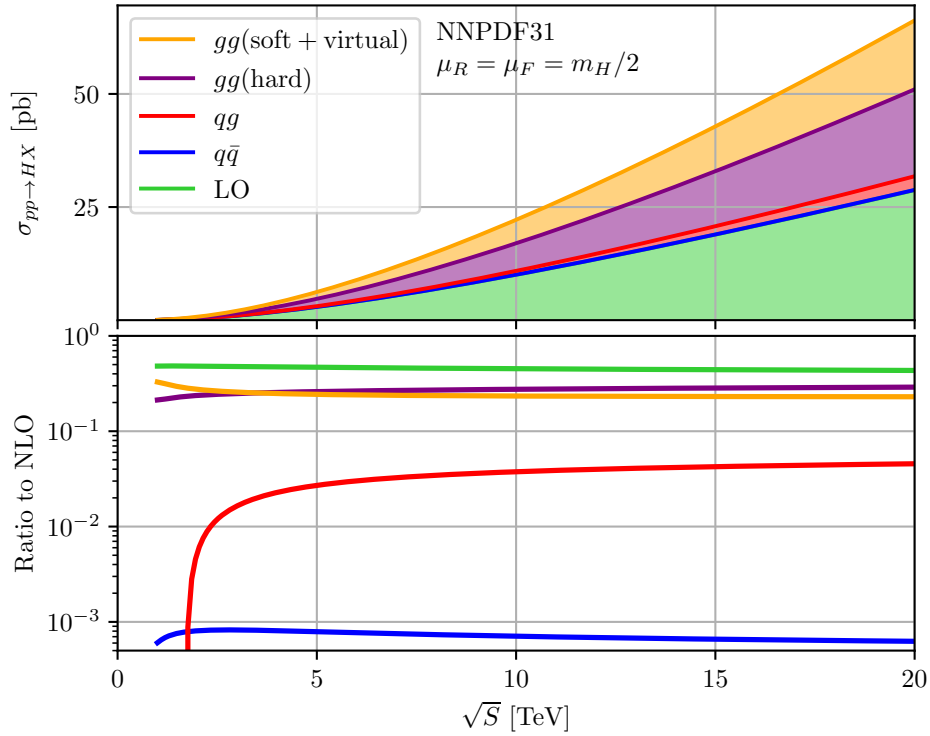
Figure 4.7: Hadronic cross section as function of the hadronic center of mass energy. The total cross section is partinioned into its various channels. The channel denoted "soft + virtual" collects the leading terms of the threshold expansion around $(1 - \xi)$ in Eq. (4.79), that is all terms proportional to $\delta(1 - \xi)$ and irreducible plus distributions. The lower plot shows the ratio of the various channels to the leading order cross section. Computational setup is described in the conventions.

After convolution of the partonic cross section with the partonic luminosity we get the hadronic cross section, which is displayed in Fig. 4.7 as a function of the hadronic center of mass energy. The cross section is split into the various channels. The "soft + virtual" channel denotes all

contributions which originate from integrating the delta function $\delta(1 - \xi)$ and irreducible plus distributions, i.e. terms of the form

$$\left(\frac{f(\xi)}{1 - \xi}\right)_{+} \mathcal{O}\big((1 - \xi)^0\big) \tag{4.82}$$

At NLO, it only comes from gluon-induced Higgs production (4.11).

The majority of the hadronic cross section is due to a gluon-gluon initial state, making up more than 95% over the full spectrum of energies. Roughly half of this contribution comes from LO. The other half is composed, yet again of roughly two equal parts, the "soft + virtual" contribution and the remaining real radiation part. The quark-gluon initial state has the second largest impact, whereas the quark-quark induced Higgs production is completely negligible, contributing below 1‰. The large suppression of the $q\bar{q}$ channel is almost entirely due to the reduced partonic luminosity of the channel. Indeed, from Fig. 2.3, we see that the $q\bar{q}$ flux is roughly 30 times smaller than the qg one. This is also the order of magnitude of the ratio of the qg and $q\bar{q}$ induced Higgs production cross section.

The gluon-gluon and quark-gluon luminosity on the other hand is rather similar, especially close to the production threshold, where most of the contributions to the cross section comes from, since larger values are suppressed by $\mathcal{L}/\tau$. Yet we observe that quark-gluon-channel contribution is almost an order of magnitude smaller than in the gluon-gluon channel. To investigate the origin of this suppression, we can look at the coefficient of the logarithm $\log(\mu^2)$ which is predetermined by the RGE

$$\frac{\partial \hat{\sigma}_{qg \to Hq}}{\partial \log \mu^2} = -\frac{\alpha_s}{2\pi} \int_0^1 \mathrm{d}\xi \, P_{gq}(\xi) \hat{\sigma}_{gg \to H}, \quad \frac{\partial \hat{\sigma}_{gg \to Hg}}{\partial \log \mu^2} = -2 \times \frac{\alpha_s}{2\pi} \int_0^1 \mathrm{d}\xi \, P_{gg}(\xi) \hat{\sigma}_{qg \to H}. \tag{4.83}$$

At the threshold, the ratio quark-gluon to gluon-gluon logarithmic coefficients is thus $C_F/(4C_A) = 1/9$, which is also roughly the ratio we observed in their contribution to the cross section. The origin of the suppression, is thus partly due to the difference in the color factor and the additional combinatorial factors in the gluon-gluon channel.

Since the NLO corrections are of the same magnitude as the LO cross section, the perturbative result is not yet reliable. One would need to go to even more loops and higher multiplicities in the hope to reach perturbative convergence.

4.3.4 Phenomenological Application

Having discussed the HTL at length, it is important to investigate how well the approximation works for phenomenological applications. In Fig. 4.8, we show the relative error of the cross section in the HTL compared to the results with a finite quark mass for different powers of α_s in the various partonic channels.

At LO, the HTL underestimates the cross section by around 6.5%. In the HTL, the Higgs-gluon form factor, is accurate up to power corrections of order $z = m_H^2/4m_t^2 \approx 13\%$, so the observed accuracy of the approximation aligns with our expectations. For radiative corrections, $m_H^2/m_t^2 \approx 52\%$ is the more natural expansion parameter and the quark-gluon as well as the quark-quark channel show, that they are indeed only roughly 50% accurate.

The gluon-gluon channel on the other hand shows a remarkable property: the accuracy of the HTL stays quite constant across perturbative orders in α_s. In our opinion, this feed is
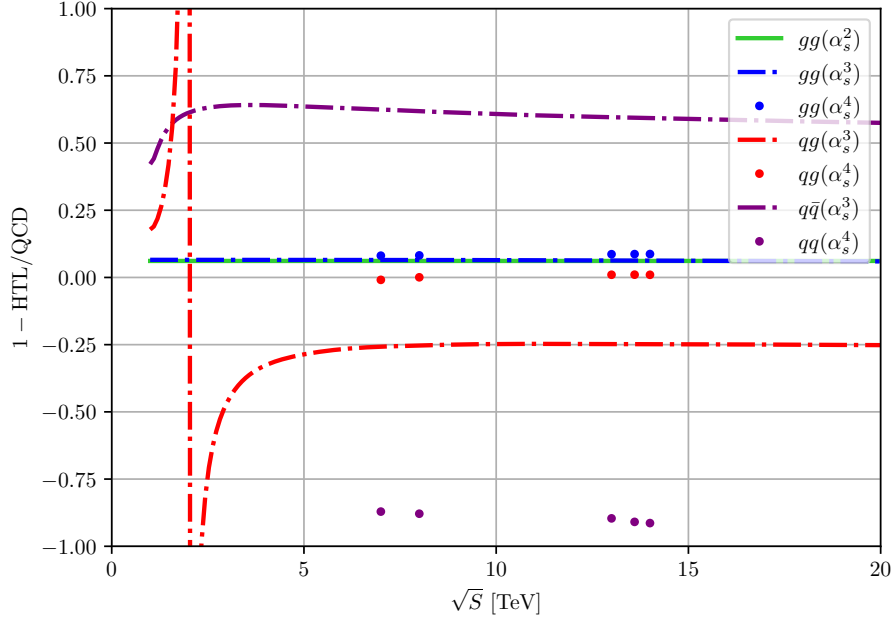
Figure 4.8: Relative error of the HTL compared to the results with finite top-quark mass for various center of mass energies. Displayed are contributions to the cross section in each partonic channels. The computational setup is described in the conventions. The methods to compute the NNLO results with finite top-quark mass are described in chapter 5.

explained by the fact, that much of the structure of the perturbative corrections is dictated by lower orders, and that, for this channel in particular, these kinds of corrections turn out to be numerically large. Indeed, we can apply *Catani's I operator* [50] to predict the poles, as well as the overall factor $(-m_H^2/\mu^2)^{-\epsilon}$, of the Higgs-Gluon form factor in Eq. (4.68). So the part of the partonic cross section which is derived from LO reads

$$
\hat{\sigma}_{gg\to H}\Big|_{\propto \sigma_{gg\to H}^{(0)}} = \frac{\pi}{576 v^2}\xi\left(\frac{\alpha_s}{\pi}\right)^2 \delta(1-\xi)
$$
$$
\times \left[\left(1+\epsilon+\mathcal{O}(\epsilon^2)\right) + \frac{\alpha_s}{\pi}\left(\frac{m_H^2}{\mu^2}\right)^{-\epsilon}\left(-\frac{3}{\epsilon^2}-\frac{3}{\epsilon}-3+\frac{3\pi^2}{2}+\mathcal{O}(\epsilon)\right)+\mathcal{O}\left(\alpha_s^2\right)\right].
$$
(4.84)

Numerically, the finite part is largely dominated by the π^2 term which originated from the analytic continuation of the Sudakov (double) logarithm. The analytic continuation needed at time-like momentum transfer thus causes a large logarithm. The logarithm on the other hand stems from a soft gluon exchange in the loop.

For the real radiation cross section, we can once again already anticipate initial state collinear as well as the soft divergences

$$
\hat{\sigma}_{gg\to Hg} = \frac{1}{576\pi^2}\frac{\alpha_s}{v}(1-\xi)^{-1-2\epsilon}\left(\frac{s}{\mu^2}\right)^{-\epsilon}\Theta(1-\xi)
$$
$$
\times \left[-\frac{1}{\epsilon}\xi(1-\xi)P_{gg}^{(0)}(\xi)\frac{2(-1+2\epsilon)\Gamma(-\epsilon)}{\Gamma(3-2\epsilon)}+(1-\xi)^2\cdot(\cdots)\right].
$$
(4.85)

The $(1-\xi)^2$ terms, which we denoted by $(\cdots)$ are finite and regular in the soft limit $\xi\to 1$. We know, that there cannot be any terms of order $(1-\xi)$ apart from those in the splitting function, because every term in the matrix element (4.71) which is constant in the soft limit,

still has collinear divergences in the phase-space. I.e. all next to soft contributions are captured in the splitting function. In fact, if we compare with the cross section in Eq. (4.76), then we see that the actual lowest order term is even $(1 - \xi)^4$.

The partonic luminosity together with the factor $1/\tau$ cause a strong enhancement of the phase-space region close to the threshold $\xi \to 1$ or $\tau \to m_H^2/S$. Therefore, the hadronic cross section will be well approximated by convoluting the inclusive cross section

$$
\hat{\sigma}_{gg \to HX}\Big|_{\propto \sigma_{gg \to H}^{(0)}} = \frac{\alpha_s^2}{576\pi v^2}\Theta(1-\xi)\bigg\{\delta(1-\xi)
$$
$$
+ \frac{\alpha_s}{\pi}\bigg[\delta(1-\xi)\pi^2\left(\frac{3}{4} + \mathcal{O}(1/\pi^2)\right) + 6\left(1 + \xi^4 + (1-\xi)^4\right)\left(\frac{\log(1-\xi)}{1-\xi}\right)_+
$$
$$
+ \xi P_{gg}(\xi)\log\left(\frac{s}{\mu^2}\right)\bigg]\bigg\}. \tag{4.86}
$$

Numerically, we find that the approximation is around 90% accurate at NLO. The main deviations are caused by the soft-virtual channel. We can therefore expect to see deviations in the rescaling factor

$$
r^{\mathrm{N}^n\mathrm{LO}} = \frac{\sigma_{pp \to HX}^{\mathrm{QCD,N}^n\mathrm{LO}}}{\sigma_{pp \to HX}^{\mathrm{HTL,N}^n\mathrm{LO}}} \tag{4.87}
$$

across perturbative orders of the order of $10\% \times z \approx 1\%$. **TODO:** Add reference to results for finite top-quark masses.

Strictly speaking, our discussion was limited to NLO. However, we claim that most of the arguments are transferable to higher orders in perturbation theory. Indeed, the factor π^2 from analytic continuation can be included to all order by resumming the Sudakov logarithm we encountered [51],i.e. the driving contribution is indeed proportional to the born cross section. This procedure is also sometimes referred to as π^2-*resummmation*. At high orders of perturbation theory, it was demonstated [49], that the quality of the resummation deteriorates, that mean that the Sudakov logarithms are no longer the driving contributor to the soft-virtual contribution. We can therefore expect to see larger deviations from the exact rescling at higher orders. Similarly, our discussion on how to obtain the leading coefficients of the threshold expansion by requiring cancelation of initial-state collinear divergences can also be transferred to higher order [52]. At N^{3}LO, one can correctly predict the three leading logarithms $\log^{5,4,3}(1-\xi)$.

We can leverage the small corrections on the rescaling parameter to improve the HTL cross section results by rescaling the HTL results by

$$
\sigma_{pp \to HX}^{\mathrm{rHTL,N}^n\mathrm{LO}} = r^{\mathrm{LO}}\sigma_{pp \to HX}^{\mathrm{HTL,N}^n\mathrm{LO}}, \tag{4.88}
$$

where the superscript "rHTL", now refers to the *rescaled heavy top limit*. Since the gluon-gluon channel is the dominant production channel and the rescaling factor remains quite constant across the perturbative orders, the rHTL cross section will yield a good approximation ($\sim 1\%$) for the Higgs production cross section[6].

---

6 Excluding the effects from light quark masses.

4.4 THEORY STATUS

Having analyzed the gluon-gluon fusion Higgs production cross section at LO, and NLO in the HTL. We are now equipped with all concepts to discuss state-of-the-art theory predictions.

As already mentioned, the most precise theoretical predictions come from N^3LO cross sections in the HTL [53, 49]. They apply the method of reverse unitarity (see section 2.2.3) to perform the phase-space integration fully analytically. The cross section is calculated in terms of a deep expansion in the threshold parameter $(1 - \xi)$

$$\hat{\sigma}_{ij \to HX} = \delta_{ig}\delta_{jg}\hat{\sigma}_{\text{SV}} + \sum_{n=0}^{N} c_{ij}^{(n)}(1 - \xi)^n, \qquad (4.89)$$

where $\hat{\sigma}_{\text{SV}}$ is the leading term, the soft-virtual contribution we already encountered. The soft-virtual contribution has been calculated in Ref. [54]. Because the partonic luminosity is concentrated heavily around the threshold region, one would expect, to see good convergence of the hadronic cross section. Indeed, Ref. [53] computed the first 37 terms of the threshold expansion found that the hadronic cross section is already well approximated by the first five terms.

In the meantime, results without reliance on the threshold expansion have become available [55], confirming the expected accuracy of the threshold expansion and shifting the total cross section by around +0.10 pb at 13 TeV.

In Fig. 4.9 we show the results for the gluon-gluon fusion cross section in the rHTL at various perturbative orders as a function of the hadronic center of mass energy.
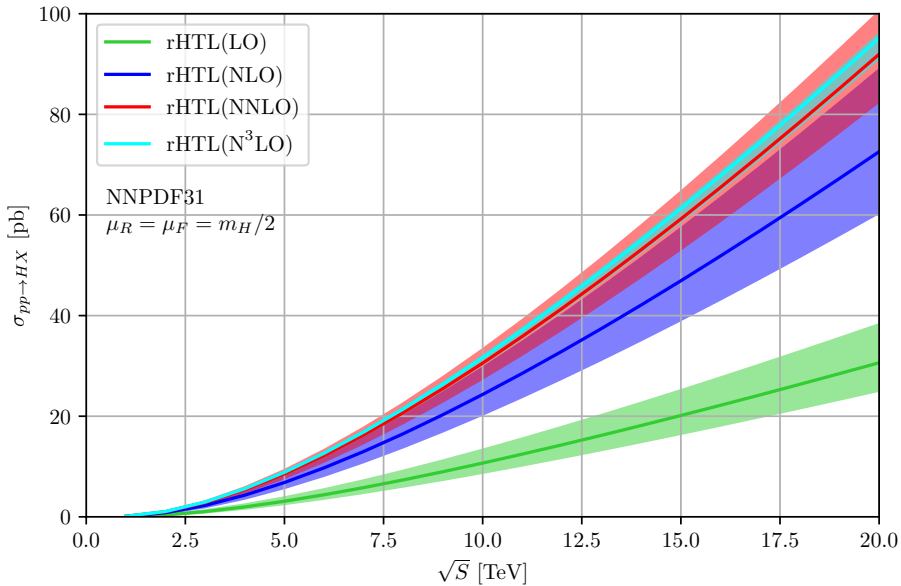
Figure 4.9: Gluon-gluon fusion hadronic cross section as a function of the center of mass energy. Displayed are results computed in the rHTL at various perturbative orders. Transparent bands indicate the scale uncertainty calculated by variation of μ_R in the range $[m_H/4, m_H]$. The computational setup is described in the conventions. The plot was created with the help of SusHi [56, 57].

As we discussed before, the NLO cross section is about twice as large as predicted in the Born approximation. NNLO corrections are still sizeable, contribution roughly 20% to the cross section. The NLO scale uncertainties underestimate the effect of higher orders, as the central NNLO cross section is outside the previous uncertainty bands. Only when we go to N^3LO do we see perturbative convergence and corrections consistent with the previous scale uncertainty bands. The scale uncertainties at this order are below 4% for the displayed collision energies.

At this level of precision, it becomes important to investigate other sources of uncertainty and perform a careful evaluation of their impact on the cross section. The most important sources are

- The Scale Uncertainties,

- The PDF uncertainties,

- Uncertainties related to electroweak corrections,

- Uncertainties related to finite top-quark masses,

- Uncertainties related to light quarks.

In the following we will discuss them one-by-one.

4.4.1 Scale Uncertainties

Scale uncertainties serve as an estimate of missing higher order corrections. They are typically computed by 7-point-scale variation, that means the cross section is evaluated at a central scale μ and the additional 6 points $(\mu_R, \mu_F) = (\mu/2, \mu/2), (\mu/2, \mu), (\mu, \mu/2), (2\mu, \mu), (\mu, 2\mu), (2\mu, 2\mu)$. The envelope of the cross section at the seven points then form the scale uncertainty. Since the renormalization and factorization scale is unphysical, physical observables like the cross section are in principle independent of the scales. However, as we are truncating the pertubative series at some fixed order, we are left with some residual dependence of the scale. The scale dependence is therefore a good indicator of missing higher orders. Even so, at low orders the scale uncertainties cannot always be trusted as Fig. 4.9 illustrates nicely.

Fig. 4.10 shows the functional dependence of the hadronc cross section on the renormalization and factorization scale for various perturbative orders. We see that there is very little dependence on the factorization scale, i.e. the vast majority of the scale uncertainties derive from the variation of renormalization scale. This also justifies, why the scale uncertainties in Fig. 4.9 are computed with a fixed factorization scale. We also observe that the dependence on the scale nicely stabilizes as we increase the perturbative precision. For the central scale, $\mu_R = \mu_F = m_H/2$ has become the de facto standard for the inclusive cross section and is also the recommendation of the Higgs Working Group [58]. The observed functional dependence in Fig. 4.10 supports this choice, as the N^3LO corrections are minor at this scale and the cross section is particularly flat in this regime. It should be noted, that the miniature dependence on the factorization scale is only observed for the total cross section. If instead, we are considering individual production channels, the functional dependence remains very large, because the DGLAP equations mix the quark and gluon PDFs.

The scale uncertainties can be further reduced by including higher order corrections. Although full N^4LO predictions are still beyond the current state-of-the-art in computational capabilities, we can predict at least some parts of the higher order corrections.
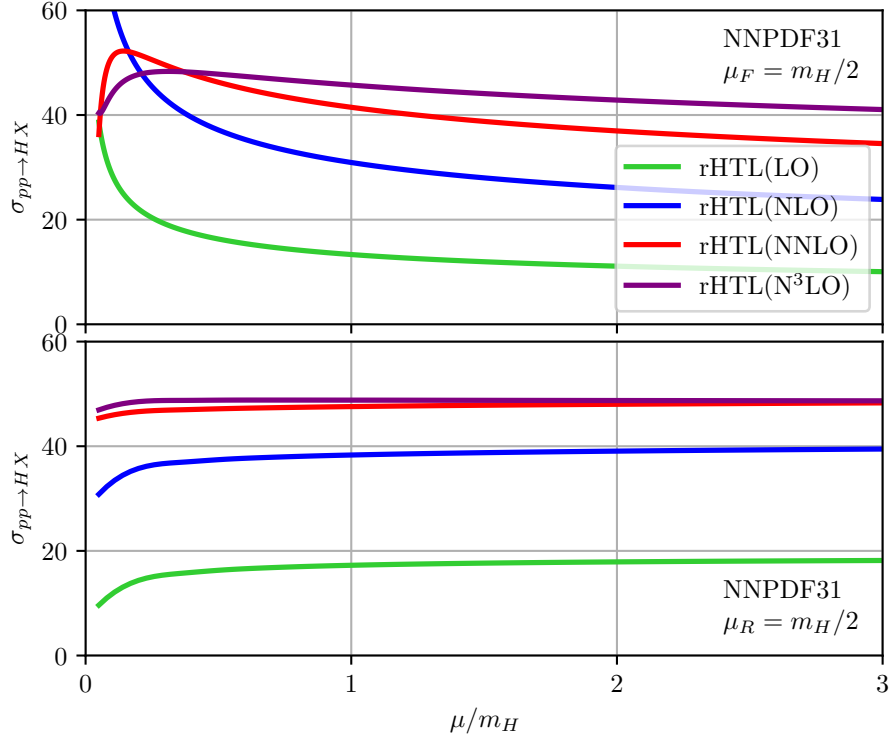
Figure 4.10: Hadronic cross section as a function of the renormalization scale (top panel) and factorization scale (bottom panel). The respective other scale is kept fixed at $m_H/2$. The computational setup is described in the conventions. The plot was created with the help of SusHi [56, 57].

Results in the soft-virtual approximation

Since the partonic luminosity is sharply peaked around the threshold (see Fig. 2.3) $\xi \to 1$ or alternatively $\tau \to m_H^2/S$, we can get a good approximation of the hadronic cross section, by expanding the partonic cross section around the threshold as seen in Eq. (4.89). The leading term, i.e. the soft-virtual approximation has been already been computed up to 3 loops [59] in the HTL. Furthermore, as we discussed in section 4.3.4, the cancelation of initial state collinear divergences can be leveraged to determine the leading 3 logarithms of the first subleading term. This means that at $\mathrm{N}^4\mathrm{LO}$ we can predict the coefficients of the logarithms[7]

$$\log^{7,6,5}(1 - \xi) \tag{4.90}$$

in $c_{ij}^{(0)}$. This is especially important to stabilize the factorization scale dependence, since otherwise we would introduce an additional contribution to the cross section which is only present in one channel, the gluon-gluon channel, which would scale with running of the PDFs.

At the central scale of $\mu_R = \mu_F = m_H/2$, the partial $\mathrm{N}^4\mathrm{LO}$ results shift the cross section by around -0.1%. Scale uncertainties are reduced from around 4% to below 2.5%. The systematic uncertainty coming from the truncation of the threshold expansion is estimated by comparing the full cross section results with the soft-virtual approximation at lower order, and rescaling the error to the $\mathrm{N}^4\mathrm{LO}$ correction. The error is estimated to be well below 1% of the total cross section. **TODO:** This seems very large. Ask Gotam!

---

7 In fact one can also get parts of the $\log^4(1 - \xi)$ coefficient.

Threshold Resummation

The threshold logarithms appearing in $c_{ij}^{(0)}$ can actually by resummed to all orders. The Hadronic cross section can be cast into the form

$$\sigma(N) = \sum_{ij} f_i(N, \mu_F) f_j(N, \mu_F) \hat{\sigma}_{ij}(N, \mu_R, \mu_F), \tag{4.91}$$

where we switched from τ-space to N-space by means of a *Mellin transform*

$$\sigma(N) = \int_0^1 \mathrm{d}\tau \, \tau^{N-1} \frac{\sigma(\tau)}{\tau}. \tag{4.92}$$

In N-space, also called *Mellin space*, the threshold region $\tau \to m_H^2/S$ corresponds to the limit $N \to \infty$. In this limit, it can be shown [60, 61, 62, 63], that the partonic cross section satisfies the resummed form

$$\hat{\sigma}_{ij}(N) = \delta_{ig}\delta_{jg}\hat{\sigma}_{gg \to H}^{\mathrm{LO}} C_{gg} \exp[\mathcal{G}_H(\log N)] + \mathcal{O}(1/N). \tag{4.93}$$

C_{gg} collects all constant contributions for $N \to \infty$ and can therefore be extracted from lower orders in the large N limit. $\mathcal{G}_H$ contains the threshold logarithms, which get resummed by exponentiation. It requires the cusp anomalous dimension, known today at four-loop accuracy [64], which enables the computation of full N³LO + next-to-next-to-next-to-leading logarithm cross section results. The results[8] [49] show, that at the central scale, the fixed and resummed cross section is nearly identical. This can be interpreted as additional validation of our scale choice. Additionally, it confirms the N⁴LO soft virtual approximation, which also found that the corrections at the central scale are very close to zero.

π^2-Resummation

In section 4.3.4, we showed that the soft-virtual contribution to the cross section is dominated by a Sudakov logarithm at time-like momentum transfer. This fact can be exploited to predict numerically large coefficients at higher orders and ultimately can be used perform an all order resummation, sometimes referred to as π^2-resummation [51].

Since the logarithm stems from a soft gluon exchange, we can apply techniques from *soft-collinear effective theory* (SCET) [65, 66] to map the Higgs-gluon form factor to a Wilson coefficients of SCET. In SCET we integrate out all the hard modes, such that we can approximate

$$G_{\mu\nu}^a G^{a\,\mu\nu} \longrightarrow C_S(-q^2)(-q^2)g_{\mu\nu}\mathcal{A}_{n\perp}^{a\,\mu}\mathcal{A}_{\bar{n}\perp}^{a\,\nu}, \tag{4.94}$$

where $\mathcal{A}_{n\perp}^{\mu\,a}$ and $\mathcal{A}_{\bar{n}\perp}^{a\,\nu}$ are effective, gauge invariant operators representing gluons traveling along the light-like directions n and $\bar{n}$ defined by the momenta of the incoming hadrons. q^2 is the square of the momentum of the operator and C_S is the Wilson coefficient. The Higgs-gluon form factor in SCET, and hence the leading logarithmic contribution to the full Higgs-gluon form factor is then simply given by **TODO:** Why?

$$\mathcal{C}(0)\Big|_{\mathrm{SCET}} = C_S(-m_H^2 - i0^+), \tag{4.95}$$

which we can use to match the Wilson coefficient

$$C_S(Q^2) = 1 + \frac{\alpha_s}{4\pi} C_A \left(-\ln^2\left(\frac{Q^2}{\mu^2}\right) + \frac{\pi^2}{6} \right). \tag{4.96}$$

---

8 The authors of that reference use a Padé approximation for the four-loop cusp anomalous dimension, as the full result was still unknown at that point in time. They claim that the approximation is highly accurate.

The key benefit of working in the SCET framework, is that we can now apply RGE methods. Indeed, the Wilson coefficient satisfies the RGE

$$\frac{\mathrm{d}C_S}{\mathrm{d}\ln\mu} = \left[\Gamma^A_{\mathrm{cusp}} \ln \frac{Q^2}{\mu^2} + \gamma^S\right] C_S,\tag{4.97}$$

where Γ^A_{cusp} is the cusp anomalous dimension of Wilson lines with light-like segments in the adjoint representation, and γ_S is the anomalous dimension of the operator. The solution of the differential equation, therefore automatically yields a resummed expression of the Higgs-gluon form factor. The solution can be written in terms of the recursive equation

$$|C_S(-m_H^2)|^2 = U(m_H^2)|C_S(-m_H^2)|^2,$$

$$\text{with} \qquad \ln U(m_H^2) = \frac{\alpha_s(m_H^2)}{\pi} \frac{C_A \pi^2}{2} \left\{ 1 + \frac{\alpha_s(m_H^2)}{4\pi} \left[C_A \left(\frac{67}{9} - \frac{\pi^2}{3} \right) - T_F n_l \frac{20}{9} \right] + \mathcal{O}(\alpha_s^2) \right\}.\tag{4.98}$$

We see that the leading π^2 term matches our findings in Eq. (4.84).

The resummation drastically improves results at low order of perturbation theory. However, at higher orders, the quality of the resummation deteriorates. This indicates, that at these orders the factors of π^2 are no longer dominant. The procedure should therefore **not** be used to "improve" the N^{3}LO cross sections.

4.4.2 PDF Uncertainties

All results presented so far, where computed using NNLO PDF sets, including all N^{3}LO cross section results. This creates a mismatch between the hard scattering matrix elements and the PDFs, and the cross sections predictions do in fact not entirely have N^{3}LO accuracy. The reason for applying PDF sets at NNLO accuracy is the lack thereof at N^{3}LO.

PDFs are usually fitted to experimental data and then evolved to the desired scale using the DGLAP equation (2.44). To achieve N^{3}LO accuracy, we therefore require

1. hard scattering amplitudes the PDFs can be matched to,

2. and the N^{3}LO splitting functions for the DGLAP evolution.

Regarding the first point, the exact N^{3}LO coefficient function for *deep-inelastic scattering* in the massless limit are known for a long time [67, 68, 69, 70, 71, 72], whereas massive coefficient functions are only available in approximation frameworks [73, 74]. Furthermore, N^{3}LO predictions for charged- and neutral-current *Drell-Yan* production are also available, both for the total [75, 76, 77] and for differential cross sections [78, 79]. These processes are especially valuable for the matching of the PDFs, since there are experimentally very clean.

In Mellin space, the DGLAP equation (2.44) transforms from an integral-differential equation to just a partial differential equation

$$\frac{\partial f_{H,i}}{\partial \log \mu} = -\gamma_{ij}(N, \alpha_s(\mu)) f_{H,j}(N, \mu),\tag{4.99}$$

where $\gamma_{ij}(N, \alpha_s)$ is related to the Mellin transform of the splitting functions

$$\gamma_{ij}(N, \alpha_s(\mu)) = -\frac{\alpha_s}{\mu} \int_0^1 \mathrm{d}x\, x^{N-1} P_{ij}(x, \alpha_s(\mu)).\tag{4.100}$$

Much progress has been made in evaluating specific moments of the splitting functions [80, 81, 82, 83, 84, 85, 86]. Additionally, parts of the splitting functions can be predicted through resummation techniques at low Bjorken-x, a leading logarithmic [87] and next-to-leading logarithmic [88, 89, 90] accuracy. Very recently, all splitting amplitudes were computed fully analytical by Mistlberger et al. [91], these describe the limit of amplitudes in which two of the external partons become collinear. It represents one important ingredient of the splitting kernel.

Although the evolution kernel are not yet fully known, the ingredients we do have can be still be used to at least construct an approximate N³LO PDF set. Results for such PDF sets were recently published by the MSHT [92] as well as the NNPDF [93] collaboration, which were then combined in Ref. [94]. They use the available data for deep-inelastic scatteing and Drell-Yan production to fit the PDFs. For the running they use (most of) the known Mellin moments of the splitting kernels and smoothly interpolate between them.

In Fig. 4.11 and Tab. 4.1, we compare the gluon-gluon fusion rHTL cross section results at N³LO computed with different approximate N³LO PDF sets. The NNPDF40_an3lo_as_01180_mhou
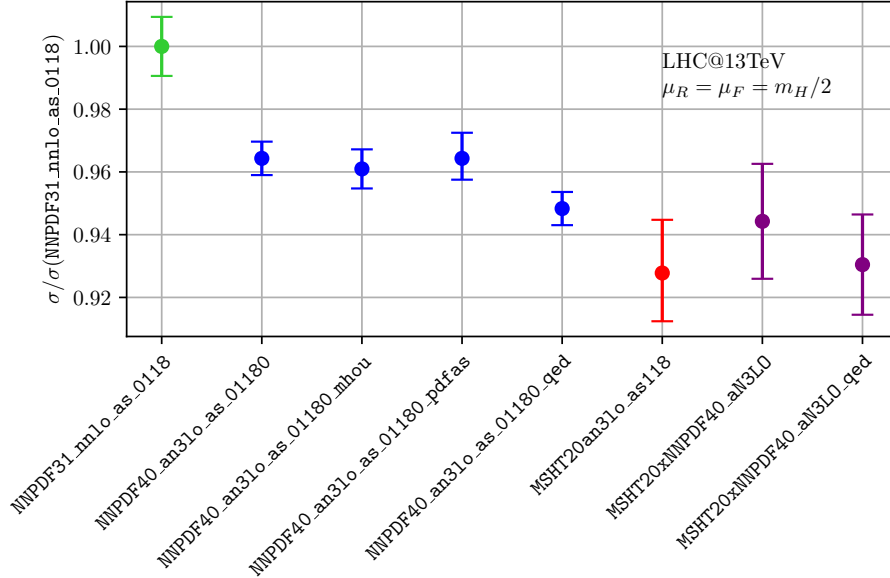
Figure 4.11: Gluon-Gluon fusion cross section in the rHTL at N³LO for various PDF sets normalized by the cross section computed with the NNPDF31_nnlo_as_0118 PDF set. The provided uncertainties only include the PDF uncertainties. The uncertainty of the normalization is not propagated. The computational setup is described in the conventions. Results were computed using iHixs 2 [95].

includes *missing higher order uncertainties*. This encompasses the scale uncertainties of the hard scattering matrix elements the PDFs are fitted to, and estimates of the omitted terms in the incomplete N³LO splitting kernels. In the NNPDF40_an3lo_as_01180_pdfas PDF set, the replicas are created with different values of α_s between $\alpha_s(m_Z) = 0.117$ and 0.119, in order to estimate the α_s uncertainties. PDF sets ending with "_qed", also include corrections from quantum electrodynamics (QED).

PDF	$\sigma_{gg \to HX}$ [pb]
NNPDF31_nnlo_as_0118	48.8 ± 0.46
NNPDF40_an3lo_as_01180	47.06 ± 0.26
NNPDF40_an3lo_as_01180_mhou	46.90 ± 0.30
NNPDF40_an3lo_as_01180_pdfas	$47.06^{+0.40}_{-0.33}$
NNPDF40_an3lo_as_01180_qed	46.28 ± 0.26
MSHT20an3lo_as118	$45.28^{+0.83}_{-0.75}$
MSHT20xNNPDF40_aN3LO	46.08 ± 0.89
MSHT20xNNPDF40_aN3LO_qed	45.41 ± 0.78

Table 4.1: Gluon-Gluon fusion cross section in the rHTL at N^{3}LO for various PDF sets. The provided uncertainties only include the PDF uncertainties. The computational setup is described in the conventions. Results were computed using `iHixs 2` [95].

Before the publication of aN^{3}LO PDF sets, the uncertainty due to the mismatch of the PDF was estimated through lower orders rescaled to N^{3}LO

$$\delta(\text{PDF} - \text{th}) = |\sigma_{gg \to HX}^{\text{NNLO,NNLO PDF}} - \sigma_{gg \to HX}^{\text{NNLO,NLO PDF}}| \times \left(\frac{\sigma_{gg \to HX}^{\text{N}^3\text{LO}}}{\sigma_{gg \to HX}^{\text{NNLO}}} - 1 \right). \qquad (4.101)$$

For the `NNPDF31_nnlo_as_0118` PDF set at 13 TeV, this uncertainty turns out to be close to 1%. However, from Fig. 4.11, we can see that with this approach the impact of the N^{3}LO PDFs is severely underestimated, as the results computed with the aN^{3}LOPDFs is shifted by around 4-6%.

We can also see that the different approaches followed by the `NNPDF` and `MSHT` collaboration, yield central values which are not compatible within the uncertainty bands. Furthermore, the PDF-uncertainty estimates differ by around a factor of three.

Provided that the provided missing higher order uncertainties are accurate, the approximations of the splitting kernel seems to be very accurate, effecting the cross sections only on the level of 1‰.

The α_s-uncertainties, make up about half of the total PDF uncertainty, as visible from the error increase between the `NNPDF40_an3lo_as_01180` and `NNPDF40_an3lo_as_01180_pdfas` PDF set.

The inclusion of QED effects shifts the cross section by around -0.6 pb at 13 TeV.

Because of considerably sized difference between the PDFs of the collaboration, we advise to use the combined PDF sets. We estimate the α_s and missing higher order uncertainties with the `NNPDF` PDF sets and rescale them by

$$\frac{\delta(\text{MSHT20xNNPDF40\_aN3LO})}{\delta(\text{NNPDF40\_an3lo\_as\_01180})} \approx 3.5, \qquad (4.102)$$

where $\delta(\text{PDF})$ is the PDF uncertainty of the total cross section.

4.4.3 Electroweak Corrections

Besides the discussed QCD corrections, we can also consider electroweak corrections. These are generally suppressed because of the smaller coupling constant $\alpha(m_Z) \approx 1/127$, but the percentage level precision of our predictions makes an investigation of electroweak effects indispensable.

The electroweak corrections to the LO QCD partonic cross section can be classified into two categories: the light-quark contributions and the top-quark contributions. The top-quark
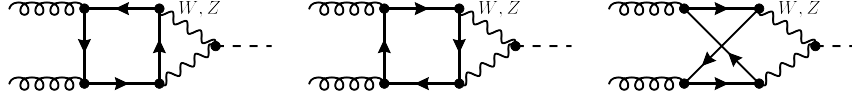
Figure 4.12: Light quark contribution to the LO electroweak corrections of the gluon-gluon fusion Higgs production cross section.
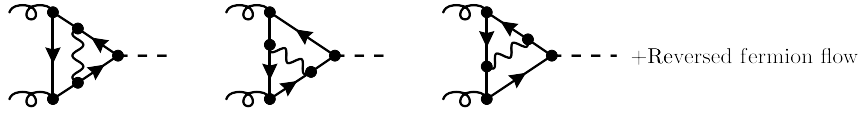
Figure 4.13: Top quark contribution to the LO electroweak corrections of the gluon-gluon fusion Higgs production cross section. The wavy line represents all electroweak gauge bosons (γ, W, Z).

contribution contains a Yukawa-coupling of the top, and the light quark contributions contains all the remaining diagrams. The respective diagrams are depicted in Fig. 4.12 and 4.13. Real radiative electroweak corrections like those depicted in Fig. 4.14, do not contribute to the cross section, since two diagrams which only differ by the direction of the fermion flow exactly cancel. Even though the preconditions are not strictly met this can be shown analogous to *Furry's theorem*[9].
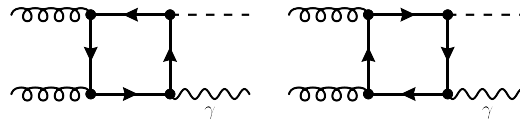
Figure 4.14: Example Feynman diagrams of radiative electroweak corrections to the gluon-gluon fusion Higgs production cross section. The remaining Feynman diagrams four diagrams can be obtained by permutation of external gluon, photon and Higgs. Two diagrams which differ only by the direction of the fermion flow exactly cancel.

The two-loop light-quark contribution to the Higgs-gluon form factor was calculated in Ref. [96]. The top-quark contribution was then worked out in Refs. [97, 98, 99]. The latter reference also includes the effect from finite bottom quark masses, including diagrams in which we encounter flavor changes due to a W-boson exchange. The leading electroweak corrections increase the

---

9 Furry's theorem states that the abelian part of the sum of two diagrams that differ only by the direction of a closed fermion vanishes, if there are an odd number of vertices proportional to the γ-matrices. In the present case, the color factor $\delta^{c_1 c_2}$, i.e.fully abelian. There is an even number of vertices, however one of the vertices is a Yukawa interaction and hence does not introduce a γ-matrix. It is easy to show that with these conditions, Furry's theorem still applies.

LO cross section by around 5%. Almost the entirety of this correction is due to the light-quark contribution.

Beyond LO in α_s, the hadronic cross section was first estimated at $\mathcal{O}(\alpha_s^3\alpha)$ using the HTL and also treating the massive vector bosons as infinitely heavy [100]. Furthermore, since the top-quark contribution was negligible at LO, the authors only considered light-quark contribution to the cross section. With this approximation, the electroweak corrections can be incorporated through a modification of the Wilson coefficient

$$
\begin{aligned}
C_1 = {} & \left[\frac{\alpha_s}{4\pi}C_1^{(0)} + \left(\frac{\alpha_s}{4\pi}\right)^2 C_1^{(1)} + \mathcal{O}(\alpha_s^3)\right] \\
& + \frac{\alpha}{4\pi}\left[\frac{\alpha_s}{4\pi}C_{1,w}^{(0)} + \left(\frac{\alpha_s}{4\pi}\right)^2 C_{1,w}^{(1)} + \mathcal{O}(\alpha_s^3)\right].
\end{aligned}
\tag{4.103}
$$

One then finds for the electroweak coefficient

$$
\begin{aligned}
C_{1,w}^{(0)} &= -\frac{2}{\sin^2\theta_W\cos^2\theta_W}\left[\frac{5}{4} - \frac{7}{3}\sin^2\theta_W + \frac{22}{9}\sin^4\theta_W\right] - \frac{4}{\sin^2\theta_W}, \\
C_{1,w}^{(1)} &= C_{1,w}^{(0)}\frac{14}{3}.
\end{aligned}
\tag{4.104}
$$

The same contribution was later reevaluated in the limit of massless electroweak gauge bosons [101], as well as in the soft-gluon approximation [102]. Even though, the approximations make completely different assumptions about the mass spectrum, the phenomenological results turn out to be quite similar, increasing the NLO cross section between 5.4 and 5.2%. This shows, that the cross section is not very sensitive to the mass of the vector bosons.

Still, results without relying on approximations would be highly desirable and were recently provided by Ref. [103]. The results found that the electroweak corrections increase the NLO cross section by around 5.1%, confirming that the previous approximations were indeed accurate. The $\mathcal{O}(\alpha_s^3\alpha^2)$ QCD predictions are rescaled to order $\mathcal{O}(\alpha_s^5\alpha^2)$ using the rHTL with electroweak corrected Wilson coefficients (see Eq. (4.103)). The electroweak corrections increase the N³LO rHTL cross section by $4.6 \pm 0.6\%$. By far the dominating error of this contribution comes from missing higher order uncertainties. Errors related to the omission of the top-quark contribution, finite quark-mass effects, or partonic channels at $\mathcal{O}(\alpha_s^3\alpha^2)$ make up less than 0.1%.

4.4.4   Finite Top-Quark Mass Effects

So far our discussion of perturbative corrections was mainly focused on the HTL approximation. In section 4.3.4, we explained how the approximation can be improved to also encompass some finite top-quark mass effects by means of rescaling the cross sections. We argued that in the dominating gluon-gluon channel especially, the rHTL appromixation will be highly accurate. Nevertheless, we also saw significant deviations, in particular for the other partonic channels, which might yield important corrections to the rHTL cross section.

This makes the higher order corrections with finite top-quark mass indispensable. The LO calculation with finite top-quark masses presented in section 4.2 was extended to NLO in Refs. [104, 105]. Later, power corrections to the HTL of the form $\mathcal{O}(m_H^4/m_t^4)$ became available at NNLO [106, 107, 108]. Still, a residual theoretical uncertainty of about 1% of the total cross

channel	$\sigma_{\text{rHTL}}^{\text{NNLO}}$ [pb] $\mathcal{O}(\alpha_s^2) + \mathcal{O}(\alpha_s^3) + \mathcal{O}(\alpha_s^4)$	$(\sigma_t^{\text{NNLO}} - \sigma_{\text{rHTL}}^{\text{NNLO}})$ [pb] $\mathcal{O}(\alpha_s^3)$	$\mathcal{O}(\alpha_s^4)$	$(\sigma_t^{\text{NNLO}} - \sigma_{1/m_t}^{\text{NNLO}})$ [pb] $\mathcal{O}(\alpha_s^4)$
	$\sqrt{S} = 8\,\text{TeV}$			
gg	$7.39 + 8.58 + 3.88$	$+0.0353$	$+0.0879$	-0.047
qg	$0.55 + 0.26$	-0.1397	-0.0153	$+0.001$
qq	$0.01 + 0.04$	$+0.0171$	-0.0191	-
total	$7.39 + 9.14 + 4.18$	-0.0873	$+0.0535$	-0.046
	$\sqrt{S} = 13\,\text{TeV}$			
gg	$16.30 + 19.64 + 8.76$	$+0.0345$	$+0.2431$	-0.145
qg	$1.49 + 0.84$	-0.3696	-0.0408	$+0.015$
qq	$0.02 + 0.10$	$+0.0322$	-0.0501	-
total	$16.30 + 21.15 + 9.70$	-0.3029	$+0.1522$	-0.130

Table 4.2: Comparison of cross sections computed in the rHTL (σ_{rHTL}), the cross section with finite top-quark masses (σ_t), and the cross section computed with power corrections (σ_{1/m_t}) at NNLO. The computational setup is described in the conventions. Exact results were extracted from Ref. [109]. The power corrections were computed using `iHixs 2` [95]. The quark-quark channel is not yet available with power corrections, which is why we do not include it in the above table. The channel is suppressed by the PDFs, i.e. the total cross section will be left almost unaffected.

section persisted. Only with the computation of the exact top-quark mass dependence of the NNLO cross section [109] could the uncertainty be eliminated.

The main results of that reference are displayed in Tab. 4.2 (also see Fig. 4.8). We also compare the cross sections with exact top-quark mass dependence with the m_H/m_t expansion. We see that the finite-top-quark-mass effects are small ($< 0.4\%$). In the gluon-gluon channel the rHTL works exceptionally well, approximating the NNLO cross section with percent-level accuracy. Again we expect this kind of accuracy on the basis of the rescaling procedure. In the other partonic channels the approximation works significantly worse, showing deviations of up to 19%. The sheer dominance of the gluon-gluon channel assures that the total cross section is approximated well by the rHTL.

The power corrections m_H^4/m_t^4 power corrections to the HTL do not significantly improve the rHTL, but they do get the order of magnitude as well as the sign right.

The residual theoretical uncertainty of the finite-top-quark-mass effects can be estimated from the scale uncertainty of difference $\sigma_t - \sigma_{\text{rHTL}}$, taking into account all correlations. Alternatively, one may proceed as suggested by the *Higgs Working Group*[10] (HWG) [58] and estimate the uncertainty based on lower orders, rescaled to the N³LO cross section. At NNLO, this turns out to be less than 0.1‰ of the total cross section and is hence completely negligible. Since it is σ_t, not the difference of $\sigma_t - \sigma_{\text{rHTL}}$, which scales approximately with the rHTL cross section, we do not belive that this is an appropriate estimate of the error, and we will estimate the uncertainty based on the 7-point scale variation going forward.

---

10 In the 2016 version of the HWG recommendations, they simply assign an uncertainty of 1$ to the missing finite top quark mass effects at NNLO. With the publication of full NNLO cross sections with exact top-quark mass dependence, the theoretical uncertainty will be estimated similarly to what is described here in the upcoming update of the HWG recommendations.

Since the perturbative series of the cross section is truncated at some fixed order, it will have some residual renormalization scheme dependence. The scheme-dependence of the cross section was investigated in Ref. [49] and by us in Ref. [4]. The difference between the on-shell and $\overline{\text{MS}}$ scheme was found to be less than 1‰ of the total cross section, rendering also the uncertainty on the scheme dependence completely negligible.

4.4.5   Effect of Light Quarks

In section 4.2, we investigated to what extent light quarks effect the gluon-gluon fusion Higgs production cross section at LO. Here, we found that the main contribution arises from the interference with top-quark induced Higgs production. The inclusion of the bottom quark lowered the cross section by around 11% at 13 TeV. The next-heavy quark—the charm—further reduced the cross section, this time by 1.9%.

Since perturbative corrections are typically quite large in gluon-gluon fusion, it is once again vital to also compute higher order corrections to the interference. The NLO cross section for arbitrary quark masses was computed in Ref. [105].

Once again, we estimate the theoretical uncertainty for missing higher orders based the assigned scale uncertainties. The HWG, instead suggests estimating the uncertainty based on lower orders and rescale them to the N³LO correction in the rHTL. Since the light-quark-mass effects are not expected to scale with the cross section of the rHTL, we do belive that this is not reliable estimate of the uncertainty and do not apply them going forward.
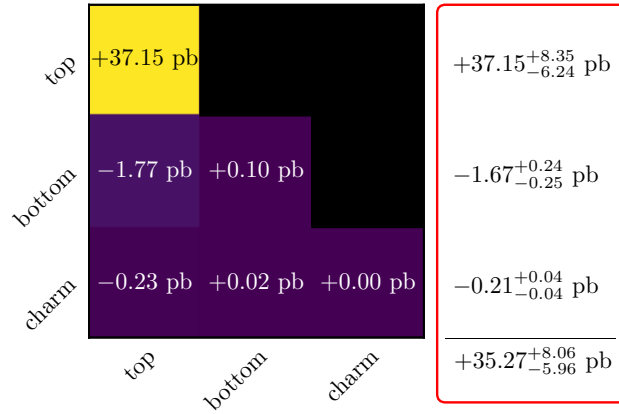
Figure 4.15: σ_i (diagonals) and $\sigma_{i \times j}$ (off-diagonals) at NLO for the three heaviest quark flavors at a hadronic center of mass energy of 13 TeV. The red box indicates the sum of each row, and hence the combined effects of each additional flavor. The computational setup is described in the conventions. We use the on-shell scheme for the top-quark mass and the $\overline{\text{MS}}$ scheme for the charm- and bottom-quark masses. The scale uncertainties are computed using 7-point variation.

The NLO results for the pure-flavor and the interference effects are displayed in Fig. 4.15. We see that the top-bottom interference contribution to the cross section increased in magnitude by 65% from LO to NLO. We once again observe that the top-bottom interference contribution is by far the most important one among the light quarks. All other light-quark mass effects are still within the scale uncertainty of the top-bottom contribution. Improving these contributions beyond NLO is therefore completely unnecessary. Interestingly, we observe that the scale

uncertainties of the pure-top and the top-bottom contribution are almost perfectly anti-correlated.

With the scale uncertainty, we can estimate that effects due to missing higher orders of the light-quark contribution to be of the order of 7‰. However, this estimate is too naïve. Indeed, if we choose a different renormalization scheme for the bottom quark mass, say the on-shell mass, the top-bottom interference contribution at NLO becomes (again at $\sqrt{S} = 13$ TeV)

$$\sigma_{t\times b} = -2.42^{+0.19}_{-0.12} \text{ pb},\qquad(4.105)$$

which differs from our previous $\overline{\text{MS}}$ renormalized cross section contribution by -0.66 pb or 38%. The large discrepancy between the results is somewhat expected, since the hard scattering amplitude in the high energy limit roughly scales with m_b^2 (see Eq. (4.10)) and the relation between the on-shell and the $\overline{\text{MS}}$ bottom-mass converges very poorly [110, 111]. Therefore, the cross section can only show a good perturbative convergence in one of the schemes if any. At NLO, we have not determined enough coefficients of the perturbation series to make a reliable argument about the convergence, making higher order predictions indispensable. If we assign the error in a way to encompass both the on-shell- and $\overline{\text{MS}}$-renormalized results, it will constitute a 1.7% uncertainty on the total cross section, making it one of the leading sources of uncertainty.

Eliminating this source of uncertainty by computing higher order corrections to the top-bottom interference contribution is one of the major aims of this PhD thesis. With these predictions we want to investigate the perturbative convergence in the different mass-renormalization schemes.

The cross sections presented in this section were all computed in the 5FS, i.e. the bottom- and charm-quark were considered massless and could appear in the initial state. Since the hard scattering matrix element vanishes for massless particles, we then proceeded to set the light quark masses to non-vanishing values in all closed quark loops which couple to the Higgs[11]. This ad hoc introduction of quark masses has become the de facto standard for light-quark mass effects in gluon-gluon fusion, but well grounded justifications of this procedure have been lacking so far. With this PhD thesis we want to close this gap, and explore the validity of this massification procedure by comparing the results of top-bottom-interference contributions to the same but computed in the 4FS, in which the quark-masses are treated consistently.

4.4.6 Differential Cross Sections

Up to this point our the main focus of our discussion has been the total cross section of the gluon-gluon fusion channel. However, differential cross sections can shine some light on the production kinematics of the Higgs and additionally offer a plethora of rich phenomenology and experimental applications. In this section, will briefly summarize the current status on differential cross sections of Higgs production in the gluon-gluon fusion channel. The possibilities to study the Higgs production cross section in terms of its kinematics are endless, so our discussion is by no means complete, instead we will focus on the most phenomenologically relevant distributions.

---

11 We will later show that this method indeed ensures gauge-invariant IR-safe cross sections.

The Higgs-p_T Distribution

Arguably the most important distribution is the Higgs-p_T distributions

$$\frac{\mathrm{d}\sigma_{pp\to HX}}{\mathrm{d}p_T}, \tag{4.106}$$

where p_T is the transverse momentum of the Higgs with respect to the beam axis. p_T-distributions have been calculated up to third order in perturbation theory using the rHTL [112, 113], including subsequent decays to photons [114] and leptons [115]. The rHTL only provides as a good approximation of the cross section up to $p_T \sim m_H$. For larger p_T, the distribution is well described by a power law, which can be understood with a simple dimensional analysis. Indeed, at large p_T, the transverse momentum is the dominant scale, and we can neglect the top-quark mass. In order to match the mass dimension, -3, of the differential partonic cross section $\mathrm{d}\sigma_{pp\to HX}/\mathrm{d}p_T$, we require the scaling behavior

$$\frac{\mathrm{d}\hat{\sigma}_{ij\to HX}}{\mathrm{d}p_T} \sim p_T^{-3}. \tag{4.107}$$

In the rHTL on the other hand, the coupling constant is proportional to $1/v^2$ and hence has a non-vanishing mass dimension. The large p_T scaling of the partonic cross section is therefore

$$\frac{\mathrm{d}\hat{\sigma}_{ij\to HX}^{\mathrm{rHTL}}}{\mathrm{d}p_T} \sim v^{-2}p_T^{-1}. \tag{4.108}$$

Consequently, the ratio of the hadronic cross section in the rHTL and the exact theory must satisfy

$$\frac{\mathrm{d}\sigma_{pp\to HX}^{\mathrm{rHTL}}}{\mathrm{d}p_T} \Big/ \frac{\mathrm{d}\sigma_{pp\to HX}}{p_T} \sim p_T^2/v^2 \tag{4.109}$$

at $p_T \gg m_H$. **TODO:** This argument is to naïve. Indeed, if we neglect all quark masses in the HEL, then the scattering matrix element becomes zero because the scalar Higgs coupling causes a helicity flip which must then be compensated by a mass (see discussion after Eq. (4.8)). This means that in the full theory, the cross section must be proportional to m_t^2. This scale must be compensated somehow, probably by some $1/m_H^2$ but I can't say where this comes from.. The inclusion of finite top quark mass effects is therefore of immense importance especially at large p_T and has been studied up to NNLO in Refs. [116, 117, 118].

At smaller transverse momentum $p_T \sim m_H/2$ we can resolve the effects of the lighter quark masses. This is particularly interesting, because it demonstrates that this region is sensitive to the Yukawa coupling of the light quarks [119, 120]. In a recent study by the CMS collaboration [121], the authors fitted experimental data to the Higgs-p_T spectrum and could indirectly determine the following constraints on the coupling modifiers

$$-1.2 < \kappa_b < 1.1, \qquad -4.9 < \kappa_c < 4.8. \tag{4.110}$$

The effect of light quark masses on the Higgs-p_T spectrum has been studied up to NNLO in Refs. [122, 123, 124, 4].

At LO and in all virtual corrections, the Higgs is produced with vanishing p_T, because there is no other final state particle, the Higgs could recoil against. The LO and all virtual corrections, will therefore only contribute to the zero-bin of the distribution. The transverse momentum hence acts as a slicing parameter. Consequently, at small transverse momentum, the cross section will receive large logarithmic enhancements because the cut-off threshold acts an

IR regulator. These logarithms cancel in the exact cross section, but due to the truncation of the perturbative series, fixed order results still suffer from their appearance and yield inaccurate results whenever these logarithms become dominant. To stabilize the behavior in these phase-space regions, the logarithms can be resummed to all orders [125, 116, 126, 127, 128, 129, 130, 131].

The Higgs-Rapdity Distribution
The Higgs rapidity is defined as

$$\eta_H \equiv \frac{1}{2} \ln \frac{p_H^0 + p_H^3}{p_H^0 - p_H^3}, \qquad (4.111)$$

where p_H is the momentum of the Higgs, and the z-axis aligns with the beam direction. The rapidity is an inclusive observable, meaning that all contributions, be it real or virtual can contribute to any bin of the distribution. Consequently, the respective distribution will not show any logarithmic enhancements that require resummation as we saw for the p_T-distribution.

The Higgs-rapidity distribution has been calculated up to N³LO in the HTL [132, 133]. The effect of finite top-quark masses has been studied at NNLO in Ref. [131]. The effect of finite bottom quark masses on the other hand was recently presented by us [4] and will be discussed in this PhD thesis.

5 | COMPUTATIONAL DETAILS

Our final goal is clear now: We want to investigate the effect of finite top- and bottom-quark masses on the Higgs production cross section, both on the inclusive and the differential cross section level. In particular, we want to study the impact of the mass renormalization scheme on the cross section to eliminate one of the main remaining uncertainties of the cross section. Furthermore, in addition to the commonly used 5FS, we want to explore the impact of alternative FSs to assess the validity of the treatment of light quark masses in the 5FS.

In this chapter, we will describe the necessary methods for computing the Higgs production cross section with full top- and bottom-quark mass dependence at NNLO.

5.1 COMPUTING THE AMPLITUDES

The base ingredients of the calculation are the scattering amplitudes. In addition to the LO amplitude for $gg \to H$ presented in section 4.2 and the NLO amplitudes computed in Ref. [105], we require amplitudes for the following partonic processes

- Real-Real Corrections (One-loop):
  1. $gg \to Hgg$
  2. $gg \to Hq\bar{q}$
  3. $q\bar{q} \to Hq'\bar{q}'$
  4. + processes related by crossing symmetry

- Real-Virtual Amplitudes (Two-loop):
  1. $gg \to Hg$
  2. $q\bar{q} \to Hg$
  3. + processes related by crossing symmetry

- Virtual-Virtual Amplitudes (Three-loop):
  1. $gg \to H$.

In the following, we discuss the computation of each element one-by-one.

In this section, we are exclusively working in the 5FS. The necessary modifications for adapting the amplitudes to the 4FS will be presented in section 5.3. When working in the 5FS, the bottom-quark mass is generally zero. Since this would imply that the total top-bottom interference contribution is vanishing, one then sets the mass to its actual value inside all closed quark loops that couple to the Higgs. Therefore in Feynman diagrams like those depicted in Fig. 5.3, the bottom quark is treated as massive, but if the top- and bottom-quark are

exchanged, the bottom quark mass is set to zero. With a massification prescription like this, it is essential to verify that gauge invariance and IR safety are not lost in the process.

The proof that it is not proceeds by the replica technique. Consider the SM but only with the following quark content: n_b identical copies of the bottom quark, $n_{b'}$ massless quarks b' serving as our massless bottom quark, and the top-quark. Without the inclusion of electroweak effects this theory is equivalent to QCD with the addition of a Yukawa interaction to the Higgs; ergo this theory is gauge invariant and free of IR-divergences. Furthermore, gauge invariance and IR-safety also hold for each individual Yukawa coupling contribution (Y_t or Y_b) and each power of n_b and $n_{b'}$, as these are arbitrary parameters from the point of QCD. This means that the parts of the amplitude which are proportional to $Y_t n_b$ are separately gauge invariant, and so are the parts which are proportional to $Y_b n_b n_{b'}$, and so on. Examples of Feynman diagrams contributing to a selection of Y_t, Y_b, n_b and $n_{b'}$ power-combinations are depicted in Fig. 5.1. Likewise, after squaring, the contribution $Y_t Y_b n_{b'} n_b$ is going to be separately IR finite.
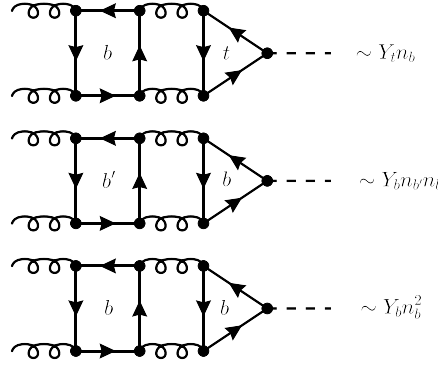
Figure 5.1: Example Feynman diagrams and their scaling with the Yukawa coupling, n_b, and $n_{b'}$.

We have thus shown, that contributions with a massive bottom-quark loop which does **not** couple to the Higgs does not mix gauge dependent terms or IR divergences with the selected contribution from our massification procedure.

5.1.1 The Real-Real Corrections

The real-real corrections only contain a single loop, with either a top or a bottom quark running in the loop. Examples of different Feynman diagrams for various partonic channels are depicted in Fig. 5.2.
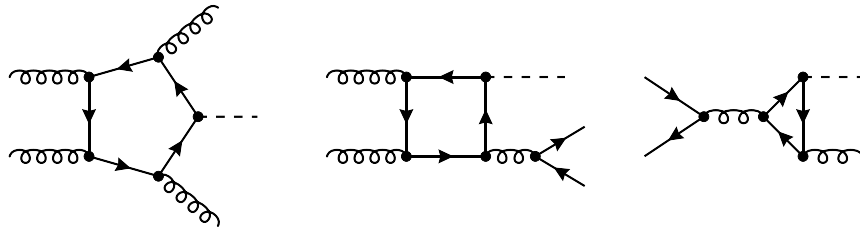
Figure 5.2: Example Feynman diagrams for one-loop real-real corrections in various partonic channels.

As one-loop amplitudes, they can be computed numerically with publically available libraries like `Recola` [134]. However, the real-real corrections often represent the bottleneck of the computation of the phase-space integrals, which makes an efficient evaluation of the amplitudes desirable. We therefore instead use the analytic form of the amplitude computed in Ref. [135]. We use the implementation of the amplitudes provided by `MCFM` [136, 137, 138], which in turn uses `QCDLoop` [139, 140] for the evaluation of one-loop integrals.

We found that with the analytic expressions, the evaluation time of the amplitudes is sped up by a factor of 20 compared to the numerical evaluation in `Recola`.

5.1.2 The Real-Virtual Corrections

For the real-virtual corrections we, for the first time encounter Feynman diagrams with two different mass scales running in the loop. Fig. 5.3 shows all (up to inversion of the fermion flow inside the triangle loops) Feynman diagrams with two internal quark loops. We observe,
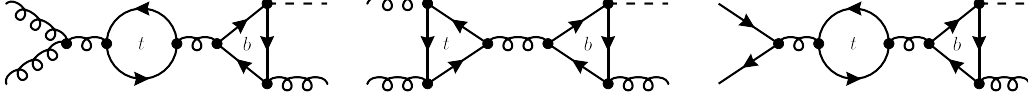
Figure 5.3: Feynman diagrams for the two-loop real-virtual corrections with two massive quarks. Amplitudes for the $qg \to Hq$ channel can be obtained via crossing from the $q\bar{q} \to Hg$ amplitudes. Triangle loops with reversed fermion flow are not explicitly shown. The external gluons must be accounted for with all permutations which render a different Feynman diagrams. In the 5FS, the bottom-quark is always coupling to the Higgs.

that all two-loop integrals actually factorize into two separate one-loop integrals making them quite straight-forward to solve.

The contributions to the scattering amplitude containing only a single massive quark involve genuine two-loop integrals. Fig. 5.4 shows a selection of contributing Feynman diagrams. Two loop integrals, especially non-planar ones, with three mass scales are very challenging
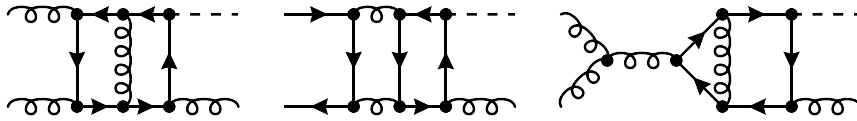
Figure 5.4: Example Feynman diagrams for the two-loop real-virtual corrections with a single massive quark in various partonic channels.

to compute analytically, even with state-of-the-art methods, and as of today the analytic computation of these amplitudes are still unknown, however approximations for a nearly massless bottom quark have been calculated relatively recently [141, 142]. We therefore decided to instead evaluate the appearing two-loop integrals numerically at fixed phase-space points and interpolate between them during the phase-space integration.

In any case, for both the one-mass and two-masses contribution we first have to reduce the amplitude to form factors. To make possible symmetries more apparent, we cross the radiated parton to the initial state, i.e. we consider the amplitudes

$$g(p_1) + g(p_2) + g(p_3) \longrightarrow H(p_4), \qquad \bar{q}(p_1) + q(p_2) + g(p_3) \longrightarrow H(p_4). \tag{5.1}$$

Projection to Form Factors

We can factor out the external polarization vectors, spinors and color factors to rewrite the amplitudes in terms of their amputated counterpart

$$\mathcal{M}_{ggg \to H} = \mathcal{M}_{\mu\nu\rho} \epsilon_1^\mu \epsilon_2^\nu \epsilon_3^\rho f^{c_1 c_2 c_3}, \qquad \mathcal{M}_{\bar{q}qg \to H} = \bar{v}(p_1) \mathcal{M}_\rho u(p_2) \epsilon_3^\rho T_{c_1 c_2}^{c_3}. \tag{5.2}$$

After squaring the amplitude and summing over the color of the external partons, we get the color factors

$$f^{c_1 c_2 c_3} f^{c_1 c_2 c_3} = C_A N_A = 24, \qquad T_{c_1 c_2}^{c_3} T_{c_2 c_1}^{c_3} = C_F N_c = 4. \tag{5.3}$$

It is convenient, to choose polarization vectors which are cyclically transverse to the external momenta, i.e.

$$\epsilon_1 = \epsilon(p_1; p_2), \quad \epsilon_2 = \epsilon(p_2; p_3), \quad \epsilon_3 = \epsilon(p_3; p_1), \tag{5.4}$$

where the second argument indicates the gauge vector. We can then propose the form factor decomposition of the amplitudes

$$\mathcal{M}^{\mu\nu\rho} = g^{\mu\nu} p_2^\rho F_1 + g^{\mu\rho} p_1^\nu F_2 + g^{\nu\rho} p_3^\mu F_3 + p_3^\mu p_1^\nu p_2^\rho F_4,$$

$$\bar{v}(p_1) \mathcal{M}^\rho u(p_2) = \bar{v}(p_1) \left[\not{p}_3 p_1^\rho - (p_1 \cdot p_3) \gamma^\rho \right] u(p_2) G_1 + \bar{v}(p_1) \left[\not{p}_3 p_2^\rho - (p_2 \cdot p_3) \gamma^\rho \right] u(p_2) G_2. \tag{5.5}$$

We used the Ward identity, to restrict the tensor coefficients in $\mathcal{M}^\rho$. $\mathcal{M}^{\mu\nu\rho}$ also satisfies Ward identity.

The tensor coefficients span a vector space with respect to the scalar product

$$\langle a_{\mu_1, \cdots \mu_{n_g}} | b^{\mu_1, \cdots \mu_{n_g}} \rangle \equiv \sum_{\text{pol.}} a_{\mu_1 \dots \mu_{n_g}}^* \left[\prod_i^{n_g} \epsilon_i^{*\mu_i} \epsilon_i^{\nu_i} \right] b_{\nu_1 \dots \nu_{n_g}} \tag{5.6}$$

where n_g is the number of external gluons, i.e. $n_g = 3$ for $ggg \to H$ and $n_g = 1$ for $\bar{q}qg \to H$ and the summation is performed over the polarizations of all external particles. The tensor coefficients hence form a—not necessary orthonormal—basis.

Any vector can be written as a linear sum over basis vectors

$$|v\rangle = \sum_i v_i |e_i\rangle. \tag{5.7}$$

Then the projector to the j-th basis vector can be found via

$$\langle e_j | P \equiv P_j = \sum_k G_{jk}^{-1} |e_k\rangle, \tag{5.8}$$

where G is the Gram-matrix

$$G_{ij} = \langle e_i | e_j \rangle. \tag{5.9}$$

With this little interlude from linear algebra it is then easy to verify that the projectors for the $F_1, \dots, F_4$ form factors are given by

$$P_1^{\mu\nu\rho} = \frac{1}{d-3} \left(g^{\mu\nu} p_2^\rho \frac{t}{su} - p_3^\mu p_1^\nu p_2^\rho \frac{1}{su} \right),$$

$$P_2^{\mu\nu\rho} = \frac{1}{d-3} \left(g^{\mu\rho} p_1^\nu \frac{u}{st} - p_3^\mu p_1^\nu p_2^\rho \frac{1}{st} \right),$$

$$P_3^{\mu\nu\rho} = \frac{1}{d-3} \left(g^{\nu\rho} p_3^\mu \frac{s}{tu} - p_3^\mu p_1^\nu p_2^\rho \frac{1}{tu} \right),$$

$$P_4^{\mu\nu\rho} = \frac{1}{d-3} \left(-g^{\mu\nu} p_2^\rho \frac{1}{su} - g^{\mu\rho} p_1^\nu \frac{1}{st} - g^{\nu\rho} p_3^\mu \frac{1}{tu} + p_3^\mu p_1^\nu p_2^\rho \frac{d}{stu} \right). \tag{5.10}$$

To be even more explicit: the form factors are given by

$$F_i = \langle e_i | P_{\mu\nu\rho} | \mathcal{M}^{\mu\nu\rho} \rangle = P_i^{\mu_1\nu_1\rho_1} \left(-g_{\mu_1\mu_2} + \frac{p_{1\,\mu_1} p_{2\,\mu_2} + p_{2\,\mu_1} p_{1\,\mu_2}}{p_1 \cdot p_2} \right)$$
$$\times \left(-g_{\nu_1\nu_2} + \frac{p_{2\,\nu_1} p_{3\,\nu_2} + p_{3\,\nu_1} p_{2\,\nu_2}}{p_2 \cdot p_3} \right) \left(-g_{\rho_1\rho_2} + \frac{p_{3\,\rho_1} p_{1\,\rho_2} + p_{1\,\rho_1} p_{3\,\rho_2}}{p_3 \cdot p_1} \right) \mathcal{M}^{\mu_2\nu_2\rho_2}. \tag{5.11}$$

Here we used the standard identity

$$\sum_\lambda \epsilon_\mu^*(p, n, \lambda) \epsilon_\nu(p, n, \lambda) = -g_{\mu\nu} + \frac{p_\mu n_\nu + p_\nu n_\mu}{p \cdot n} \tag{5.12}$$

to rewrite the sum over the polarization vectors.

Similarly, using

$$\sum_\lambda u(p, \lambda) \bar{u}(p, \lambda) = \slashed{p}, \quad \text{and} \quad \sum_\lambda v(p, \lambda) \bar{v}(p, \lambda) = \slashed{p}, \tag{5.13}$$

we find the projectors of G_1 and G_2[1]

$$\bar{v}(p_1) P_1^\mu u(p_2) = \frac{1}{2st(d-3)} \bar{v}(p_1) \left[\frac{d-2}{t} \left(\slashed{p}_3 p_1^\mu - \frac{t}{2} \gamma^\mu \right) - \frac{d-4}{u} \left(\slashed{p}_3 p_2^\mu - \frac{u}{2} \gamma^\mu \right) \right] u(p_2),$$
$$\bar{v}(p_1) P_2^\mu u(p_2) = \frac{1}{2su(d-3)} \bar{v}(p_1) \left[\frac{d-2}{u} \left(\slashed{p}_3 p_2^\mu - \frac{u}{2} \gamma^\mu \right) - \frac{d-4}{t} \left(\slashed{p}_3 p_1^\mu - \frac{t}{2} \gamma^\mu \right) \right] u(p_2). \tag{5.14}$$

These allow the extraction of the form factors via

$$G_i = \langle e_i | P_\mu | \mathcal{M}^\mu \rangle = \left(-g_{\mu_1\mu_2} + \frac{p_{3\,\mu_1} p_{1\,\mu_2} + p_{1\,\mu_1} p_{3\,\mu_2}}{p_3 \cdot p_1} \right) \text{tr}\{ P_i^{\mu_1} \mathcal{M}^{\mu_2} \}, \tag{5.15}$$

where we have used Eq. (5.13) once again, to rewrite the polarization sum in terms of a Dirac-trace.

Helicity Amplitudes

Since the form factors dependent on the choice of our tensor basis, we would rather express our end result in terms of helicity amplitudes

$$\mathcal{M}_{ggg \to H}^{\lambda_1\lambda_2\lambda_3} = \mathcal{M}_{\mu\nu\rho} \epsilon^\mu(p1, p_2, \lambda_1) \epsilon_2^\nu(p_2, p_3, \lambda_2) \epsilon_3^\rho(p_3, p_1, \lambda_3),$$
$$\mathcal{M}_{\bar{q}qg \to H}^{\lambda_1\lambda_2\lambda_3} = \bar{v}(p_1, \lambda_1/2) \mathcal{M}_\rho u(p_2, \lambda_2/2) \epsilon_3^\rho(p_3, p_1, \lambda_3). \tag{5.16}$$

To find the relation between the form factors and the helicity amplitudes, we consider all independent helicity configurations and use the *spinor-helicity formalism* (see Ref. [143] for a pedagogical introduction to the topic) to rewrite them in terms of spinor products

$$\langle ij \rangle \equiv \bar{u}(p_i, -1/2) u(p_j, 1/2), \qquad [ij] \equiv \bar{u}(p_i, 1/2) u(p_j, -1/2). \tag{5.17}$$

The results for the $ggg \to H$ amplitudes read

$$\mathcal{M}_{ggg \to H}^{+++} = \frac{1}{\sqrt{2}} \frac{su}{\langle 12 \rangle \langle 23 \rangle \langle 31 \rangle} \left(F_1 + \frac{t}{u} F_2 + \frac{t}{s} F_3 + \frac{t}{2} F_4 \right),$$

$$\mathcal{M}_{ggg \to H}^{++-} = \frac{1}{\sqrt{2}} \frac{[12]^3}{[13][23]} \frac{u}{s} \left(F_1 + \frac{t}{2} F_4 \right),$$

$$\mathcal{M}_{ggg \to H}^{+-+} = \frac{1}{\sqrt{2}} \frac{[13]^3}{[12][23]} \frac{s}{t} \left(F_2 + \frac{u}{2} F_4 \right),$$

$$\mathcal{M}_{ggg \to H}^{-++} = \frac{1}{\sqrt{2}} \frac{[23]^3}{[12][13]} \frac{t}{u} \left(F_3 + \frac{s}{2} F_4 \right). \tag{5.18}$$

---

1 Note that the projectors are defined as the entire left-hand side.

The other four helicity amplitudes can be determined via charge conjugation

$$\mathcal{M}^{\lambda_1,\lambda_2,\lambda_3} = \mathcal{M}^{-\lambda_1,-\lambda_2,-\lambda_3}\big|_{\langle ij\rangle \leftrightarrow [ji]}. \tag{5.19}$$

Similarly, for the $\bar{q}qg \to H$ process we find the helicity amplitudes

$$
\begin{aligned}
\mathcal{M}^{-++}_{\bar{q}qg\to H} &= -\frac{1}{\sqrt{2}}\frac{[13]^2}{[12]}sF_1, \\
\mathcal{M}^{+-+}_{\bar{q}qg\to H} &= \frac{1}{\sqrt{2}}\frac{[23]^2}{[12]}sF_2.
\end{aligned}
\tag{5.20}
$$

The $+--$ and $-+-$ amplitudes can be determined with Eq. (5.19) and all other helicity configurations render vanishing amplitudes due to the conservation of angular momentum.

The form factors, amplitudes and helicity amplitudes admit a perturbative expansion in α_s. We define

$$\mathcal{M}^{\lambda_1\lambda_2\lambda_3}_{ijk\to H} = \frac{4\pi}{v}\left(\alpha_s\right)^{3/2}\sum_{i=0}\left(\frac{\alpha_s}{4\pi}\right)^i \mathcal{M}^{(i),\lambda_1\lambda_2\lambda_3}. \tag{5.21}$$

Mapping to Topologies and the Reduction to Master Integrals

We generate all diagrams with `DiaGen/IdSolver`, our in-house software tool for the generation of Feynman diagrams. As output, we obtain `FORM` [144, 145] code we can further manipulate. We apply the color algebra and project to the form factors as described above. `DiaGen/IdSolver` is also capable to find *prototypes*, i.e. it automatically identifies a minimal set of integral families and assigns appearing integrals accordingly.

In principle, `DiaGen/IdSolver` is also able to find relations between appearing Feynman integrals, so called *integration-by-parts identities* (IBP), by means of the *Laporta algorithm* [146]. However, due to the immense complexity of the problem at hand, intermediate expressions are prone to become very large. This makes solving the appearing linear system of equation by traditional methods like Gaussian elimination highly inefficient. The appearance of large intermediate expressions can be circumvented by using *finite field* methods. In a nutshell, one inserts fractional samples for the appearing kinematic invariants and then performs the Laporta algorithm with reduced kinematics, making it much simpler to solve. The final IBP identities relate the master integrals by rational functions, one can then reconstruct the functional dependence on the kinematic variables through repeated sampling, like when performing a fit. The rational values are mapped to finite fields—explaining the name of the method—which allows computations without loss of precision. We use this workflow implemented in the publically available tool chain `Kira` $\oplus$ `Firefly` [147, 148, 149].

After application of the IBP identities we end up with three integral families for amplitudes with a single internal massive quark. We adapt the definition provided in Ref. [141]. The propagators of the each family are printed in Tab. 5.1. Notice, that the Feynman diagrams can never have more than seven internal lines, meaning that integrals appearing in physical amplitudes are missing at least two of the propagators. The physical subsector of the integral families are depicted graphically in Figs. 5.5, 5.6, and 5.7. For the contributions containing two massive internal quarks, we do not provide the integral families since the two-loop integrals factorize to one-loop integrals.

UV-Renormalization, IR-Subtraction and LSZ-Reduction

So far our analysis was concerned with bare amplitudes regulated in dimensional regularization. The UV-poles are eliminated through renormalization of the coupling constant and the quark masses. Following the description in section 2.2 we replace the bare coupling constant and

#	Planar 1 (PL1)	Planar 2 (PL2)	Non-planar (NPL)
1	k_1^2	$k_1^2 - m^2$	$k_1^2 - m^2$
2	$(k_1 - p_1)^2$	$(k_1 - p_1)^2 - m^2$	$(k + p_1)^2 - m^2$
3	$(k_1 - p_1 - p_2)^2$	$(k_1 - p_1 - p_2)^2 - m^2$	$(k_1 - p_2 - p_3)^2 - m^2$
4	$(k_1 - p_1 - p_2 - p_3)^2$	$(k_1 - p_1 - p_2 - p_3)^2 - m^2$	$k_2^2 - m^2$
5	$k_2^2 - m^2$	$k_2^2 - m^2$	$(k_2 + p_1)^2 - m^2$
6	$(k_2 - p_1)^2 - m^2$	$(k_2 - p_1)^2 - m^2$	$(k_2 - p_3)^2 - m^2$
7	$(k_2 - p_1 - p_2)^2 - m^2$	$(k_2 - p_1 - p_2)^2 - m^2$	$(k_1 - k_2)^2$
8	$(k_2 - p_1 - p_2 - p_3)^2 - m^2$	$(k_2 - p_1 - p_2 - p_3)^2 - m^2$	$(k_1 - k_2 - p_2)^2$
9	$(k_1 - k_2)^2 - m^2$	$(k_1 - k_2)^2$	$(k_1 - k_2 - p_2 - p_3)^2$

Table 5.1: Integral families for all contributions with only one internal massive quark as defined in Ref. [141]. m is the mass of the internal top- or bottom-quark.
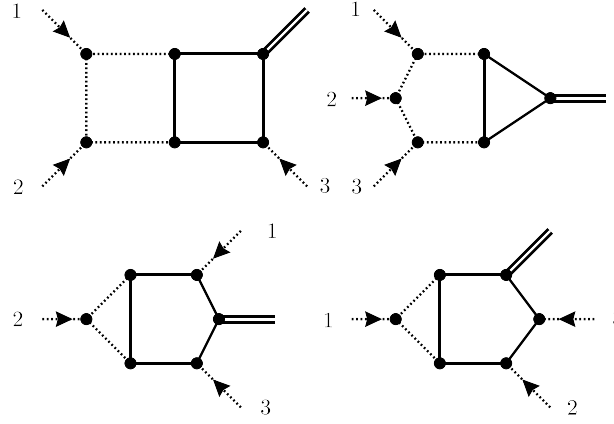
Figure 5.5: Graphical representation of the physical sectors embedded in the first integral family (PL1). Dotted lines represent massless propagators, while solid lines have the quark mass in the propagator.

masses by their renormalized counterparts and subsequently expand in α_s. The $\alpha_s^{5/2}$ term is singled out to get the NNLO correction to the amplitude. We employ the $\overline{\text{MS}}$ scheme for the α_s, and—for now—the OS scheme for all the quark masses.

To obtain physical amplitudes, we employ the LSZ reduction formula. This means for each external particle, multiplying by the square root of the corresponding LSZ-constant. In dimensional regularization, the LSZ constants only get contributions from heavy fields, since all other contributions render scaleless integrals. This means that the gluon LSZ constants are already non-trivial at one-loop, whereas the quark LSZ constants only gets non-trivial corrections at two-loop, which makes them irrelevant for the calculation at hand. Since bottom-quarks are treated as massless whenever they are not coupling to the Higgs, they do not contribute to the LSZ constants, i.e. only the top-quark mass enters the LSZ constants.

The remaining poles are of IR origin. They would cancel against poles arising during phase-space integration, so we can subtract them already on the amplitude level. We employ the $\overline{\text{MS}}$ scheme and subtract only the divergences predicted by the **Z** operator (see for example Ref. [29]).
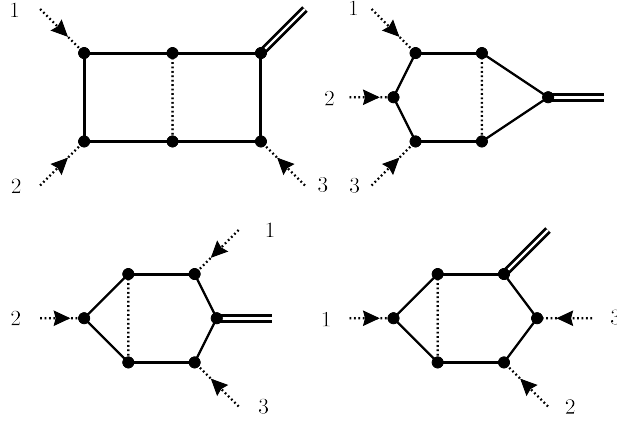
Figure 5.6: Same as Fig. 5.5 but for the second integral family (PL2).
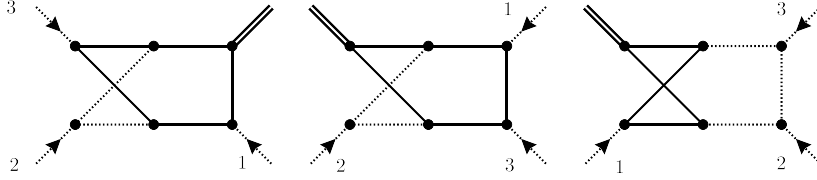
Figure 5.7: Same as Fig. 5.5 but for the third non-planar integral family (NPL).

Results for the Contributions with Two Heavy Quarks

Once we performed all the above steps, we separate the contributions which contain two heavy quark loops from the rest of the amplitude. The **Z** operator, i.e. the IR-poles, do not receive contributions from heavy internal lines and is therefore irrelevant for this contribution. The LSZ constants of the gluons on the other hand, do contribute. In the coupling renormalization constants, we single out the contributions from the top quark, i.e. we set the number of fermions to

$$n_f = n_l + n_h \tag{5.22}$$

Here n_l is the number of light quarks, and n_h is the number of heavy quarks. In the 5FS we have $n_l = 5$ and $n_h = 1$. The renormalization constant in the $\overline{\text{MS}}$ scheme then reads

$$Z_g = 1 - \frac{\alpha_s}{4\pi} 2\beta_0 \frac{1}{\epsilon} + \mathcal{O}(\alpha_s^2) = 1 + \frac{\alpha_s}{4\pi} \frac{1}{\epsilon} \left(-\frac{11}{6} C_A + \frac{2}{3}(n_l + n_h)T_F \right) + \mathcal{O}(\alpha_s^2). \tag{5.23}$$

To single out the contributions from the top-quark we only take terms proportional to n_h and set n_h to one afterwards. We can then apply the decoupling relations of Eq. (4.57) to replace the coupling constant by its decoupled counterpart in the lower order amplitudes[2]. We can absorb these terms into the renormalization of the coupling constant, such that we end up with the effective renormalization constant

$$Z_g^{(n_l)}\big|_{\propto n_h} = \frac{\alpha_s}{4\pi} \frac{2}{3} T_F \left(\frac{1}{\epsilon} - \ln\left(\frac{m_t^2}{\mu^2}\right) \right) + \mathcal{O}(\alpha_s^2). \tag{5.24}$$

This is nothing else than the top-quark contribution to the OS coupling renormalization constant. The decoupling constants were specifically introduced to cure the $\overline{\text{MS}}$ scheme from

---

2 In the renormalization constants we can simply set $\alpha_s^{(n_l+n_h)} = \alpha_s^{(n_l)}$ at this order in perturbation theory.

the appearance of non-decoupling effects. In the OS scheme this issue does not arise because of the Appelquist-Carrazone theorem (see section 4.3.2). It therefore comes to no ones surprise that the effective renormalization constant matches the OS one.

At one-loop, the top-quark contribution to the renormalization constant is of abelian nature. In QED, the Ward identity implies the all order relation $Z_e = Z_3^{-1/2}$. We can therefore conclude, or verify explicitly that the one-loop renormalization constant is also related to the gluon LSZ constant

$$2Z_g^{(n_l)}\big|_{\propto n_h} = -Z_3 + \mathcal{O}(\alpha_s^2). \tag{5.25}$$

This has the profound effect, that if the external number of gluons is identical to the power of the coupling constant (at lower order), then the contributions exactly cancel. This is for example the case in the $ggg \to H$ amplitude.

The result for the helicity amplitude of the $ggg \to H$ amplitude read

$$
\begin{aligned}
\mathcal{M}_{ggg \to H}^{(1),+++}\Big|_{2\text{ masses}} &= \frac{1}{\sqrt{2}} \frac{1}{\langle 12 \rangle \langle 23 \rangle \langle 31 \rangle} \Bigg\{ -\frac{4m_t^2 stu}{(s+t)} \tilde{C}_0(u, m_t^2) \Big[\tilde{B}(m_H^2, m_b^2) \\
&\quad + \frac{s+t}{u} + 2\frac{m_b^2}{u} \left(4m_b^2 - s - t \right) \tilde{C}_1(u, m_H^2, m_b^2) - \frac{4m_b^2}{s+t} \tilde{B}(u, m_l^2) \Big] \\
&\qquad + (s \to t, t \to u, u \to s) + (s \to u, u \to t, t \to s) \Bigg\}
\end{aligned}
\tag{5.26}
$$

$$
\begin{aligned}
\mathcal{M}_{ggg \to H}^{(1),-++}\Big|_{2\text{ masses}} &= -\frac{1}{\sqrt{2}} \frac{[23]^3}{[12][13]} \frac{4m_t^2 st}{u(s+t)} \tilde{C}_0(u, m_t^2) \Big[\tilde{B}(m_H^2, m_b^2) \\
&\quad + \frac{s+t}{u} + 2\frac{m_b^2}{u} \left(4m_b^2 - s - t \right) \tilde{C}_1(u, m_H^2, m_b^2) - \frac{4m_b^2}{(s+t)} \tilde{B}(u, m_b^2) \Big]
\end{aligned}
\tag{5.27}
$$

Where we defined the auxiliary functions[3]

$$
\begin{aligned}
\tilde{B}(s, m^2) &\equiv \beta(s, m^2) \log\left(-\frac{1 - \beta(s, m^2)}{1 + \beta(s, m^2)} + i0^+ \right), \\
\tilde{C}_0(s, m^2) &\equiv \frac{1}{2s} \log^2\left(-\frac{1 - \beta(s, m^2)}{1 + \beta(s, m^2)} + i0^+ \right) + \frac{2}{s} \left(\tilde{B}(s, m^2) + 2 \right), \\
\tilde{C}_1(s_1, s_2, m^2) &\equiv \frac{1}{2} \frac{1}{s_1 - s_2} \left[\log^2\left(-\frac{1 - \beta(s_1, m^2)}{1 + \beta(s_2, m^2)} + i0^+ \right) - \log^2\left(-\frac{1 - \beta(s_2, m^2)}{1 + \beta(s_2, m^2)} + i0^+ \right) \right],
\end{aligned}
$$

with $\quad \beta(s, m^2) \equiv \sqrt{1 - \frac{4m^2}{s}}.$

$$\tag{5.28}$$

All other helicity amplitudes are either related via charge conjugation (5.19), or by relabeling of the external momenta

$$\mathcal{M}_{ggg \to H}^{+-+} = \mathcal{M}_{ggg \to H}^{-++}\Big|_{p_1 \leftrightarrow p_2}, \qquad \mathcal{M}_{ggg \to H}^{++-} = \mathcal{M}_{ggg \to H}^{-++}\Big|_{p_1 \leftrightarrow p_3}. \tag{5.29}$$

Note that the Mandelstam variables are defined in terms of incoming gluon momenta, i.e.

$$s = (p_1 + p_2)^2, \quad t = (p_1 + p_3)^2, \quad u = (p_2 + p_3)^2. \tag{5.30}$$

---

3 The functions are closely related to the finite part of the bubble integrals, and the triangle integrals with on-shell, and one off-shell leg. The functions are modified slightly to simplify the expressions, however we keep the standard notation, where B functions indicate bubbles and C functions triangle integrals. The tilde is added to make the distinction from the original integrals more apparent.

For the quark channel the result reads

$$
\left.\mathcal{M}^{(1),-++}_{\bar{q}qg\to H}\right|_{2\,\text{masses}} = \frac{1}{\sqrt{2}}\frac{[13]^2}{[12]}\frac{4}{9(t+u)}\left(5s+12m_t^2+(3s+6m_t^2)\tilde{B}(s,m_t^2)\right)\left[\tilde{B}(m_H^2,m_b^2)\right.
$$
$$
\left. +\frac{t+u}{s}+2\frac{m_b^2}{s}\left(4m_b^2-t-u\right)\tilde{C}_1(s,m_H^2,m_b^2)-\frac{4m_b^2}{t+u}\tilde{B}(s,m_b^2)\right].
$$
$$(5.31)$$

Once again all other amplitudes can be obtained through a relabeling of the external momenta and charge conjugation. We see that the functional dependence on the Mandelstams is identical in all amplitudes in Eqs. (5.26), (5.27), and (5.31). This is because the expression is related to the off-shell gluon-Higgs form factor, appearing in all Feynman diagrams of this contribution (see Fig. 5.3).

Contributions With One Heavy Quark

For completeness, we also reproduce the LO helicity amplitudes computed in Ref. [150].

$$
\mathcal{M}^{(0),+++}_{ggg\to H} = \frac{1}{\sqrt{2}}\frac{16m^2stu}{\langle 12\rangle\langle 23\rangle\langle 31\rangle}\left\{-8\left[\frac{1}{ut}+\frac{1}{tt_1}+\frac{1}{uu_1}\right]-\frac{8}{s}\left[\frac{2s+t}{u_1^2}B_1(u)+\frac{2s+u}{t_1^2}B_1(t)\right]\right.
$$
$$
-\frac{2(s-4m^2)}{stu}\left[s_1C_1(s)+(u-s)C_1(t)+(t-s)C_1(u)\right]-16m^2\left[\frac{1}{tt_1}C_1(t)+\frac{1}{uu_1}C_1(u)\right]
$$
$$
\left. +\frac{8m^2}{s}D(u,t)+\frac{s-4m^2}{stu}\left[stD(s,t)+usD(u,s)-utD(u,t)\right]-\frac{4}{s^2}E(u,t)\right\}
$$
$$(5.32)$$

$$
\mathcal{M}^{(0),-++}_{ggg\to H} = \frac{1}{\sqrt{2}}\frac{[23]^3}{[12][13]}\frac{16m^2st}{u}\left\{\frac{8m_H^2}{stu}+\frac{2(m_H^2-4m^2)}{stu}\left[s_1C_1(s)+u_1C_1(u)+t_1C_1(t)\right]\right.
$$
$$
\left. -\frac{m_H^2-4m^2}{stu}\left[stD(s,t)+usD(u,s)+utD(u,t)\right]\right\}
$$
$$(5.33)$$

$$
\mathcal{M}^{(0),-++}_{\bar{q}q\to H} = \frac{1}{\sqrt{2}}\frac{[13]^2}{[12]}\frac{m^2}{s_1}\left[2+2\frac{s}{s_1}B_1(s)+\left(4m^2-u-t\right)C_1(s)\right]
$$
$$(5.34)$$

Here m is the internal quark mass and we defined

$$
s_1 = s - m_H^2, \quad t_1 = t - m_H^2, \quad u_1 = u - m_H^2.
$$
$$(5.35)$$

The appearing functions are directly linked to standard Feynman integrals which we provide in Appendix B. **TODO:** Check numerically

Although there is one less scale in the contributions with only one quark mass, the two-loop amplitudes are a lot more complex because the integrals do no longer factorize. Instead of attempting to solve the remaining integrals analytically, we followed a numerical approach, where the amplitudes are evaluated at fixed phase-space points. These points can then be used as grid points for interpolations during the phase-space integration. For the numerical evaluation of the master integrals we follow the strategy outlined in Ref. [109], which itself is based on methods presented in Ref. [151]. The general idea is to derive a system of differential equation for each integral family, find suitable boundary conditions analytically, and then solve the differential equations numerically.

The amplitude is a function of four variables, e.g. s, t, u and the quark mass m. The Higgs mass is not a free parameter since it can be expressed as a sum over the Mandelstams. We can

however simply factor our one scale, say the collision scale s to make everything dimensionless, and we are left with only three. We choose to parametrize the amplitude in terms of the dimensionless variables

$$z \equiv -\frac{t+u}{s}, \quad \lambda \equiv \frac{t}{t+u}, \quad x \equiv \frac{m^2}{s} = \frac{m^2}{m_H^2}(1-z). \tag{5.36}$$

These variables are advantageous because they parametrize soft and collinear limits. Indeed, soft limits are described with $z \to 0$, whereas the collinear limits are captured by $\lambda \to 0$ for the t-collinear and $\lambda \to 1$ for u-collinear. Furthermore, z and λ are bounded by

$$0 \le z \le 1, \quad 0 \le \lambda \le 1, \quad \text{and} \quad 0 \le x \tag{5.37}$$

for physical production kinematics.

To apply the method of differential equations, we need to apply derivatives with respect to our variables, but the master integrals are functions of the external momenta. We can apply the chain rule to relate the derivatives

$$
\begin{aligned}
\left(z\frac{\partial}{\partial z} \right) &= \left(t\frac{\partial}{\partial t} \right) + \left(u\frac{\partial}{\partial u} \right) + \frac{t+u}{s+t+u}\left(x\frac{\partial}{\partial x} \right) \\
&= \left(p_3^\mu \frac{\partial}{\partial p_3^\mu} \right) - \frac{z}{1-z}\left(x\frac{\partial}{\partial x} \right),
\end{aligned} \tag{5.38}
$$

$$
\begin{aligned}
\left(\lambda\frac{\partial}{\partial \lambda} \right) &= \left(t\frac{\partial}{\partial t} \right) - \frac{\lambda}{1-\lambda}\left(u\frac{\partial}{\partial u} \right) \\
&= \frac{1}{2}\left(\left(p_1^\mu \frac{\partial}{\partial p_1^\mu} \right) - \left(p_2^\mu \frac{\partial}{\partial p_2^\mu} \right) + (1-2\lambda)\left(p_3^\mu \frac{\partial}{\partial p_3^\mu} \right) \right).
\end{aligned} \tag{5.39}
$$

The derivative with respect to x remains unchanged. One can now proceed to apply the differential operators onto the master integrals. The derivatives result in new integrals, which we can relate to our master integrals through the repeated use of IBPs.

We found that it is advantageous shift almost all the appearing master integrals from $d = 4 - 2\epsilon$ to $d+2$ dimensions, by application of *dimension-shift relations* (see Ref. [6] for a comprehensive introduction). This way, all spurious poles of the top-level sector are removed, and the integrals must only be computed up to ϵ^0. As a byproduct, we found that the coefficients in front of the master integrals are significantly reduced in complexity.

In order to solve the differential equation, we need to find suitable boundary conditions. Since the HTL has already been extensively studied, it suggests itself to use it as boundary conditions. To this end, we expand the integrals in the limit of a large internal mass $m, x \to \infty$ by means of the *large mass expansion* (see Ref. [152] for a comprehensive introduction). It allows expanding integrals in the limit of large masses already at the integral level, i.e. the remaining integrals are devoid of the large mass. The expansion is implemented in the workflow of `DiaGen/IdSolver`. The only required integrals are massless four-point functions and vacuum integrals which can be found in the appendix of Ref. [153].

The solutions found at the boundary $x \to \infty$ can now be transported to the physical plane, i.e. to finite quark masses by solving the differential equation in the x-direction. This strategy is illustrated in Fig. 5.8. The differential equation is solved numerically using the *Bulirsch-Stoer algorithm*. Since we are working within the physical parameter space defined by Eq. (5.36), we can no longer relate the various matrix elements by means of crossing relations Eq. (5.29). We
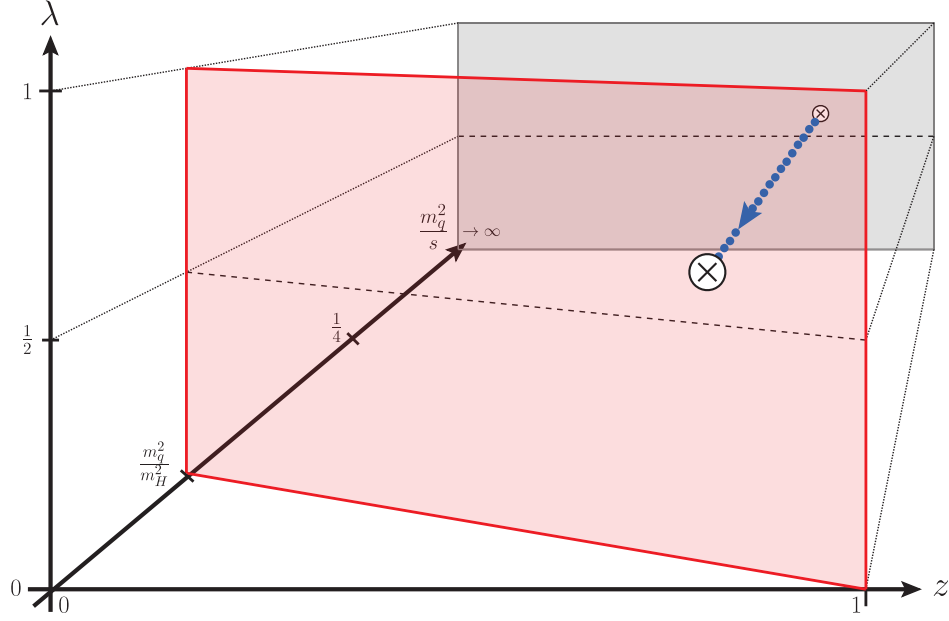
Figure 5.8: Graphical illustration of the parameter space and the strategy for transporting the boundary conditions at $x \to \infty$ to the physical plane shown in red. Figure taken (with slight modification) from Ref. [153].

will therefore have to switch to a physical momentum configuration and compute all matrix elements[4]

$$
\begin{aligned}
&\mathcal{M}^{+++}_{gg \to Hg}, \mathcal{M}^{-++}_{gg \to gH}, \mathcal{M}^{+-+}_{gg \to gH}, \mathcal{M}^{++-}_{gg \to gH}, \mathcal{M}^{+++}_{gg \to gH}, \\
&\mathcal{M}^{-++}_{\bar{q}q \to gH}, \mathcal{M}^{+-+}_{\bar{q}q \to gH}, \mathcal{M}^{+-+}_{g\bar{q} \to \bar{q}H}, \mathcal{M}^{++-}_{g\bar{q} \to \bar{q}H}, \mathcal{M}^{++-}_{qg \to qH}, \mathcal{M}^{-++}_{qg \to qH}
\end{aligned}
\tag{5.40}
$$

individually. Notice that we can still apply the charge conjugation identity in Eq. (5.19) if we first pull out the spinor-helicity factors. Nevertheless, the exchange of the first two momenta does not take us out of the physical parameter space and hence the crossing symmetry (followed by charge conjugation) can still be exploited.

$$
|\mathcal{M}^{\lambda_1 \lambda_2 \lambda_3}_{gg \to gH}|^2(\lambda, z, x) = |\mathcal{M}^{\lambda_2 \lambda_1 \lambda_3}_{gg \to gH}|^2(1 - \lambda, z, x),
\tag{5.41}
$$

$$
|\mathcal{M}^{\lambda_1 \lambda_2 \lambda_3}_{\bar{q}q \to gH}|^2(\lambda, z, x) = |\mathcal{M}^{\lambda_2 \lambda_1 \lambda_3}_{\bar{q}q \to gH}|^2(1 - \lambda, z, x),
\tag{5.42}
$$

$$
|\mathcal{M}^{\lambda_1 \lambda_2 \lambda_3}_{qg \to qH}|^2(\lambda, z, x) = |\mathcal{M}^{\lambda_2 \lambda_1 \lambda_3}_{g\bar{q} \to \bar{q}H}|^2(1 - \lambda, z, x).
\tag{5.43}
$$

We relate the squared amplitudes to avoid phase factors arising from the spinor-helicity factors. The physical parameter space is therefore effectively cut in half. Consequently, we only have to solve the amplitude for $1/2 \leq \lambda \leq 1$ and can infer the remaining space with these symmetry relations.

We therefore choose initial conditions which are just above the symmetry line $\lambda = 1/2$, and then sample different values in z. The solutions of the differential equation in x for these samples then serve as initial conditions for the differential equation in λ. This is illustrated in Fig. 5.9. At $z \to 0$, we encounter a soft divergence. These divergences will cancel in the end, but it is therefore important to map out this parameter space with particular care. We therefore sample z logarithmically. Furthermore, for $z \to 1$ the poles of the differential equation

---

4 The helicities are assigned to the partons in the order they appear in the corresponding process, i.e. the first helicity belongs to the first appearing parton, the second to the second, and the third to the third.
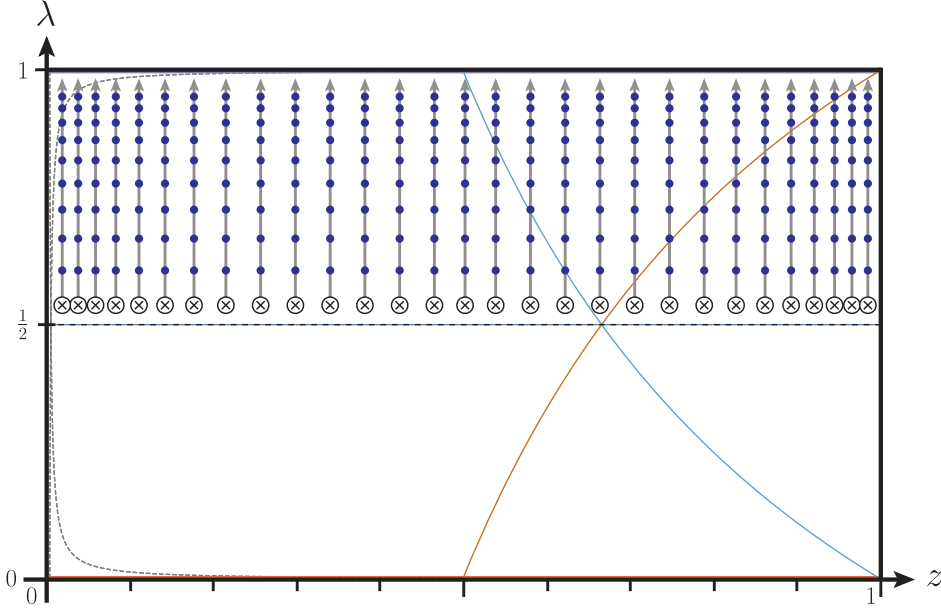
Figure 5.9: Illustration of the physical plane (shown in red in Fig. 5.8) for a bottom quark with a mass ratio of $m_b^2/m_H^2 = 1/684$. The colored thin lines indicate poles of the differential equation in λ. The circled crosses with the errors indicate the boundary condition for the differential equation in λ and the path along which the differential equation is solved. The integration paths are not to scale and are for illustrative purposes only.

are very close together. This once again causes large cancellations. To avoid mismodelling the amplitudes in these regions of the parameter space we therefore also sample more points close to this boundary. In the end we sample around 1000 values of z, ranging from 10^{-4} to $1 - 10^{-4}$.

The poles of the differential equation in λ are dealt with via a contour deformation in the complex plane. Once again we sample λ logarithmically, such that we obtain more points towards the IR-sensitive $\lambda \to 1$ region. In total, we sample around 500 points, yielding dense grid of the physical plane of around 10^6 grid points.

Around the IR sensitive regions $z \to 0$ and $\lambda \to 0, 1$, the amplitudes are dominated by the singularities $1/z$ and $1/\sqrt{\lambda}$, a contribution which will eventually cancel against other IR divergences. On the other hand, the dominance of the singularity will negatively impact the precision of the interpolation for the non-divergent terms. We would therefore like to subtract the IR-divergences before performing the interpolation. It is well known, that the leading IR behavior factorizes from the amplitude. Consider for example, the limit of two almost collinear outgoing partons with momenta

$$p_1^\mu = z_1 p^\mu + k_\perp^\mu - \frac{k_\perp^2}{z_1} \frac{n^\mu}{2p \cdot n}, \qquad p_2^\mu = (1 - z_1)p^\mu - k_\perp - \frac{k_\perp^2}{1 - z} \frac{n^\mu}{2p \cdot n}, \qquad (5.44)$$

where $k_\perp \cdot p = k_\perp \cdot n = 0$, and p and n are on-shell ($p^2 = n^2 = 0$). Further p and n are not collinear, i.e. $p \cdot n \sim \mathcal{O}(p^0 n^0)$. The collinear limit is therefore parametrized by $k_\perp \to 0$. Then the leading power behavior of the one-loop averaged squared matrix element is given by

$$
\begin{aligned}
2\mathrm{Re}&\overline{\langle \mathcal{M}^{(0)}_{a_1 a_2, \cdots}(p_1, p_2, \ldots) | \mathcal{M}^{(1)}_{a_1 a_2, \cdots}(p_1, p_2, \ldots)\rangle} \simeq \\
&4\pi\alpha_s \frac{1}{p_1 \cdot p_2} \left[\langle P^{(0)}_{a_1 a_2}(z_1)\rangle \times 2\mathrm{Re}\overline{\langle \mathcal{M}^{(0)}_{a,\cdots}(p,\ldots)|\mathcal{M}^{(1)}_{a,\cdots}(p,\ldots)\rangle} \right. \\
&\left. \qquad + \frac{\alpha_s}{4\pi} \langle P^{(1)}_{a_1 a_2}(z_1)\rangle \, \overline{\langle \mathcal{M}^{(0)}_{a,\cdots}(p,\ldots)|\mathcal{M}^{(0)}_{a,\cdots}(p,\ldots)\rangle} \right].
\end{aligned}
\tag{5.45}
$$

Here a_1 and a_2 denote the flavor of the respective parton, while the flavor a is set by flavor conservation. $\langle P^{(0,1)}_{a_1 a_2}(z_1)\rangle$ are the tree-level and one-loop averaged splitting functions. For reasons that will be explained below, the exact structure of the one-loop splitting functions is of no concern to us. The tree-level averaged splitting functions in four dimensions read

$$
\begin{aligned}
\langle P^{(0)}_{gg}(z_1)\rangle &= 2C_A \left(\frac{z_1}{1-z_1} + \frac{1-z_1}{z_1} + z_1(1-z_1) \right), \\
\langle P^{(0)}_{q\bar{q}}(z_1)\rangle = \langle P^{(0)}_{\bar{q}q}(z_1)\rangle &= T_F \left(1 - 2z_1(1-z_1)\right), \\
\langle P^{(0)}_{qg}(z_1)\rangle = \langle P^{(0)}_{\bar{q}g}(z_1)\rangle &= C_F \frac{1+z_1^2}{1-z_1} \\
\langle P^{(0)}_{gq}(z_1)\rangle = \langle P^{(0)}_{g\bar{q}}(z)\rangle &= \langle P^{(0)}_{qg}(1-z)\rangle.
\end{aligned}
\tag{5.46}
$$

Initial state collinear divergences can be recovered by replacing $p_2 \to -p_2$ as well as $P_{a_1 a_2} \to (-1)^{2s_a + 2s_{a_1}} P_{a_1 a_2}$, where s_a and s_{a_1} are the spins of the respective partons.

Likewise, in the limit where one of the external gluons becomes soft, $q \to 0$, the factorization of the one-loop squared amplitude with external partons reads

$$
\begin{aligned}
2\mathrm{Re}\,&\langle \mathcal{M}^{(0)}_{g,a_1,\cdots}(q, p_1, \ldots)|\mathcal{M}^{(1)}_{g,a_1,\cdots}(q, p_1, \ldots)\rangle \simeq \\
&-4\pi\alpha_s \Bigg\{ \sum_{(i,j)} (\mathcal{S}_{ij}(q) - \mathcal{S}_{ii}(q)) \, 2\mathrm{Re}\,\langle \mathcal{M}^{(0)}_{a_1,\cdots}(p_1,\ldots)|\mathbf{T}_i \cdot \mathbf{T}_j|\mathcal{M}^{(1)}_{a_1,\cdots}(p_1,\ldots)\rangle \\
&\qquad + \frac{\alpha_s}{4\pi}\Bigg[\sum_{(i,j)} (\mathcal{S}_{ij}(q) - \mathcal{S}_{ii}(q)) \, R_{ij} \, \langle \mathcal{M}^{(0)}_{a_1,\cdots}(p_1,\ldots)|\mathbf{T}_i \cdot \mathbf{T}_j|\mathcal{M}^{(0)}_{a_1,\cdots}(p_1,\ldots)\rangle \\
&\qquad\qquad - 4\pi \sum_{(i,j,k)} \mathcal{S}_{ik}(q) I_{ij} \, \langle \mathcal{M}^{(0)}_{a_1,\cdots}(p_1,\ldots)|f^{abc}\mathbf{T}_i^a \mathbf{T}_j^b \mathbf{T}_k^c|\mathcal{M}^{(1)}_{a_1,\cdots}(p_1,\ldots)\rangle \Bigg] \Bigg\}
\end{aligned}
\tag{5.47}
$$

The sums run over distinct parton indices. $\mathbf{T}_i$ denotes the color operator of the i-th particle, i.e. it is the generator of the SU(3) group in the representation of that particle: fundamental for quarks, complex-conjugated for anti-quarks, adjoint for gluons and trivial for colorless particles. Once again, the exact structure of the one-loop coefficients I_{ij}, R_{ij} is irrelevant to us (see Ref. [151] for a definition). The eikonal factor is given by

$$
\mathcal{S}_{ij}(q) = \frac{p_i \cdot p_j}{(p_i \cdot q)(p_j \cdot q)}.
\tag{5.48}
$$

We claim that the regulated averaged squared amplitudes[5]

$$
\begin{aligned}
\overline{\langle \mathcal{M}_{gg \to gH}^{(0)} | \mathcal{M}_{gg \to gH}^{(1)} \rangle}\big|_{\text{regulated}} &\equiv \overline{\langle \mathcal{M}_{gg \to gH}^{(0)} | \mathcal{M}_{gg \to gH}^{(1)} \rangle} - \overline{\langle \mathcal{M}_{gg \to gH}^{(0),\text{rHTL}} | \mathcal{M}_{gg \to gH}^{(1),\text{rHTL}} \rangle} \\
&- \overline{\langle \mathcal{M}_{gg \to H}^{(0)} | \mathcal{M}_{gg \to H}^{(1)} - \mathcal{M}_{gg \to H}^{(1),\text{rHTL}} \rangle} \times
\begin{cases}
\frac{8\pi\alpha_s}{t} \langle P_{gg}^{(0)}\left(\frac{s}{s+u}\right) \rangle & \text{if } |t| < |u| \\
\frac{8\pi\alpha_s}{u} \langle P_{gg}^{(0)}\left(\frac{s}{s+t}\right) \rangle & \text{if } |u| < |t|
\end{cases},
\end{aligned}
$$

$$
\begin{aligned}
\overline{\langle \mathcal{M}_{qg \to qH}^{(0)} | \mathcal{M}_{qg \to qH}^{(1)} \rangle}\big|_{\text{regulated}} &\equiv \overline{\langle \mathcal{M}_{qg \to qH}^{(0)} | \mathcal{M}_{qg \to qH}^{(1)} \rangle} - \overline{\langle \mathcal{M}_{qg \to qH}^{(0),\text{rHTL}} | \mathcal{M}_{qg \to qH}^{(1),\text{rHTL}} \rangle} \\
&+ \overline{\langle \mathcal{M}_{gg \to H}^{(0)} | \mathcal{M}_{gg \to H}^{(1)} - \mathcal{M}_{gg \to H}^{(1),\text{rHTL}} \rangle} \times \frac{8\pi\alpha_s}{t} \langle P_{q\bar{q}}^{(0)}\left(\frac{s}{s+u}\right) \rangle,
\end{aligned}
$$

$$
\overline{\langle \mathcal{M}_{q\bar{q} \to gH}^{(0)} | \mathcal{M}_{q\bar{q} \to gH}^{(1)} \rangle}\big|_{\text{regulated}} \equiv \overline{\langle \mathcal{M}_{q\bar{q} \to gH}^{(0)} | \mathcal{M}_{q\bar{q} \to gH}^{(1)} \rangle} - \overline{\langle \mathcal{M}_{q\bar{q} \to gH}^{(0),\text{rHTL}} | \mathcal{M}_{q\bar{q} \to gH}^{(1),\text{rHTL}} \rangle},
$$

(5.49)

are free of IR divergences. The averaged splitting functions are

$$
\langle P_{gg}^{(0)}(z) \rangle = 2C_A \left(\frac{z}{1-z} + \frac{1-z}{z} + z(1-z) \right) \quad \text{and} \quad \langle P_{q\bar{q}}^{(0)}(z) \rangle = T_F \left(1 - 2z(1-z) \right).
$$

(5.50)

By subtracting the amplitude in the rHTL we are eliminating all infrared divergences coming from one-loop splitting functions or soft functions in Eqs. (5.45) and (5.47). These functions only act upon the difference of the LO Higgs-gluon form factor in QCD and in the rHTL. But this difference is zero by definition of the rHTL. Notice that the factor used for rescaling the cross section in the HTL for the interference contributions is now defined in terms of

$$
r_{t \times b}^{\text{LO}} = \frac{\hat{\sigma}_{t \times b}^{\text{LO}}}{\hat{\sigma}_{t \times b}^{\text{LO},\text{rHTL}}},
$$

(5.51)

which for on-shell masses yields approximately -0.129. In contrast to the rescaling factor for the pure top-quark contribution, this rescaling factor has no direct phenomenological relevance, in the sense that it can incorporate finite quark mass effects, and is used only as a computational trick.

After subtraction of the rHTL squared amplitudes, the difference still exhibits divergences from tree-level splitting and soft functions. For the $gg \longrightarrow gH$ amplitude the divergence can be handled by subtracting

$$
\overline{\langle \mathcal{M}_{gg \to H}^{(0)} | \mathcal{M}_{gg \to H}^{(1)} - \mathcal{M}_{gg \to H}^{(1),\text{rHTL}} \rangle} \times
\begin{cases}
\frac{8\pi\alpha_s}{t} \langle P_{gg}^{(0)}\left(\frac{s}{s+u}\right) \rangle & \text{if } |t| < |u| \\
\frac{8\pi\alpha_s}{u} \langle P_{gg}^{(0)}\left(\frac{s}{s+t}\right) \rangle & \text{if } |u| < |t|
\end{cases}
$$

(5.52)

from the difference. To see this, let us first consider the t-collinear limit, i.e. $p_1 \cdot p_3 \to 0$. We can choose the anti-collinear direction to be along p_2 and then determine[6]

$$
z_1 = \frac{p_1 \cdot p_2}{p_1 \cdot p_2 - p_3 \cdot p_2} = \frac{s}{s-u}.
$$

(5.53)

Hence, Eq. (5.52) has exactly the structure required from a collinear limit (5.45). The u-collinear limit works analogously. The soft limit, where t and u tend to zero, we can expand the splitting functions and get

$$
(5.52) \to \overline{\langle \mathcal{M}_{gg \to H}^{(0)} | \mathcal{M}_{gg \to H}^{(1)} - \mathcal{M}_{gg \to H}^{(1),\text{rHTL}} \rangle} \times \frac{8\pi\alpha_s}{t} 2C_A \frac{s}{u}.
$$

(5.54)

---

5 **TODO:** Notice the different signs infront of the splitting functions compared to Ref. [4].

6 Note that z is only unique up to power corrections.

Remembering that the Higgs-gluon form factor was diagonal in color-space, i.e. proportional to $\delta^{c_1 c_2}$, we see that this is exactly the soft divergence predicted by Eq. (5.47).

Lacking a final state gluon, the qg-channel can not develop a soft divergence. The initial state collinear divergence is subtracted with the corresponding splitting functions analogous to the gg channel. The different sign comes from the splitting function, which generates a minus sign if a fermion is crossed to the initial state.

Lastly, after subtraction of the squared amplitude of the rHTL the $q\bar{q}$-channel does not exhibit any IR singularity, due to the lack of available Born processes.
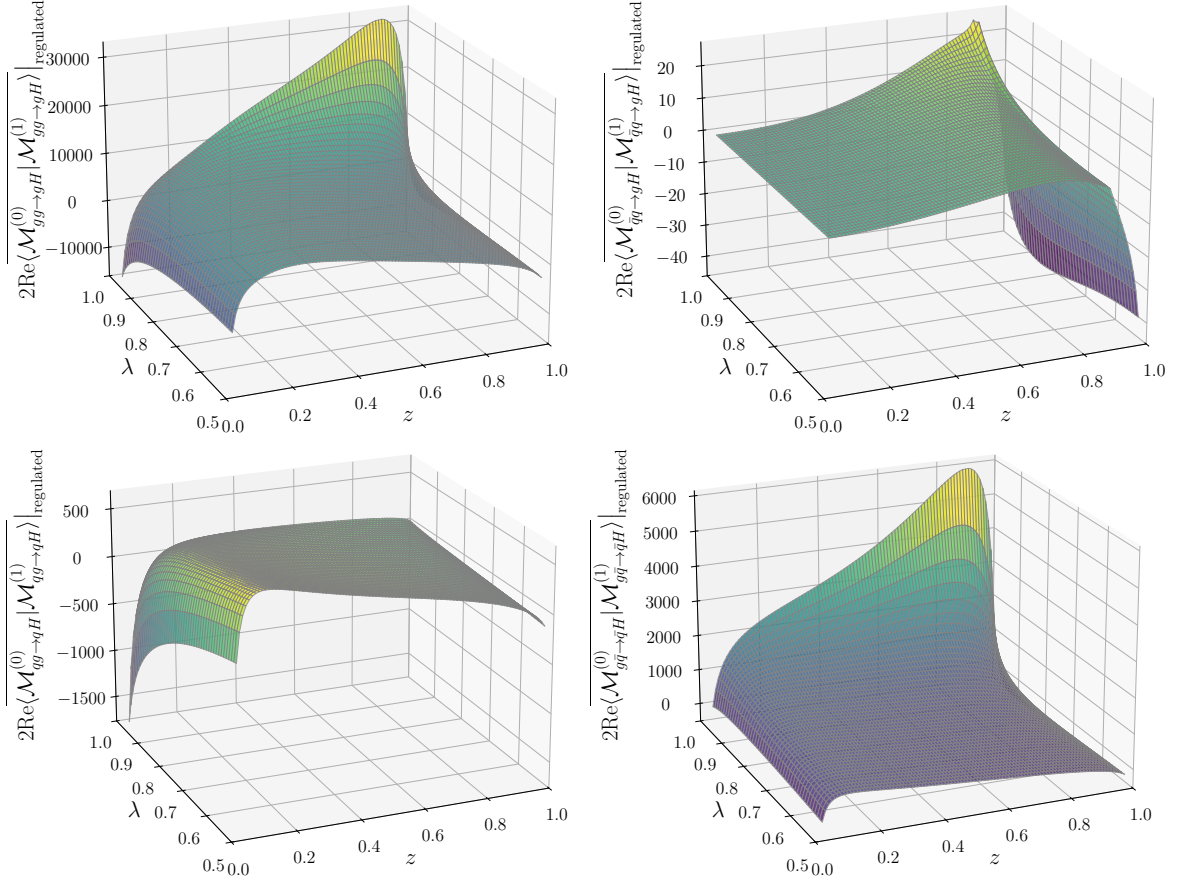
We repeat this procedure for nine different quark masses listed in Tab. 5.2, which are in the vicinity of the bottom- and top-quark mass, allowing us to interpolate in x-space as well.

5.1.3 The Virtual-Virtual Corrections

5.2 $\overline{\mathrm{MS}}$-SCHEME

5.3 THE 4-FLAVOUR SCHEME

5.4 PERFORMING THE PHASE-SPACE INTEGRATION
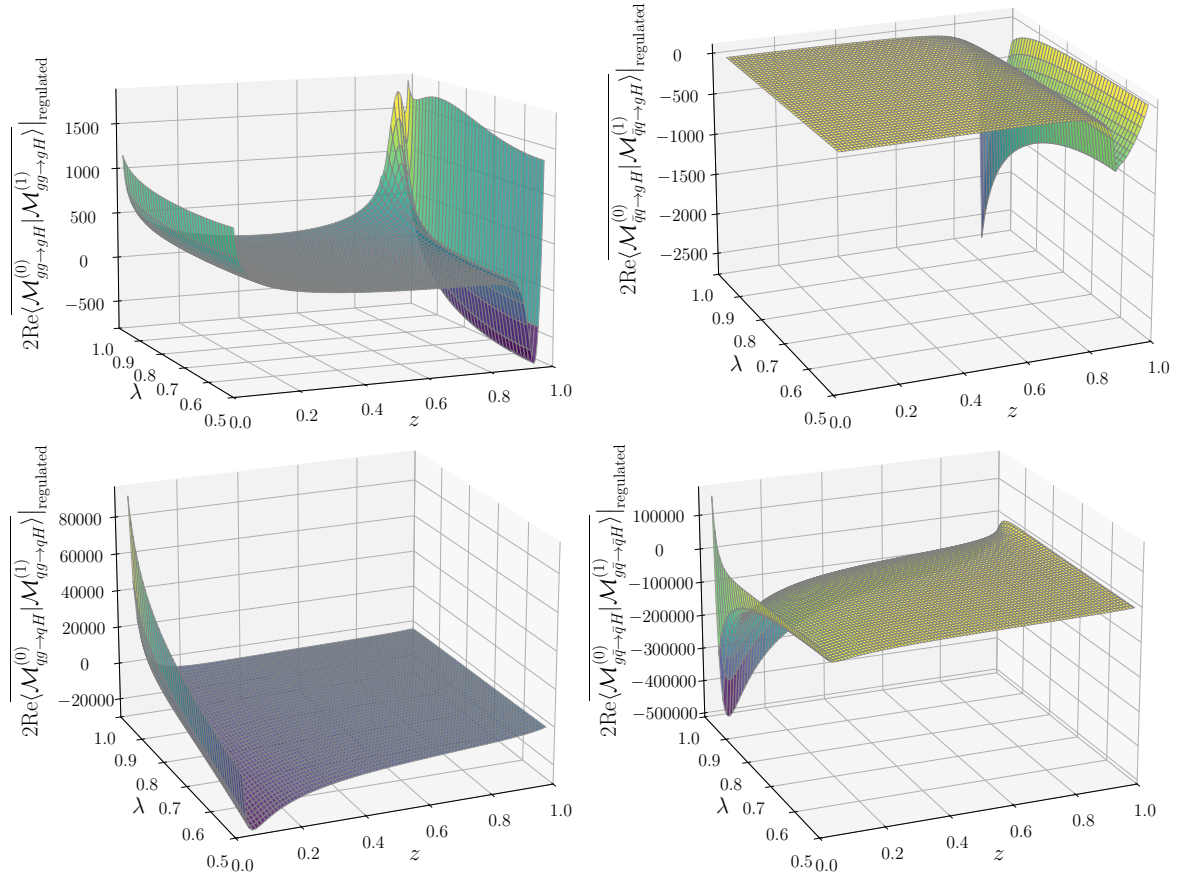
Grid mass	Value [GeV]	Approximate ratio $m_{b,t}^2/m_H^2$	Relative error [‰]
m_b	4.78	$\frac{1}{684}$	0.2
$\overline{m}_b(m_H)$	2.789	$\frac{1}{2011}$	0.9
$\overline{m}_b(m_H/2)$	2.961	$\frac{1}{1782}$	0.2
$\overline{m}_b(m_H/4)$	3.170	$\frac{1}{1557}$	1.0
$\overline{m}_b^{\min}$	1.67	$\frac{1}{5602}$	0.1
m_t	172.4	$\frac{23}{12}$	4
$\overline{m}_t(m_H)$	166.1	$\frac{136}{77}$	0.0
$\overline{m}_t(m_H/2)$	176.2	$\frac{149}{75}$	0.0
$\overline{m}_t(m_H/4)$	188.2	$\frac{213}{94}$	0.0

Table 5.2: Mass ratios squared, m_b^2/m_H^2 and m_t^2/m_H^2, used for the generation of numerical values of the two-loop four-point amplitudes. We chose values corresponding to the OS masses, according to PDG recommendations [154], and $\overline{\text{MS}}$-masses at scales relevant for 7-point variation w.r.t. to a central scale of $m_H/2$. For the latter, we used $\overline{m}_b(\overline{m}_b) = 4.18$ GeV, as recommended by the PDG and $\overline{m}_t(\overline{m}_t) = 162.7$ GeV. The dynamic scale **TODO:** Add reference ot dynamic scale used for our differential cross-section predictions can exceed m_H, and reaches values of up to 1 TeV. At this high scale, the bottom-quark mass is $\overline{m}_b(1 \text{ TeV}) = 2.41$ GeV. To avoid extrapolations outside our numerical grids for the amplitudes, we therefore included another mass value, $\overline{m}_b^{\min}$, below this minimum.

6 | RESULTS AND DISCUSSION

Description of this chapter.

6.1 TOTAL CROSS SECTION

6.1.1 Effects of Finite Top-Quark Masses

6.1.2 Effects of Finite Bottom-Quark Masses

6.2 DIFFERENTIAL CROSS SECTION

7 | CONCLUSIONS

Here are my conclusions.

A | FEYNMAN RULES OF THE STANDARD MODEL
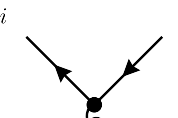
In this chapter we list all Feynman rules of the SM. We choose to work in a unitary gauge, meaning that the all Goldstone-bosons decouple and there are no unphysical particles in the electroweak sector. In the QCD sector, we work in the R_ξ gauge, i.e. we have unphysical particles in the form of *Faddeev-Popov ghosts*. If not otherwise specified, the momenta on every line are defined as incoming.

Propagators:
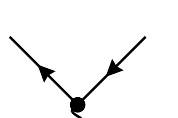
$$a,\mu \quad \overset{k}{\text{→}} \quad b,\nu \quad = i\frac{\delta^{ab}}{k^2+i0^+}\left[-g_{\mu\nu}+(1-\xi)\frac{k_\mu k_\nu}{k^2+i0^+}\right]$$

$$i \quad \overset{k}{\longrightarrow} \quad j \quad = i\delta_{ij}\frac{\slashed{k}+m}{k^2-m^2+i0^+}$$

$$\overset{k}{\dashrightarrow} \quad = i\frac{1}{k^2-m_H^2+i0^+}$$

$$\mu \quad \overset{k}{\underset{\gamma}{\wwww}} \quad \nu \quad = i\frac{-g_{\mu\nu}}{k^2+i0^+}$$

$$\mu \quad \overset{k}{\underset{W}{\wwww}} \quad \nu \quad = i\frac{1}{k^2-m_W^2+i0^+}\left(-g_{\mu\nu}+\frac{k_\mu k_\nu}{m_W^2+i0^+}\right)$$

$$\mu \quad \overset{k}{\underset{Z}{\wwww}} \quad \nu \quad = i\frac{1}{k^2-m_Z^2+i0^+}\left(-g_{\mu\nu}+\frac{k_\mu k_\nu}{m_Z^2+i0^+}\right)$$

$$a \quad \overset{k}{\cdots\blacktriangleright\cdots} \quad b \quad = i\frac{\delta^{ab}}{k^2+i0^+}$$

Fermion–Gauge-Boson Vertices:

$$= ig\gamma^\mu T_{ij}^a$$

$$= -ie\gamma^\mu Q$$
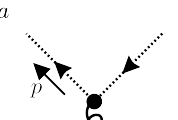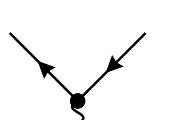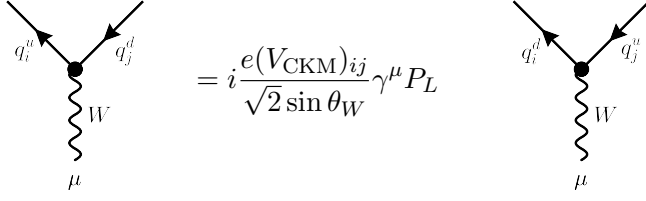
$$= gf^{abc}p^\mu$$

$$= i\frac{e}{\sin\theta_W\cos\theta_W}\gamma^\mu$$
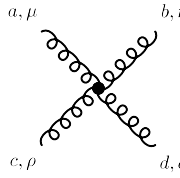$$\times\left(I^3 P_L - Q\sin^2\theta_W\right)$$
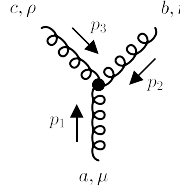
$$= i\frac{e(V_{\mathrm{CKM}})_{ij}}{\sqrt{2}\sin\theta_W}\gamma^\mu P_L$$

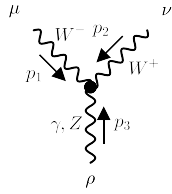$$= i\frac{e(V_{\mathrm{CKM}})^*_{ji}}{\sqrt{2}\sin\theta_W}\gamma^\mu P_L$$
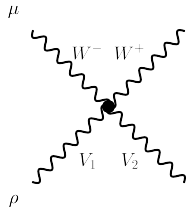
Gauge-Boson Self Interactions:

$$\begin{aligned} = g f^{abc}(&(p_1^\rho - p_2^\rho)g^{\mu\nu}\\ &+ (p_2^\mu - p_3^\mu)g^{\nu\rho} + (p_3^\nu - p_1^\nu)g^{\rho\mu}) \end{aligned}$$

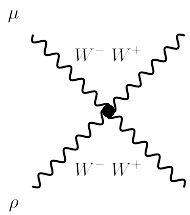$$\begin{aligned} = -ig^2\big(&f^{abe}f^{cde}(g^{\mu\rho}g^{\nu\sigma} - g^{\mu\sigma}g^{\nu\rho})\\ &+ f^{ace}f^{bde}(g^{\mu\nu}g^{\rho\sigma} - g^{\mu\sigma}g^{\nu\rho})\\ &+ f^{ade}f^{bce}(g^{\mu\nu}g^{\rho\sigma} - g^{\mu\rho}g^{\nu\sigma})\big) \end{aligned}$$

$$\begin{aligned} = i\frac{e}{\sin\theta_W}(&(p_1^\rho - p_2^\rho)g^{\mu\nu} + (p_2^\mu - p_3^\mu)g^{\nu\rho}\\ &+ (p_3^\nu - p_1^\nu)g^{\rho\mu}) \times \begin{cases} -\sin\theta_W & \text{for } \gamma\\ \cos\theta_W & \text{for } Z \end{cases} \end{aligned}$$

$$= i\frac{e^2}{\sin^2\theta_W}(g^{\mu\sigma}g^{\nu\rho} + g^{\mu\rho}g^{\nu\sigma} - 2g^{\mu\nu}g^{\rho\sigma}) \times \prod_{i=1}^2 \begin{cases} -\sin\theta_W & \text{if } V_i = \gamma\\ \cos\theta_W & \text{if } V_i = Z \end{cases}$$
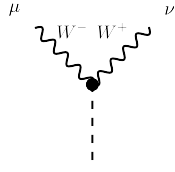

$$= i\frac{e^2}{\sin^2\theta_W}(2g^{\mu\rho}g^{\nu\sigma} - g^{\mu\nu}g^{\rho\sigma} - g^{\mu\sigma}g^{\nu\rho})$$
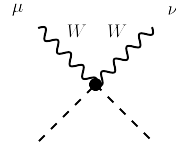
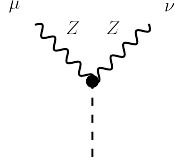**Higgs Interactions:**

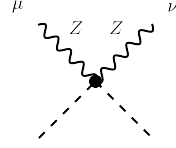$$= -i\frac{m_q}{v}\delta_{ij}$$

$$= -i\frac{3m_H^2}{v}$$

$$= i\frac{e}{\sin\theta_W}m_W g^{\mu\nu}$$

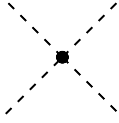

$$= i\frac{e^2}{2\sin^2\theta_W}g^{\mu\nu}$$

$$= i\frac{e}{\sin\theta_W\cos\theta_W}m_Z g^{\mu\nu}$$

$$= i\frac{e^2}{2\sin^2\theta_W\cos^2\theta_W}g^{\mu\nu}$$

$$= -i\frac{3m_H^2}{v^2}$$

B | FEYNMAN INTEGRALS

In this appendix we collect some common one-loop Feynman integrals which appear frequently throughout this PhD thesis.

Bubble

We define the function $B(p^2)$ as the finite part of the bubble integral

$$B(p^2) = 2 - \log\left(\frac{m^2}{\mu^2}\right) + \beta(p^2, m^2) \log\left(-\frac{1 - \beta(p^2, m^2)}{1 + \beta(p^2, m^2)} + i0^+\right). \tag{B.1}$$

The function $\beta(s, m^2)$ is defined in Eq. (5.28). We further define

$$B_1(p^2) \equiv B(p^2) - B(m_H^2). \tag{B.2}$$

Triangle

The one-loop on-shell triangle integral is

$$C(s) = C(p_1, p_2) = \frac{1}{2s} \log^2\left(-\frac{1 - \beta(p^2, m^2)}{1 + \beta(p^2, m^2)} + i0^+\right). \tag{B.3}$$

The triangle integral with one off-shell leg is related via

$$s_1 C_1(s) \equiv s C(s) - m_H^2 C(m_H^2). \tag{B.4}$$

Box

The one-loop box integral reads

$$
\begin{aligned}
D(s,t) &= D(p_1, p_2, p_3) \\
&= \int \frac{\mathrm{d}^4 l}{i\pi^2} \frac{1}{[l^2 - m^2][(l + p_1)^2 - m^2][(l + p_1 + p_2)^2 - m^2][(l + p_1 + p_2 + p_3)^2 - m^2]} \\
&= -\frac{2}{st\beta(st/u, m^2)} \left\{ \mathrm{Li}_2\left(\frac{1 - \beta(st/u, m^2)}{-\beta(st/u, m^2) - \beta(m_H^2, m^2 - i0^+)}\right) \right. \\
&\quad - \mathrm{Li}_2\left(\frac{1 + \beta(st/u, m^2)}{\beta(st/u, m^2) - \beta(m_H^2, m^2 - i0^+)}\right) + \mathrm{Li}_2\left(\frac{1 - \beta(st/u, m^2)}{\beta(m_H^2, m^2 - i0^+) - \beta(st/u, m^2)}\right) \\
&\quad - \mathrm{Li}_2\left(\frac{1 + \beta(st/u, m^2)}{\beta(m_H^2, m^2 - i0^+) + \beta(st/u, m^2)}\right) \\
&\quad + \log\left(-\frac{1 - \beta(st/u, m^2)}{\beta(st/u, m^2) + 1}\right) \log\left(1 - \frac{m_H^2}{4m^2}(1 - \beta^2(st/u, m^2) - i0^+)\right) \\
&\quad \left. - (m_H^2 \to s) - (m_H^2 \to t) \right\}
\end{aligned}
\tag{B.5}
$$

where $p_1^2 = p_2^2 = p_3^2 = 0$. We further define the auxiliary function

$$E(u, t) = uC(u) + tC(t) + u_1 C_1(u) + t_1 C_1(t) - ut D(u, t). \tag{B.6}$$

BIBLIOGRAPHY

[1] Michał Czakon, Felix Eschment, and Tom Schellenberger. "Revisiting the double-soft asymptotics of one-loop amplitudes in massless QCD." In: *JHEP* 04 (2023), p. 065. DOI: `10.1007/JHEP04(2023)065`. arXiv: `2211.06465 [hep-ph]`.

[2] Michał Czakon, Felix Eschment, and Tom Schellenberger. "Subleading effects in soft-gluon emission at one-loop in massless QCD." In: *JHEP* 12 (2023), p. 126. DOI: `10.1007/JHEP12(2023)126`. arXiv: `2307.02286 [hep-ph]`.

[3] Michał Czakon et al. "Top-Bottom Interference Contribution to Fully Inclusive Higgs Production." In: *Phys. Rev. Lett.* 132.21 (2024), p. 211902. DOI: `10.1103/PhysRevLett.132.211902`. arXiv: `2312.09896 [hep-ph]`.

[4] Michał Czakon et al. "Quark mass effects in Higgs production." In: *JHEP* 10 (2024), p. 210. DOI: `10.1007/JHEP10(2024)210`. arXiv: `2407.12413 [hep-ph]`.

[5] Izaak Neutelings. *Izaak neutelings*. Mar. 2024. URL: `https://tikz.net/sm_particles/`.

[6] Stefan Weinzierl. *Feynman Integrals. A Comprehensive Treatment for Students and Researchers*. UNITEXT for Physics. Springer, 2022. ISBN: 978-3-030-99557-7, 978-3-030-99560-7, 978-3-030-99558-4. DOI: `10.1007/978-3-030-99558-4`. arXiv: `2201.03593 [hep-th]`.

[7] Gerard 't Hooft. "Renormalizable Lagrangians for Massive Yang-Mills Fields." In: *Nucl. Phys. B* 35 (1971). Ed. by J. C. Taylor, pp. 167–188. DOI: `10.1016/0550-3213(71)90139-8`.

[8] Gerard 't Hooft and M. J. G. Veltman. "Regularization and Renormalization of Gauge Fields." In: *Nucl. Phys. B* 44 (1972), pp. 189–213. DOI: `10.1016/0550-3213(72)90279-9`.

[9] Andy Buckley et al. "LHAPDF6: parton density access in the LHC precision era." In: *Eur. Phys. J. C* 75 (2015), p. 132. DOI: `10.1140/epjc/s10052-015-3318-8`. arXiv: `1412.7420 [hep-ph]`.

[10] Richard D. Ball et al. "Parton distributions from high-precision collider data." In: *Eur. Phys. J. C* 77.10 (2017), p. 663. DOI: `10.1140/epjc/s10052-017-5199-5`. arXiv: `1706.00428 [hep-ph]`.

[11] John C. Collins, Davison E. Soper, and George F. Sterman. "Factorization of Hard Processes in QCD." In: *Adv. Ser. Direct. High Energy Phys.* 5 (1989), pp. 1–91. DOI: `10.1142/9789814503266_0001`. arXiv: `hep-ph/0409313`.

[12] Yuri L. Dokshitzer. "Calculation of the Structure Functions for Deep Inelastic Scattering and e+ e- Annihilation by Perturbation Theory in Quantum Chromodynamics." In: *Sov. Phys. JETP* 46 (1977), pp. 641–653.

[13] V. N. Gribov and L. N. Lipatov. "Deep inelastic e p scattering in perturbation theory." In: *Sov. J. Nucl. Phys.* 15 (1972), pp. 438–450.

[14] Guido Altarelli and G. Parisi. "Asymptotic Freedom in Parton Language." In: *Nucl. Phys. B* 126 (1977), pp. 298–318. DOI: `10.1016/0550-3213(77)90384-4`.

[15] T. Kinoshita and A. Ukawa. "Mass Singularities of Feynman Amplitudes." In: *Lect. Notes Phys.* 39 (1975). Ed. by Huzihiro Araki, pp. 55–58. DOI: `10.1007/BFb0013300`.

[16] T. D. Lee and M. Nauenberg. "Degenerate Systems and Mass Singularities." In: *Phys. Rev.* 133 (1964). Ed. by G. Feinberg, B1549–B1562. DOI: `10.1103/PhysRev.133.B1549`.

[17] Charalampos Anastasiou and Kirill Melnikov. "Higgs boson production at hadron colliders in NNLO QCD." In: *Nucl. Phys. B* 646 (2002), pp. 220–256. DOI: `10.1016/S0550-3213(02)00837-4`. arXiv: `hep-ph/0207004`.

[18] Falko Dulat et al. "Higgs-differential cross section at NNLO in dimensional regularisation." In: *JHEP* 07 (2017), p. 017. DOI: `10.1007/JHEP07(2017)017`. arXiv: `1704.08220 [hep-ph]`.

[19] Markus A. Ebert, Bernhard Mistlberger, and Gherardo Vita. "N-jettiness beam functions at N^{3}LO." In: *JHEP* 09 (2020), p. 143. DOI: `10.1007/JHEP09(2020)143`. arXiv: `2006.03056 [hep-ph]`.

[20] Daniel Baranowski et al. "Zero-jettiness soft function to third order in perturbative QCD." In: (Sept. 2024). arXiv: `2409.11042 [hep-ph]`.

[21] Daniel Baranowski et al. "Triple real-emission contribution to the zero-jettiness soft function at N3LO in QCD." In: (Dec. 2024). arXiv: `2412.14001 [hep-ph]`.

[22] John M. Campbell et al. "The NNLO QCD soft function for 1-jettiness." In: *Eur. Phys. J. C* 78.3 (2018), p. 234. DOI: `10.1140/epjc/s10052-018-5732-1`. arXiv: `1711.09984 [hep-ph]`.

[23] Thomas Becher and Guido Bell. "The gluon jet function at two-loop order." In: *Phys. Lett. B* 695 (2011), pp. 252–258. DOI: `10.1016/j.physletb.2010.11.036`. arXiv: `1008.1936 [hep-ph]`.

[24] Thomas Becher and Matthias Neubert. "Toward a NNLO calculation of the anti-B —> X(s) gamma decay rate with a cut on photon energy. II. Two-loop result for the jet function." In: *Phys. Lett. B* 637 (2006), pp. 251–259. DOI: `10.1016/j.physletb.2006.04.046`. arXiv: `hep-ph/0603140`.

[25] Radja Boughezal, Xiaohui Liu, and Frank Petriello. "N-jettiness soft function at next-to-next-to-leading order." In: *Phys. Rev. D* 91.9 (2015), p. 094035. DOI: `10.1103/PhysRevD.91.094035`. arXiv: `1504.02540 [hep-ph]`.

[26] Michał Czakon et al. "Single-jet inclusive rates with exact color at $\mathcal{O}(\alpha_s^4)$." In: *JHEP* 10 (2019), p. 262. DOI: `10.1007/JHEP10(2019)262`. arXiv: `1907.12911 [hep-ph]`.

[27] M. Czakon. "A novel subtraction scheme for double-real radiation at NNLO." In: *Phys. Lett. B* 693 (2010), pp. 259–268. DOI: `10.1016/j.physletb.2010.08.036`. arXiv: `1005.0274 [hep-ph]`.

[28] H. M. Georgi et al. "Higgs Bosons from Two Gluon Annihilation in Proton Proton Collisions." In: *Phys. Rev. Lett.* 40 (1978), p. 692. DOI: `10.1103/PhysRevLett.40.692`.

[29] M. Czakon and D. Heymes. "Four-dimensional formulation of the sector-improved residue subtraction scheme." In: *Nucl. Phys. B* 890 (2014), pp. 152–227. DOI: `10.1016/j.nuclphysb.2014.11.006`. arXiv: `1408.2500 [hep-ph]`.

[30] Michał Czakon and Marco Niggetiedt. "Exact quark-mass dependence of the Higgs-gluon form factor at three loops in QCD." In: *JHEP* 05 (2020), p. 149. DOI: `10.1007/JHEP05(2020)149`. arXiv: `2001.03008 [hep-ph]`.

[31] S. Dawson. "Radiative corrections to Higgs boson production." In: *Nucl. Phys. B* 359 (1991), pp. 283–300. DOI: `10.1016/0550-3213(91)90061-2`.

[32] H. Kluberg-Stern and J. B. Zuber. "Ward Identities and Some Clues to the Renormalization of Gauge Invariant Operators." In: *Phys. Rev. D* 12 (1975), pp. 467–481. DOI: `10.1103/PhysRevD.12.467`.

[33] Satish D. Joglekar and Benjamin W. Lee. "General Theory of Renormalization of Gauge Invariant Operators." In: *Annals Phys.* 97 (1976), p. 160. DOI: `10.1016/0003-4916(76)90225-6`.

[34] Marc Henneaux, Axel Kleinschmidt, and Gustavo Lucena Gómez. "Remarks on Gauge Invariance and First-class Constraints." In: *Ann. U. Craiova Phys.* 21 (2011), S1–S10.

[35] David J. Gross and Frank Wilczek. "Ultraviolet Behavior of Nonabelian Gauge Theories." In: *Phys. Rev. Lett.* 30 (1973). Ed. by J. C. Taylor, pp. 1343–1346. DOI: `10.1103/PhysRevLett.30.1343`.

[36] H. David Politzer. "Reliable Perturbative Results for Strong Interactions?" In: *Phys. Rev. Lett.* 30 (1973). Ed. by J. C. Taylor, pp. 1346–1349. DOI: `10.1103/PhysRevLett.30.1346`.

[37] *Proceedings, Colloquium on Renormalization of Yang-Mills Fields, Marseille, June 19-23, 1972.* 1972.

[38] William E. Caswell. "Asymptotic Behavior of Nonabelian Gauge Theories to Two Loop Order." In: *Phys. Rev. Lett.* 33 (1974), p. 244. DOI: `10.1103/PhysRevLett.33.244`.

[39] D. R. T. Jones. "Two Loop Diagrams in Yang-Mills Theory." In: *Nucl. Phys. B* 75 (1974), p. 531. DOI: `10.1016/0550-3213(74)90093-5`.

[40] E. Egorian and O. V. Tarasov. "Two Loop Renormalization of the QCD in an Arbitrary Gauge." In: *Teor. Mat. Fiz.* 41 (1979), pp. 26–32.

[41] Bernd A. Kniehl and Michael Spira. "Two loop O (alpha-s G(F) $m(t)^2$ correction to the $H \to b\bar{b}$ decay rate." In: *Nucl. Phys. B* 432 (1994), pp. 39–48. DOI: `10.1016/0550-3213(94)90592-4`. arXiv: `hep-ph/9410319`.

[42] Bernd A. Kniehl and Michael Spira. "Low-energy theorems in Higgs physics." In: *Z. Phys. C* 69 (1995), pp. 77–88. DOI: `10.1007/s002880050007`. arXiv: `hep-ph/9505225`.

[43] K. G. Chetyrkin, Bernd A. Kniehl, and M. Steinhauser. "Decoupling relations to O (alpha-s**3) and their connection to low-energy theorems." In: *Nucl. Phys. B* 510 (1998), pp. 61–87. DOI: `10.1016/S0550-3213(97)00649-4`. arXiv: `hep-ph/9708255`.

[44] Thomas Appelquist and J. Carazzone. "Infrared Singularities and Massive Fields." In: *Phys. Rev. D* 11 (1975), p. 2856. DOI: `10.1103/PhysRevD.11.2856`.

[45] K. G. Chetyrkin, Bernd A. Kniehl, and M. Steinhauser. "Strong coupling constant with flavor thresholds at four loops in the MS scheme." In: *Phys. Rev. Lett.* 79 (1997), pp. 2184–2187. DOI: `10.1103/PhysRevLett.79.2184`. arXiv: `hep-ph/9706430`.

[46] Y. Schroder and M. Steinhauser. "Four-loop decoupling relations for the strong coupling." In: *JHEP* 01 (2006), p. 051. DOI: `10.1088/1126-6708/2006/01/051`. arXiv: `hep-ph/0512058`.

[47] K. G. Chetyrkin, Johann H. Kuhn, and Christian Sturm. "QCD decoupling at four loops." In: *Nucl. Phys. B* 744 (2006), pp. 121–135. DOI: `10.1016/j.nuclphysb.2006.03.020`. arXiv: `hep-ph/0512060`.

[48] Robert V. Harlander and William B. Kilgore. "Next-to-next-to-leading order Higgs production at hadron colliders." In: *Phys. Rev. Lett.* 88 (2002), p. 201801. DOI: `10.1103/PhysRevLett.88.201801`. arXiv: `hep-ph/0201206`.

[49] Charalampos Anastasiou et al. "High precision determination of the gluon fusion Higgs boson cross-section at the LHC." In: *JHEP* 05 (2016), p. 058. DOI: `10.1007/JHEP05(2016)058`. arXiv: `1602.00695 [hep-ph]`.

[50] S. Catani and M. H. Seymour. "A General algorithm for calculating jet cross-sections in NLO QCD." In: *Nucl. Phys. B* 485 (1997). [Erratum: Nucl.Phys.B 510, 503–504 (1998)], pp. 291–419. DOI: `10.1016/S0550-3213(96)00589-5`. arXiv: `hep-ph/9605323`.

[51] Valentin Ahrens et al. "Origin of the Large Perturbative Corrections to Higgs Production at Hadron Colliders." In: *Phys. Rev. D* 79 (2009), p. 033013. DOI: `10.1103/PhysRevD.79.033013`. arXiv: `0808.3008 [hep-ph]`.

[52] Charalampos Anastasiou et al. "Higgs Boson GluonFfusion Production Beyond Threshold in N^3LO QCD." In: *JHEP* 03 (2015), p. 091. DOI: `10.1007/JHEP03(2015)091`. arXiv: `1411.3584 [hep-ph]`.

[53] Charalampos Anastasiou et al. "Higgs Boson Gluon-Fusion Production in QCD at Three Loops." In: *Phys. Rev. Lett.* 114 (2015), p. 212001. DOI: `10.1103/PhysRevLett.114.212001`. arXiv: `1503.06056 [hep-ph]`.

[54] Charalampos Anastasiou et al. "Higgs boson gluon–fusion production at threshold in N^3LO QCD." In: *Phys. Lett. B* 737 (2014), pp. 325–328. DOI: `10.1016/j.physletb.2014.08.067`. arXiv: `1403.4616 [hep-ph]`.

[55] Bernhard Mistlberger. "Higgs boson production at hadron colliders at N^3LO in QCD." In: *JHEP* 05 (2018), p. 028. DOI: `10.1007/JHEP05(2018)028`. arXiv: `1802.00833 [hep-ph]`.

[56] Robert V. Harlander, Stefan Liebler, and Hendrik Mantler. "SusHi: A program for the calculation of Higgs production in gluon fusion and bottom-quark annihilation in the Standard Model and the MSSM." In: *Comput. Phys. Commun.* 184 (2013), pp. 1605–1617. DOI: `10.1016/j.cpc.2013.02.006`. arXiv: `1212.3249 [hep-ph]`.

[57] Robert V. Harlander, Stefan Liebler, and Hendrik Mantler. "SusHi Bento: Beyond NNLO and the heavy-top limit." In: *Comput. Phys. Commun.* 212 (2017), pp. 239–257. DOI: `10.1016/j.cpc.2016.10.015`. arXiv: `1605.03190 [hep-ph]`.

[58] D. de Florian et al. "Handbook of LHC Higgs Cross Sections: 4. Deciphering the Nature of the Higgs Sector." In: 2/2017 (Oct. 2016). DOI: `10.23731/CYRM-2017-002`. arXiv: `1610.07922 [hep-ph]`.

[59] G. Das, S. Moch, and A. Vogt. "Approximate four-loop QCD corrections to the Higgs-boson production cross section." In: *Phys. Lett. B* 807 (2020), p. 135546. DOI: `10.1016/j.physletb.2020.135546`. arXiv: `2004.00563 [hep-ph]`.

[60] Stefano Catani et al. "Soft gluon resummation for Higgs boson production at hadron colliders." In: *JHEP* 07 (2003), p. 028. DOI: `10.1088/1126-6708/2003/07/028`. arXiv: `hep-ph/0306211`.

[61] George F. Sterman. "Summation of Large Corrections to Short Distance Hadronic Cross-Sections." In: *Nucl. Phys. B* 281 (1987), pp. 310–364. DOI: `10.1016/0550-3213(87)90258-6`.

[62] S. Catani and L. Trentadue. "Resummation of the QCD Perturbative Series for Hard Processes." In: *Nucl. Phys. B* 327 (1989), pp. 323–352. DOI: `10.1016/0550-3213(89)90273-3`.

[63] S. Catani and L. Trentadue. "Comment on QCD exponentiation at large x." In: *Nucl. Phys. B* 353 (1991), pp. 183–186. DOI: `10.1016/0550-3213(91)90506-S`.

[64]   Andreas von Manteuffel, Erik Panzer, and Robert M. Schabinger. "Cusp and collinear anomalous dimensions in four-loop QCD from form factors." In: *Phys. Rev. Lett.* 124.16 (2020), p. 162001. DOI: `10.1103/PhysRevLett.124.162001`. arXiv: `2002.04617 [hep-ph]`.

[65]   Christian W. Bauer, Dan Pirjol, and Iain W. Stewart. "Soft collinear factorization in effective field theory." In: *Phys. Rev. D* 65 (2002), p. 054022. DOI: `10.1103/PhysRevD.65.054022`. arXiv: `hep-ph/0109045`.

[66]   Christian W. Bauer et al. "Hard scattering factorization from effective field theory." In: *Phys. Rev. D* 66 (2002), p. 014017. DOI: `10.1103/PhysRevD.66.014017`. arXiv: `hep-ph/0202088`.

[67]   J. A. M. Vermaseren, A. Vogt, and S. Moch. "The Third-order QCD corrections to deep-inelastic scattering by photon exchange." In: *Nucl. Phys. B* 724 (2005), pp. 3–182. DOI: `10.1016/j.nuclphysb.2005.06.020`. arXiv: `hep-ph/0504242`.

[68]   S. Moch, J. A. M. Vermaseren, and A. Vogt. "The Longitudinal structure function at the third order." In: *Phys. Lett. B* 606 (2005), pp. 123–129. DOI: `10.1016/j.physletb.2004.11.063`. arXiv: `hep-ph/0411112`.

[69]   S. Moch, M. Rogal, and A. Vogt. "Differences between charged-current coefficient functions." In: *Nucl. Phys. B* 790 (2008), pp. 317–335. DOI: `10.1016/j.nuclphysb.2007.09.022`. arXiv: `0708.3731 [hep-ph]`.

[70]   S. Moch, J. A. M. Vermaseren, and A. Vogt. "Third-order QCD corrections to the charged-current structure function F(3)." In: *Nucl. Phys. B* 813 (2009), pp. 220–258. DOI: `10.1016/j.nuclphysb.2009.01.001`. arXiv: `0812.4168 [hep-ph]`.

[71]   J. Davies et al. "Non-singlet coefficient functions for charged-current deep-inelastic scattering to the third order in QCD." In: *PoS* DIS2016 (2016), p. 059. DOI: `10.22323/1.265.0059`. arXiv: `1606.08907 [hep-ph]`.

[72]   J. Blümlein et al. "The massless three-loop Wilson coefficients for the deep-inelastic structure functions F_2, F_L, xF_3 and g_1." In: *JHEP* 11 (2022), p. 156. DOI: `10.1007/JHEP11(2022)156`. arXiv: `2208.14325 [hep-ph]`.

[73]   H. Kawamura et al. "On the next-to-next-to-leading order QCD corrections to heavy-quark production in deep-inelastic scattering." In: *Nucl. Phys. B* 864 (2012), pp. 399–468. DOI: `10.1016/j.nuclphysb.2012.07.001`. arXiv: `1205.5727 [hep-ph]`.

[74]   Niccolò Laurenti. "Construction of a next-to-next-to-next-to-leading order approximation for heavy flavour production in deep inelastic scattering with quark masses." In: (Jan. 2024). arXiv: `2401.12139 [hep-ph]`.

[75]   Julien Baglio et al. "Inclusive production cross sections at N^{3}LO." In: *JHEP* 12 (2022), p. 066. DOI: `10.1007/JHEP12(2022)066`. arXiv: `2209.06138 [hep-ph]`.

[76]   Claude Duhr, Falko Dulat, and Bernhard Mistlberger. "Charged current Drell-Yan production at N^{3}LO." In: *JHEP* 11 (2020), p. 143. DOI: `10.1007/JHEP11(2020)143`. arXiv: `2007.13313 [hep-ph]`.

[77]   Claude Duhr and Bernhard Mistlberger. "Lepton-pair production at hadron colliders at N^{3}LO in QCD." In: *JHEP* 03 (2022), p. 116. DOI: `10.1007/JHEP03(2022)116`. arXiv: `2111.10379 [hep-ph]`.

[78]   Xuan Chen et al. "Dilepton Rapidity Distribution in Drell-Yan Production to Third Order in QCD." In: *Phys. Rev. Lett.* 128.5 (2022), p. 052001. DOI: `10.1103/PhysRevLett.128.052001`. arXiv: `2107.09085 [hep-ph]`.

[79] Xuan Chen et al. "Transverse mass distribution and charge asymmetry in W boson production to third order in QCD." In: *Phys. Lett. B* 840 (2023), p. 137876. DOI: `10.1016/j.physletb.2023.137876`. arXiv: `2205.11426 [hep-ph]`.

[80] S. Moch et al. "Four-Loop Non-Singlet Splitting Functions in the Planar Limit and Beyond." In: *JHEP* 10 (2017), p. 041. DOI: `10.1007/JHEP10(2017)041`. arXiv: `1707.08315 [hep-ph]`.

[81] S. Moch et al. "Low moments of the four-loop splitting functions in QCD." In: *Phys. Lett. B* 825 (2022), p. 136853. DOI: `10.1016/j.physletb.2021.136853`. arXiv: `2111.15561 [hep-ph]`.

[82] J. Davies et al. "Large-nf contributions to the four-loop splitting functions in QCD." In: *Nucl. Phys. B* 915 (2017), pp. 335–362. DOI: `10.1016/j.nuclphysb.2016.12.012`. arXiv: `1610.07477 [hep-ph]`.

[83] G. Falcioni et al. "The double fermionic contribution to the four-loop quark-to-gluon splitting function." In: *Phys. Lett. B* 848 (2024), p. 138351. DOI: `10.1016/j.physletb.2023.138351`. arXiv: `2310.01245 [hep-ph]`.

[84] Thomas Gehrmann et al. "Complete N_f^2 contributions to four-loop pure-singlet splitting functions." In: *JHEP* 01 (2024), p. 029. DOI: `10.1007/JHEP01(2024)029`. arXiv: `2308.07958 [hep-ph]`.

[85] G. Falcioni et al. "Four-loop splitting functions in QCD – The quark-quark case." In: *Phys. Lett. B* 842 (2023), p. 137944. DOI: `10.1016/j.physletb.2023.137944`. arXiv: `2302.07593 [hep-ph]`.

[86] Thomas Gehrmann et al. "The NfCF3 contribution to the non-singlet splitting function at four-loop order." In: *Phys. Lett. B* 849 (2024), p. 138427. DOI: `10.1016/j.physletb.2023.138427`. arXiv: `2310.12240 [hep-ph]`.

[87] T. Jaroszewicz. "Gluonic Regge Singularities and Anomalous Dimensions in QCD." In: *Phys. Lett. B* 116 (1982), pp. 291–294. DOI: `10.1016/0370-2693(82)90345-8`.

[88] Richard D. Ball and Stefano Forte. "Summation of leading logarithms at small x." In: *Phys. Lett. B* 351 (1995), pp. 313–324. DOI: `10.1016/0370-2693(95)00395-2`. arXiv: `hep-ph/9501231`.

[89] Richard D. Ball and Stefano Forte. "The Small x behavior of Altarelli-Parisi splitting functions." In: *Phys. Lett. B* 465 (1999), pp. 271–281. DOI: `10.1016/S0370-2693(99)01013-8`. arXiv: `hep-ph/9906222`.

[90] Marco Bonvini and Simone Marzani. "Four-loop splitting functions at small x." In: *JHEP* 06 (2018), p. 145. DOI: `10.1007/JHEP06(2018)145`. arXiv: `1805.06460 [hep-ph]`.

[91] Xin Guan et al. "Splitting amplitudes at N³LO in QCD." In: *JHEP* 01 (2025), p. 090. DOI: `10.1007/JHEP01(2025)090`. arXiv: `2408.03019 [hep-ph]`.

[92] J. McGowan et al. "Approximate N³LO parton distribution functions with theoretical uncertainties: MSHT20aN³LO PDFs." In: *Eur. Phys. J. C* 83.3 (2023). [Erratum: Eur.Phys.J.C 83, 302 (2023)], p. 185. DOI: `10.1140/epjc/s10052-023-11236-0`. arXiv: `2207.04739 [hep-ph]`.

[93] Richard D. Ball et al. "The path to N³LO parton distributions." In: *Eur. Phys. J. C* 84.7 (2024), p. 659. DOI: `10.1140/epjc/s10052-024-12891-7`. arXiv: `2402.18635 [hep-ph]`.

[94] Thomas Cridge et al. "Combination of aN³LO PDFs and implications for Higgs production cross-sections at the LHC." In: (Nov. 2024). arXiv: `2411.05373 [hep-ph]`.

[95] Falko Dulat, Achilleas Lazopoulos, and Bernhard Mistlberger. "iHixs 2 — Inclusive Higgs cross sections." In: *Comput. Phys. Commun.* 233 (2018), pp. 243–260. DOI: `10.1016/j.cpc.2018.06.025`. arXiv: `1802.00827 [hep-ph]`.

[96] U. Aglietti et al. "Two loop light fermion contribution to Higgs production and decays." In: *Phys. Lett. B* 595 (2004), pp. 432–441. DOI: `10.1016/j.physletb.2004.06.063`. arXiv: `hep-ph/0404071`.

[97] Giuseppe Degrassi and Fabio Maltoni. "Two-loop electroweak corrections to Higgs production at hadron colliders." In: *Phys. Lett. B* 600 (2004), pp. 255–260. DOI: `10.1016/j.physletb.2004.09.008`. arXiv: `hep-ph/0407249`.

[98] Stefano Actis et al. "NNLO Computational Techniques: The Cases H —> gamma gamma and H —> g g." In: *Nucl. Phys. B* 811 (2009), pp. 182–273. DOI: `10.1016/j.nuclphysb.2008.11.024`. arXiv: `0809.3667 [hep-ph]`.

[99] Stefano Actis et al. "NLO Electroweak Corrections to Higgs Boson Production at Hadron Colliders." In: *Phys. Lett. B* 670 (2008), pp. 12–17. DOI: `10.1016/j.physletb.2008.10.018`. arXiv: `0809.1301 [hep-ph]`.

[100] Charalampos Anastasiou, Radja Boughezal, and Frank Petriello. "Mixed QCD-electroweak corrections to Higgs boson production in gluon fusion." In: *JHEP* 04 (2009), p. 003. DOI: `10.1088/1126-6708/2009/04/003`. arXiv: `0811.3458 [hep-ph]`.

[101] Charalampos Anastasiou et al. "Mixed QCD-electroweak corrections to Higgs production via gluon fusion in the small mass approximation." In: *JHEP* 03 (2019), p. 162. DOI: `10.1007/JHEP03(2019)162`. arXiv: `1811.11211 [hep-ph]`.

[102] Marco Bonetti, Kirill Melnikov, and Lorenzo Tancredi. "Higher order corrections to mixed QCD-EW contributions to Higgs boson production in gluon fusion." In: *Phys. Rev. D* 97.5 (2018). [Erratum: Phys.Rev.D 97, 099906 (2018)], p. 056017. DOI: `10.1103/PhysRevD.97.056017`. arXiv: `1801.10403 [hep-ph]`.

[103] Matteo Becchetti et al. "Next-to-leading order corrections to light-quark mixed QCD-EW contributions to Higgs boson production." In: *Phys. Rev. D* 103.5 (2021), p. 054037. DOI: `10.1103/PhysRevD.103.054037`. arXiv: `2010.09451 [hep-ph]`.

[104] A. Djouadi, M. Spira, and P. M. Zerwas. "Production of Higgs bosons in proton colliders: QCD corrections." In: *Phys. Lett. B* 264 (1991), pp. 440–446. DOI: `10.1016/0370-2693(91)90375-Z`.

[105] D. Graudenz, M. Spira, and P. M. Zerwas. "QCD corrections to Higgs boson production at proton proton colliders." In: *Phys. Rev. Lett.* 70 (1993), pp. 1372–1375. DOI: `10.1103/PhysRevLett.70.1372`.

[106] Robert V. Harlander and Kemal J. Ozeren. "Finite top mass effects for hadronic Higgs production at next-to-next-to-leading order." In: *JHEP* 11 (2009), p. 088. DOI: `10.1088/1126-6708/2009/11/088`. arXiv: `0909.3420 [hep-ph]`.

[107] Robert V. Harlander et al. "Higgs production in gluon fusion at next-to-next-to-leading order QCD for finite top mass." In: *Eur. Phys. J. C* 66 (2010), pp. 359–372. DOI: `10.1140/epjc/s10052-010-1258-x`. arXiv: `0912.2104 [hep-ph]`.

[108] Alexey Pak, Mikhail Rogal, and Matthias Steinhauser. "Finite top quark mass effects in NNLO Higgs boson production at LHC." In: *JHEP* 02 (2010), p. 025. DOI: `10.1007/JHEP02(2010)025`. arXiv: `0911.4662 [hep-ph]`.

[109] M. Czakon et al. "Exact Top-Quark Mass Dependence in Hadronic Higgs Production." In: *Phys. Rev. Lett.* 127.16 (2021). [Erratum: Phys.Rev.Lett. 131, 179901 (2023)], p. 162002. DOI: `10.1103/PhysRevLett.127.162002`. arXiv: `2105.04436 [hep-ph]`.

[110] Peter Marquard et al. "Quark Mass Relations to Four-Loop Order in Perturbative QCD." In: *Phys. Rev. Lett.* 114.14 (2015), p. 142002. DOI: `10.1103/PhysRevLett.114.142002`. arXiv: `1502.01030 [hep-ph]`.

[111] Peter Marquard et al. "Four-loop relation between the $\overline{MS}$ and on-shell quark mass." In: *PoS* RADCOR2015 (2016), p. 094. DOI: `10.22323/1.235.0094`. arXiv: `1601.03748 [hep-ph]`.

[112] X. Chen et al. "Precise QCD predictions for the production of Higgs + jet final states." In: *Phys. Lett. B* 740 (2015), pp. 147–150. DOI: `10.1016/j.physletb.2014.11.021`. arXiv: `1408.5325 [hep-ph]`.

[113] Kathrin Becker et al. "Precise predictions for boosted Higgs production." In: *SciPost Phys. Core* 7 (2024), p. 001. DOI: `10.21468/SciPostPhysCore.7.1.001`. arXiv: `2005.07762 [hep-ph]`.

[114] X. Chen et al. "Fully Differential Higgs Boson Production to Third Order in QCD." In: *Phys. Rev. Lett.* 127.7 (2021), p. 072002. DOI: `10.1103/PhysRevLett.127.072002`. arXiv: `2102.07607 [hep-ph]`.

[115] Xuan Chen et al. "NNLO QCD Corrections for Higgs-plus-jet Production in the Four-lepton Decay Mode." In: *PoS* RADCOR2019 (2019), p. 003. DOI: `10.22323/1.375.0003`. arXiv: `1912.03560 [hep-ph]`.

[116] Massimiliano Grazzini and Hayk Sargsyan. "Heavy-quark mass effects in Higgs boson production at the LHC." In: *JHEP* 09 (2013), p. 129. DOI: `10.1007/JHEP09(2013)129`. arXiv: `1306.4581 [hep-ph]`.

[117] Malte Buschmann et al. "Mass Effects in the Higgs-Gluon Coupling: Boosted vs Off-Shell Production." In: *JHEP* 02 (2015), p. 038. DOI: `10.1007/JHEP02(2015)038`. arXiv: `1410.5806 [hep-ph]`.

[118] S. P. Jones, M. Kerner, and G. Luisoni. "Next-to-Leading-Order QCD Corrections to Higgs Boson Plus Jet Production with Full Top-Quark Mass Dependence." In: *Phys. Rev. Lett.* 120.16 (2018). [Erratum: Phys.Rev.Lett. 128, 059901 (2022)], p. 162001. DOI: `10.1103/PhysRevLett.120.162001`. arXiv: `1802.00349 [hep-ph]`.

[119] Fady Bishara et al. "Constraining Light-Quark Yukawa Couplings from Higgs Distributions." In: *Phys. Rev. Lett.* 118.12 (2017), p. 121801. DOI: `10.1103/PhysRevLett.118.121801`. arXiv: `1606.09253 [hep-ph]`.

[120] Gage Bonner and Heather E. Logan. "Constraining the Higgs couplings to up and down quarks using production kinematics at the CERN Large Hadron Collider." In: (Aug. 2016). arXiv: `1608.04376 [hep-ph]`.

[121] Albert M Sirunyan et al. "Measurement and interpretation of differential cross sections for Higgs boson production at $\sqrt{s} = 13$ TeV." In: *Phys. Lett. B* 792 (2019), pp. 369–396. DOI: `10.1016/j.physletb.2019.03.059`. arXiv: `1812.06504 [hep-ex]`.

[122] Jonas M. Lindert et al. "Top-bottom interference effects in Higgs plus jet production at the LHC." In: *Phys. Rev. Lett.* 118.25 (2017), p. 252002. DOI: `10.1103/PhysRevLett.118.252002`. arXiv: `1703.03886 [hep-ph]`.

[123] Fabrizio Caola et al. "Bottom-quark effects in Higgs production at intermediate transverse momentum." In: *JHEP* 09 (2018), p. 035. DOI: `10.1007/JHEP09(2018)035`. arXiv: `1804.07632 [hep-ph]`.

[124] Roberto Bonciani et al. "Next-to-leading-order QCD corrections to Higgs production in association with a jet." In: *Phys. Lett. B* 843 (2023), p. 137995. DOI: `10.1016/j.physletb.2023.137995`. arXiv: `2206.10490 [hep-ph]`.

[125] Hendrik Mantler and Marius Wiesemann. "Top- and bottom-mass effects in hadronic Higgs production at small transverse momenta through LO+NLL." In: *Eur. Phys. J. C* 73.6 (2013), p. 2467. DOI: `10.1140/epjc/s10052-013-2467-x`. arXiv: `1210.8263 [hep-ph]`.

[126] Keith Hamilton, Paolo Nason, and Giulia Zanderighi. "Finite quark-mass effects in the NNLOPS POWHEG+MiNLO Higgs generator." In: *JHEP* 05 (2015), p. 140. DOI: `10.1007/JHEP05(2015)140`. arXiv: `1501.04637 [hep-ph]`.

[127] Emanuele Bagnaschi and Alessandro Vicini. "The Higgs transverse momentum distribution in gluon fusion as a multiscale problem." In: *JHEP* 01 (2016), p. 056. DOI: `10.1007/JHEP01(2016)056`. arXiv: `1505.00735 [hep-ph]`.

[128] Emanuele Bagnaschi et al. "Resummation ambiguities in the Higgs transverse-momentum spectrum in the Standard Model and beyond." In: *JHEP* 01 (2016), p. 090. DOI: `10.1007/JHEP01(2016)090`. arXiv: `1510.08850 [hep-ph]`.

[129] Rikkert Frederix et al. "Heavy-quark mass effects in Higgs plus jets production." In: *JHEP* 08 (2016), p. 006. DOI: `10.1007/JHEP08(2016)006`. arXiv: `1604.03017 [hep-ph]`.

[130] Fabrizio Caola et al. "The Higgs transverse momentum spectrum with finite quark masses beyond leading order." In: *JHEP* 08 (2016), p. 150. DOI: `10.1007/JHEP08(2016)150`. arXiv: `1606.04100 [hep-ph]`.

[131] Marco Niggetiedt and Marius Wiesemann. "Higgs-boson production in the full theory at NNLO+PS." In: *Phys. Lett. B* 858 (2024), p. 139043. DOI: `10.1016/j.physletb.2024.139043`. arXiv: `2407.01354 [hep-ph]`.

[132] Falko Dulat, Bernhard Mistlberger, and Andrea Pelloni. "Precision predictions at N^{3}LO for the Higgs boson rapidity distribution at the LHC." In: *Phys. Rev. D* 99.3 (2019), p. 034004. DOI: `10.1103/PhysRevD.99.034004`. arXiv: `1810.09462 [hep-ph]`.

[133] Falko Dulat, Bernhard Mistlberger, and Andrea Pelloni. "Differential Higgs production at N^{3}LO beyond threshold." In: *JHEP* 01 (2018), p. 145. DOI: `10.1007/JHEP01(2018)145`. arXiv: `1710.03016 [hep-ph]`.

[134] Stefano Actis et al. "RECOLA: REcursive Computation of One-Loop Amplitudes." In: *Comput. Phys. Commun.* 214 (2017), pp. 140–173. DOI: `10.1016/j.cpc.2017.01.004`. arXiv: `1605.01090 [hep-ph]`.

[135] Lucy Budge et al. "The one-loop amplitudes for Higgs + 4 partons with full mass effects." In: *JHEP* 05 (2020), p. 079. DOI: `10.1007/JHEP05(2020)079`. arXiv: `2002.04018 [hep-ph]`.

[136] John Campbell and Tobias Neumann. "Precision Phenomenology with MCFM." In: *JHEP* 12 (2019), p. 034. DOI: `10.1007/JHEP12(2019)034`. arXiv: `1909.09117 [hep-ph]`.

[137] John M. Campbell and R. Keith Ellis. "An Update on vector boson pair production at hadron colliders." In: *Phys. Rev. D* 60 (1999), p. 113006. DOI: `10.1103/PhysRevD.60.113006`. arXiv: `hep-ph/9905386`.

[138] John M. Campbell, R. Keith Ellis, and Ciaran Williams. "Vector Boson Pair Production at the LHC." In: *JHEP* 07 (2011), p. 018. DOI: `10.1007/JHEP07(2011)018`. arXiv: `1105.0020 [hep-ph]`.

[139] R. Keith Ellis and Giulia Zanderighi. "Scalar one-loop integrals for QCD." In: *JHEP* 02 (2008), p. 002. DOI: `10.1088/1126-6708/2008/02/002`. arXiv: `0712.1851 [hep-ph]`.

[140] Stefano Carrazza, R. Keith Ellis, and Giulia Zanderighi. "QCDLoop: a comprehensive framework for one-loop scalar integrals." In: *Comput. Phys. Commun.* 209 (2016), pp. 134–143. DOI: `10.1016/j.cpc.2016.07.033`. arXiv: `1605.03181 [hep-ph]`.

[141] Kirill Melnikov, Lorenzo Tancredi, and Christopher Wever. "Two-loop $gg \to Hg$ amplitude mediated by a nearly massless quark." In: *JHEP* 11 (2016), p. 104. DOI: `10.1007/JHEP11(2016)104`. arXiv: `1610.03747 [hep-ph]`.

[142] Kirill Melnikov, Lorenzo Tancredi, and Christopher Wever. "Two-loop amplitudes for $qg \to Hq$ and $q\bar{q} \to Hg$ mediated by a nearly massless quark." In: *Phys. Rev. D* 95.5 (2017), p. 054012. DOI: `10.1103/PhysRevD.95.054012`. arXiv: `1702.00426 [hep-ph]`.

[143] Lance J. Dixon. "Calculating scattering amplitudes efficiently." In: *Theoretical Advanced Study Institute in Elementary Particle Physics (TASI 95): QCD and Beyond*. Jan. 1996, pp. 539–584. arXiv: `hep-ph/9601359`.

[144] J. A. M. Vermaseren. "New features of FORM." In: (Oct. 2000). arXiv: `math-ph/0010025`.

[145] Ben Ruijl, Takahiro Ueda, and Jos Vermaseren. "FORM version 4.2." In: (July 2017). arXiv: `1707.06453 [hep-ph]`.

[146] S. Laporta. "High-precision calculation of multiloop Feynman integrals by difference equations." In: *Int. J. Mod. Phys. A* 15 (2000), pp. 5087–5159. DOI: `10.1142/S0217751X00002159`. arXiv: `hep-ph/0102033`.

[147] Philipp Maierhöfer, Johann Usovitsch, and Peter Uwer. "Kira—A Feynman integral reduction program." In: *Comput. Phys. Commun.* 230 (2018), pp. 99–112. DOI: `10.1016/j.cpc.2018.04.012`. arXiv: `1705.05610 [hep-ph]`.

[148] Philipp Maierhöfer and Johann Usovitsch. "Kira 1.2 Release Notes." In: (Dec. 2018). arXiv: `1812.01491 [hep-ph]`.

[149] Jonas Klappert et al. "Integral reduction with Kira 2.0 and finite field methods." In: *Comput. Phys. Commun.* 266 (2021), p. 108024. DOI: `10.1016/j.cpc.2021.108024`. arXiv: `2008.06494 [hep-ph]`.

[150] U. Baur and E. W. Nigel Glover. "Higgs Boson Production at Large Transverse Momentum in Hadronic Collisions." In: *Nucl. Phys. B* 339 (1990), pp. 38–66. DOI: `10.1016/0550-3213(90)90532-I`.

[151] Michał Czakon et al. "The $(Q_7, Q_{1,2})$ contribution to $\overline{B} \to X_s\gamma$ at $\mathcal{O}\left(\alpha_s^2\right)$." In: *JHEP* 04 (2015), p. 168. DOI: `10.1007/JHEP04(2015)168`. arXiv: `1503.01791 [hep-ph]`.

[152] Vladimir A. Smirnov. "Applied asymptotic expansions in momenta and masses." In: *Springer Tracts Mod. Phys.* 177 (2002), pp. 1–262.

[153] Marco Niggetiedt. "Quark mass effects in form factors and hadronic Higgs production." PhD thesis. 2023. DOI: `10.18154/RWTH-2023-11198`.

[154] R. L. Workman et al. "Review of Particle Physics." In: *PTEP* 2022 (2022), p. 083C01. DOI: `10.1093/ptep/ptac097`.